

**STUDY OF PARTICLE DYNAMICS IN DUSTY PLASMA
SYSTEM USING STOCHASTIC MODELS**

CHEW WEI XIANG

**DISSERTATION SUBMITTED IN FULFILMENT OF
THE REQUIREMENTS FOR THE DEGREE OF
MASTER OF SCIENCE**

**DEPARTMENT OF PHYSICS
FACULTY OF SCIENCE
UNIVERSITY OF MALAYA
KUALA LUMPUR**

2013

UNIVERSITI MALAYA

ORIGINAL LITERARY WORK DECLARATION

Name of Candidate: CHEW WEI XIANG (I.C/Passport No: 870613-06-5501)

Registration/Matric No: SGR090150

Name of Degree: MASTER OF SCIENCE

Title of Project Paper/Research Report/Dissertation/Thesis ("this Work"):

STUDY OF PARTICLE DYNAMICS IN DUSTY PLASMA SYSTEM USING STOCHASTIC MODELS

Field of Study:

I do solemnly and sincerely declare that:

- (1) I am the sole author/writer of this Work;
- (2) This Work is original;
- (3) Any use of any work in which copyright exists was done by way of fair dealing and for permitted purposes and any excerpt or extract from, or reference to or reproduction of any copyright work has been disclosed expressly and sufficiently and the title of the Work and its authorship have been acknowledged in this Work;
- (4) I do not have any actual knowledge nor do I ought reasonably to know that the making of this work constitutes an infringement of any copyright work;
- (5) I hereby assign all and every rights in the copyright to this Work to the University of Malaya ("UM"), who henceforth shall be owner of the copyright in this Work and that any reproduction or use in any form or by any means whatsoever is prohibited without the written consent of UM having been first had and obtained;
- (6) I am fully aware that if in the course of making this Work I have infringed any copyright whether intentionally or otherwise, I may be subject to legal action or any other action as may be determined by UM.

Candidate's Signature

Date

9 July 2013

Subscribed and solemnly declared before,

Witness's Signature

Date

Name:

9 July 2013

Designation:

Abstract

Dusty plasma typically consists of electrons and ions with micron-size charged dust particles. Due to complex inter-species interactions, the system accommodates rich phenomena such as formation of strongly-coupled states, structural phase transition, formation of linear and non-linear waves, and anomalous diffusion behavior that violates the Fick's law. Particles motion in dusty plasma can be modeled using Brownian motion, but this model is inadequate to fully capture the detailed dynamics. In this study, charged dust particle dynamics is investigated using stochastic process with fractal characteristics based on the fractional calculus. Dusty plasma is generated using a capacitively coupled 13.56 MHz radio frequency (rf) gas discharge system and different particle states are observed by varying the neutral gas pressure. Particle motion are probed by monitoring the intensity fluctuation of scattered light in dynamic light scattering (DLS) experiment and particle trajectories obtained from particle tracking using digital video camera. In DLS experiment, particle transport mechanisms are deduced by fitting empirical intensity correlation functions using different transport models, which include purely ballistic, purely diffusive, and hybrid ballistic-diffusive transport model with the assumption of monodisperse particles. The hybrid model is found to be most accurate in describing the particle transport. A new correlation model based on a non-standard fractional Langevin equation is introduced to model polydisperse dust particles dynamics. In particle tracking experiment, time-dependent scaling behavior in particles' mean-square-displacement (MSD) is observed. This is consistent with the results from DLS experiment that shows dust particles undergo fast ballistic transport at short time scale and slow dynamic at longer time duration. Transient anomalous diffusion is described using a simple generalization of Riemann-Liouville fractional Brownian motion. The study is concluded with a brief discussion on how the DLS and MSD approaches can be corroborated to give useful insights into complex particle transport in dusty plasmas.

Abstrak

Plasma berdebu biasanya terdiri daripada electron, ion dan zarah debu yang bersaiz mikron. Interaksi antara spesies-spesies dalam plasma berdebu membentuk pelbagai fenomena yang menarik seperti pembentukan fasa terganding tinggi, peralihan fasa, pembentukan gelombang linear dan bukan linear, dan resapan anomali yang bertentangan dengan hukum Fick. Gerakan zarah dalam plasma berdebu boleh dimodelkan dengan menggunakan gerakan Brown, tetapi model ini tidak mencukupi untuk menggambarkan dinamik zarah dengan terperinci. Dalam kajian ini, dinamik zarah debu dikaji menggunakan proses stokastik dengan ciri-ciri fraktal berdasarkan kalkulus pecahan. Sistem plasma berdebu ini menggunakan sistem radio frekuensi 13.56 MHz terganding kapasitif. Plasma berdebu yang berlainan fasa telah diperhatikan apabila tekanan gas neutral diubah. Gerakan zarah diamati dengan menganalisis fluktuasi keamatan cahaya yang diserakan oleh zarah-zarah debu dalam eksperimen penyerakan cahaya dinamik. Selain itu, gerakan zarah juga dikaji melalui trajektori zarah yang diperolehi dari penjejakan zarah menggunakan kamera video digital. Dalam eksperimen penyerakan cahaya dinamik, jenis dinamik zarah ditentukan oleh mengkaji korelasi keamatan cahaya menggunakan model dinamik yang berlainan yang termasuk balistik, resapan, hibrid balistik-resapan dengan andaian zarah bersaiz sama. Antara model-model ini, model hibrid didapati paling tepat dalam menerangkan dinamik zarah. Satu model korelasi baru berdasarkan persamaan *non-standard fractional Langevin* diperkenalkan untuk model dinamik zarah yang berlainan saiz. Dalam eksperimen penjejakan zarah debu, sifat penskalaan dalam sesaran purata kuasa dua yang bergantung kepada masa telah diperhatikan. Ini adalah selaras dengan keputusan dari eksperimen penyerakan cahaya dinamik yang menunjukkan zarah debu menjalani gerakan balistik pada skala masa yang singkat dan dinamik perlahan pada tempoh masa yang lebih panjang. Resapan anomali ini boleh dimodel oleh model *Riemann-Liouville fractional Brownian motion*. Kajian ini diakhiri dengan perbincangan ringkas mengenai bagaimana pendekatan penyerakan cahaya dinamik dan sesaran purata kuasa dua boleh memberikan pandangan yang berguna kepada dinamik zarah dalam sistem plasma berdebu yang kompleks.

Acknowledgment

I would like to express my utmost appreciation to my supervisor Prof Dr. Sithi Vinayakam Muniandy and co-supervisor Prof Dr. Wong Chiow San. Without their continuous support, encouragement and constructive discussion throughout this project and dissertation writing, it may have been impossible for me to complete this MSc thesis.

I am also indebted to my colleagues and friends Mr. Lee Yen Sian, Ms. Siti Sarah Saffai, Dr. Hossein Asgari, Mr. Ngoi Siew Kien, Mr. Lee Seng Huat, Mr. Lim Lian Kuang, Mrs. Chan li San, Mr. Tay Wee Horng, Mr Neoh Yuen Sim and Dr Lim Yat Yuen who willingly gave me invaluable advice and helping hand when I was in trouble. Not to forget Mr. Jasbir Singh, who played a very important role in our research laboratory especially in providing administrative and technical assistance.

This research was made possible by the supports of University of Malaya Research Grant RG062/09AFR, RG162/11AFR and the University of Malaya Postgraduate Research Fund. I am also grateful to the University of Malaya Fellowship Scheme for providing monetary support throughout the candidature.

Last but not least, I would also like to thank my family members and fellow friends for their understanding and mental support during my master study.

Research Outputs

ISI Publications

- Muniandy, S.V., Chew, W.X. & Wong, C.S. (2011). Fractional dynamics in the light scattering intensity fluctuation in dusty plasma. *Physics of Plasmas* 18, 013701, pg.1-8
- Chew, W. X., Muniandy, S. V., Wong, C. S., Yap, S. L. & Tan, K. S. (2011). Diffusion Dynamics of Charged Dust Particles in Capacitively Coupled RF Discharge System. American Institute of Physics Conf. Proc. Vol. 1328, pg.1-3.
- Muniandy, S. V., Chew, W. X., Asgari, H., Wong, C. S., & Lim, S. C. (2011). Fractional Dynamics of Single File Diffusion in Dusty Plasma Ring. American Institute of Physics Conf. Proc. Vol. 1397, pg. 431-432.

Submitted manuscript

- Muniandy, S. V., Chew, W. X., Safaai, S. S., Asgari, H., Yap, S. L., Wong, C. S.. Fractal Dynamics of Light Scattering Intensity Fluctuation in Disordered Dusty Plasmas. *Physica A* (submitted in July, 2012).

Presentations

- National Conference on Physics (PERFIK 2010), 28-30th October 2010, Swiss-Garden Golf Resort & Spa Damai Laut, Perak, Malaysia (poster presentation).
- The 6th Mathematics and Physical Sciences Graduate Congress, 13-15th December 2010, University of Malaya, Malaysia (oral presentation).
- The 7th Mathematics and Physical Sciences Graduate Congress, 12-14th December 2011, National University of Singapore, Singapore (oral presentation).
- Hands on Research in Complex Systems, 17-29th June 2012, Shanghai Jiao Tong University, China (poster presentation).

Table of Contents

Abstract	ii
Abstrak	iii
Acknowledgement	iv
Research Outputs	v
Table of Contents	vi
List of Figures	ix
List of Tables	xi
Chapter 1 Introduction	1
1.1 Dusty plasma	1
1.2 Complex physical phenomena in dusty plasma	2
1.3 Motivation of study	3
1.4 Objectives	4
1.5 Thesis layout	4
 Chapter 2 Literature review	 6
2.1 Dusty plasma	6
2.2 Physical phenomena	7
2.2.1 Particle charging	7
2.2.2 Particle mechanics	10
2.2.3 Collective behaviors	13
2.3 Diagnostic method	18
2.3.1 Dynamic light scattering	19
2.3.2 Visualization and particle tracking	26

2.3.3 Spatial correlation function	27
2.4 Stochastic models	28
2.4.1 Fractional calculus	30
2.4.2 Ornstein-Uhlenbeck and fractional Ornstein-Uhlenbeck process	31
2.4.3 Fractional Brownian motion	35
Chapter 3 Experiments	38
3.1 Capacitively coupled radio frequency plasma system	38
3.2 Visualization system	45
3.2.1 Experiment setup	46
3.2.2 Image processing	47
3.2.3 Pair correlation	48
3.2.4 Particle tracking	50
3.3 Dynamic light scattering system	51
3.3.1 Experiment setup	51
3.3.2 Signal processing	52
3.3.3 Correlation models	52
Chapter 4 Results and Discussions	54
4.1 Structural states of dusty plasma	54
4.2 Dynamic light scattering experiment	57
4.2.1 Intensity fluctuation at different pressures	57
4.2.2 Correlation analysis and model fitting	58
4.3 Particle tracking analysis	62
4.3.1 Particle trajectories	62

	4.3.2 Mean-square-displacement	63
Chapter5	Conclusions	66
References		69
Appendices	A Research outputs	
	B Matlab scripts	

List of Figures

Figure 1.1	Negatively charged dust particles in plasma environment consist of ions and neutrals.	1
Figure 2.1	Shielding of dust grain Coulomb potential.	2
Figure 2.2	Void formation in polystyrene dust cloud.	10
Figure 2.3	Vertical chains across several dusty plasma layers.	13
Figure 2.4	Phase diagram of Yukawa system in the (Γ, κ) plane, after (Hamaguchi et al., 1997).	14
Figure 2.5	Dust particle trajectories at different structural states: (a) crystal, (b) melting, (c) disordered gas (Lai & I, 2002).	15
Figure 2.6	Light scattering diagram.	19
Figure 3.1	Schematic diagram of capacitively coupled radio frequency plasma system.	39
Figure 3.2	Photo of the capacitively coupled radio frequency plasma system	39
Figure 3.3	(a) Sketch schematic diagram of a cross-sectional top view of plasma chamber and (b) its photo.	40
Figure 3.4	Vacuum chamber covered by top plate with viewing window at the center.	41
Figure 3.5	Circuit of matching network.	42
Figure 3.6	(a) Side view and (b) top view of dust dispenser system	43
Figure 3.7	SEM images of poly-disperse titanium dioxide particles.	44
Figure 3.8	Cylindrical depression on the bottom electrode.	45
Figure 3.9	(a) Side view of the bottom electrode with dust particles levitating at the sheath region, (b) Position of levitating dust particles in plasma.	45
Figure 3.10	(a) A schematic diagram and (b) photo of the particle visualization setup.	46
Figure 3.11	(a) Two-dimensional hexagonal crystal lattice (Pieper, Goree, & Quinn, 1996) and (b) its estimated pair correlation function.	47
Figure 3.12	(a) Dusty plasma ordered liquid (Boesse, 2005) and (b) its estimated pair correlation function.	47

Figure 3.13	(a) Randomly distributed dots and (b) its estimated pair correlation function.	47
Figure 3.14	(a) The schematic diagram and (b) photo of dynamic light scattering setup.	51
Figure 4.1	Snapshots of dusty plasma at different neutral gas pressures: (a) 0.1 mbar, (b) 0.3 mbar, and (c) 0.5 mbar.	54
Figure 4.2	Pair correlation functions of dusty plasma at different pressures. Radial distance is normalized by nearest inter-particle distance.	55
Figure 4.3	Distributions of particles' speed at different pressures.	56
Figure 4.4	Intensity fluctuations of dynamic light scattering signal at different gas pressures and absence of dust.	57
Figure 4.5	Empirical auto-correlation functions of intensity fluctuation at (a) 0.1 mbar, (b) 0.3 mbar, and (c) 0.5 mbar fitted with ballistic, diffusive, ballistic-diffusive and fractional dynamical model.	59
Figure 4.6	Selected particle trajectories at (a) 0.1 mbar, (b) 0.3 mbar, and (c) 0.5 mbar with the same time duration (0.6 s) and spatial scale (d) magnified single particle trajectory at 0.5 mbar with duration of 0.6 s.	62
Figure 4.7	Particles' mean-square-displacement at different pressures.	63
Figure 4.8	Auto-correlation function of trajectories' increments at different pressures.	65

List of Tables

Table 4.1	Fitting parameters of ballistic, diffusive, ballistic and fractional Ornstein-Uhlenbeck correlation model.	60
Table 4.2	Scaling exponents of mean square displacement at different pressures and time regimes.	64

Chapter 1

Introduction

1.1 Dusty plasma

Dusty plasma is loosely defined as normal electron-ion plasma with additional highly charged (10^3 - 10^5 elementary charges) components of micron-or submicron-sized particulates (10^{10} - 10^{12} ion masses) (Shukla & Mamun, 2002). Figure 1.1 shows a depiction of negatively charged dust in plasma environment. The large particle size and slow time-scale of particle motion (in a fraction of a second) enable direct observation at the kinetic level by using simple fast video camera.

In most naturally occurring and some artificial cases, dust particles coexist in the plasma. These dust particles can be charged either negatively or positively depending on their surrounding plasma environment and the charging mechanisms. The physics of dusty plasmas received its first major boost in the early 80s when Voyager space probes identified nearly radial ‘spokes’ around outer portion of Saturn’s B ring which was later explained by the presence of fine dust (Smith et al., 1982).

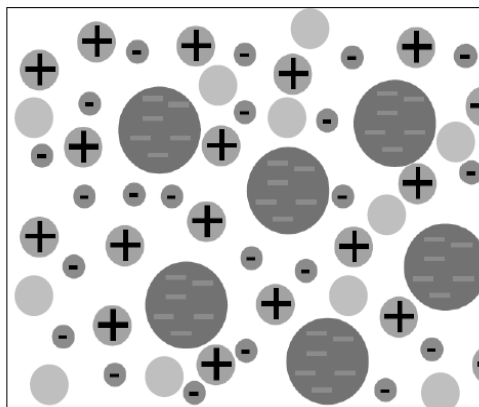


Figure 1.1 Negatively charged dust particles in plasma environment consist of ions and neutrals.

The second major advancement occurred in late 80s in the semiconductor industries where issues of particle contamination caused problem in semiconductor industries wafer production. Through laser scattering experiments, it was found that particles are formed and growing in the gas phase before falling onto the wafer. The inclusion of nano- or micrometer-sized particle in a controlled industrial/ laboratory processes have opened a wide range of new applications, such as flat-panel displays, thin film transistors, solar cells, charged aerosols and particulate powders used for material synthesis (Boufendi & Bouchoule, 2002).

1.2 Complex physical phenomena in dusty plasmas

The interaction between charged particles and the ambient environment is a many-body problem. The forces acting on one single dust particle include neutral drag force, gravitational force, ion drag force, thermophoresis force, and photophoresis force. Due to the highly charged nature, the electrostatic coupling between particles is strong enough to enable the formation of strongly coupled, ordered (crystalline and liquid) plasma phases. When the dusty plasma system's thermal energy is increased, one can get disordered liquid state and gaseous state dominated by binary collision will form at higher temperature. The real plasma is never in a quiescent state due to the long-range interaction, thus the collective nature of the plasma dominates its behavior. The particles act synchronously by organizing themselves as waves, modes, vortices or streamers, which may interact among themselves or with individual particles. The presence of charged dust in plasma not only changes the existing plasma wave's characteristics, but also introduces a number of new modes such as dust acoustic waves, dust ion acoustic waves, and dust lattice waves (Rao, Shukla, & Yu, 1990; Verheest, 2000).

1.3 Motivation of study

The rich dynamical process in dusty plasma can be described using the Yukawa model (Hou, Piel, & Shukla, 2009; Ott & Bonitz, 2009). The model considers charged particles levitated in a confinement potential well and interact with each other via isotropic screened Coulomb potential (or Yukawa / Debye-Huckel potential). Particles are coupled to the background neutrals through frictional force and stochastic momentum gain that follow white Gaussian noise. Such model predicts transient anomalous diffusive behavior that violates the Fick's law (Bouchaud & Georges, 1990). At longer time scales, the transport behavior converges to normal diffusion. However, the model does not fully consider the complexity of dusty plasma system such as the attractive inter-particle potential due to shadowing and focusing effects (Trottenberg, Melter, & Piel, 1995), anisotropy plasma environment near the sheath region (Hutchinson, 2005) and etc. In this study, the particle dynamics is investigated using stochastic process with fractal characteristics based on the framework of fractional calculus (Miller & Ross, 1993). One of the distinctive features of the stochastic process introduced in this work is its long-range correlation property that does not exist in the traditional diffusion model based on Brownian motion. The application of fractional calculus based approaches for studying complex dynamics in dusty plasma is relatively new in spite of its extensive use in many other areas (Miller & Ross, 1993).

1.4 Objectives

The aims of this work can be summarized as following:

- To setup the optical diagnostic technique for studying particle dynamics in dusty plasma,
- To investigate temporal fluctuation of light scattering signal,
- To determine the particle transport dynamics based on visualization technique.

1.5 Thesis layout

Following this chapter, the introduction to dusty plasma and related physical phenomena with emphasis on transport behavior are given in Chapter 2. Previous studies on anomalous diffusion processes in dusty plasma are also reviewed. The chapter also includes brief descriptions of the two most common diagnostic methods in dusty plasma, namely dynamic light scattering and particle visualization technique. Theoretical concepts on relevant stochastic processes and fractional calculus are given in this chapter, which will serve as the tools for modeling fluctuation as well as transport phenomena. Chapter 3 contains the experimental setup of the radio-frequency capacitively coupled dusty plasma system and the optical diagnostic system: dynamic light scattering and particle visualization technique. The image processing routines and particle location identification algorithm are described here. The main findings of this study are presented in Chapter 4 with two main sections on particle diagnosis, one focusing on the dynamic light scattering experiment and the other on the particle tracking analysis for particle transport characterization. The results are also discussed in the same chapter with a perspective towards providing a coherent interpretation of the transport behavior in disordered gas and liquid state as observed and analyzed using

DLS and particle tracking analysis. The study is concluded in Chapter 5 with a brief remark on stochastic modeling of DLS signal and anomalous diffusion plus some potential avenues for further investigation.

Chapter 2

Literature review

Some fundamental concepts in dusty plasmas such as particle charging process, particle mechanics, phase transition and collective behaviors are briefly discussed at the beginning of this chapter. One type of collective behaviors that have received great attention in recent years is the particle transport phenomena, particularly the anomalous diffusion process. In order to study particle dynamics in dusty plasma, two most common diagnostic methods used to study particle dynamics in dusty plasmas, namely the dynamic light scattering and particle visualization technique are used. The observed transport process and associated fluctuation behavior are analyzed and modeled using stochastic model formulated using fractional calculus.

2.1 Dusty plasma

Dusty plasma is a collection of electrons, ions, neutrals, and macroscopic dust particle of nano to micrometer size. Depending on the charging mechanism, the dust particle can be positively or negatively charged. However, in a laboratory environment, dust particle charged by inflow of electrons and ions will acquire a net negative charge due to the higher mobility of electrons. Typical dust charge can get up to the order of 10^3 - 10^5 elementary charges, resulting in strong coupling in dust particles than the background plasma. The negatively charged dust grain attracts the plasma species, forming a Debye layer which shields the grain potential as depicted in Figure 2.1.

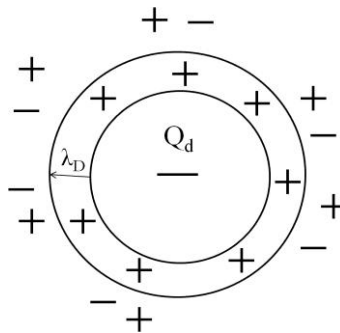


Figure 2.1 Shielding of dust grain Coulomb potential.

In laboratory plasma system, micron-sized dust grains can be confined in a capacitively coupled radio frequency (rf) discharge by the balance between external forces acting on the dust, which includes gravity, ion drag force and the electric force in the plasma sheath of the lower electrode. Dust grain in plasma undergoes anomalous heating due to ion focusing, stochastic fluctuations and spatial variations of particle charge and ion streaming instabilities (Fortov, Ivlev, Khrapak, Khrapak, & Morfill, 2005). The thermal motion is damped by background gas by friction and when the electrostatic interaction energy of the dust grains exceeds their thermal energy, a strongly coupled state would be formed. When particles are close to each other, they interact through screened Coulomb potential or the Debye-Huckel (Yukawa) potential in the form of $V = Q_d \exp(-\Delta/\lambda_D) / \Delta$, where Q_d is the charge of dust grain, λ_D is the Debye screening length and Δ is the inter-particle distance.

2.2 Physical phenomena

2.2.1 Particle charging

Strong coupling of dust particles is one of the key features in dusty plasma systems. To understand the origin of strong coupling, it is important to comprehend the charging mechanism of dust particle first. The charging mechanism on an isolated dust grain is similar to a probe immersed in plasma. Fluxes of electrons and ions flow onto the grain surface determine the charging provided the electron emission processes are negligible. Since in low temperature rf plasma electrons have higher velocity, hence the dust grain will get negatively charged. The increasing negative charge of dust will repel electrons and attracts positive ions, until a balance between electron and ions fluxes Φ_e and Φ_i is reached (Goree, 1994). The variation of charge in an equilibrium state can be expressed as

$$\frac{dQ_d}{dt} = \Phi_e + \Phi_i = 0. \quad (2.1)$$

The electron and ions fluxes are calculated with the assumption of electrons and ions inside the grain potential follow orbital-type motion with Maxwellian energy distributions. This approach is termed Orbital Motion Limited (OML) theory. According to the OML theory, the first approximation of the fluxes can be written as (Allen, 1992)

$$\Phi_e = 4\pi r_d^2 n_e e \sqrt{\frac{k_B T_e}{2\pi m_e}} \exp\left(\frac{eV}{k_B T_e}\right) \quad (2.2)$$

$$\Phi_i = 4\pi r_d^2 n_i e \sqrt{\frac{k_B T_i}{2\pi m_i}} \left(1 - \frac{eV}{k_B T_i}\right) \quad (2.3)$$

where n_e and n_i are the electron and ion densities, T_e and T_i are the electron and ion temperatures, m_e and m_i are the electron and ion mass respectively, e is the elementary charge, k_B is the Boltzmann constant, V is the dust surface potential and r_d is the particle radius. By equating the particle fluxes $\Phi_e = -\Phi_i$, one gets

$$1 - \frac{eV}{k_B T_i} = \sqrt{\frac{m_i T_e}{m_e T_i}} \frac{n_e}{n_i} \exp\left(\frac{eV}{k_B T_e}\right) \quad (2.4)$$

and the grain potential V is then solved numerically (Goree, 1994). For a spherical dust particle with radius r_d , the grain charge is $Q_d = Z_d e = C_d V$, where Z_d is the number of charges on dust grain and $C_d = 4\pi\epsilon_0 r_d (1 + r_d/\lambda_D)$ is the capacitance of a spherical conductor (Fortov, Ivlev, Khrapak, Khrapak, & Morfill, 2005). By considering an isolated charged grain, which implies $\lambda_D \gg r_d$, one can obtain $Q_d = 4\pi\epsilon_0 r_d V$.

Orbital Motion Limited charging model is only applicable in the most idealized scenario. In real experimental condition, there are some other factors that need to be considered as well. For a certain type of grain potential, the potential barrier reflects

ions that are supposed to be collected according to the OML theory. This contributes to the reduction of ion current collected by the negatively charged dust grain (Fortov et al., 2005). The other factor that OML theory has neglected is the ion-neutral collision. Ion loses energy from the collision with neutral atom as it travels toward the dust grain. Because of that, these ions are more likely to be captured by the grain attraction, and that increases the ion fluxes into the dust grain (Lampe et al., 2003).

In the presence of many dust particles, consideration of an isolated dust grain is not a realistic assumption. In such condition, inter-particle distance can be smaller than Debye length, which means that the trajectories of ions and electrons flowing toward a dust grain will be affected by neighboring particles. The large number of dust grains will also deplete the plasma species and hence affecting the local plasma potential (Barkan, Dangelo, & Merlino, 1994). This causes a reduction of potential difference between local plasma and grain surface, thus grain potential becomes more positive (Goertz, 1989).

In rf experimental setup, dust particles are levitated in the plasma sheath region where the plasma is not isotropic, thus they do not follow the Maxwell-Boltzmann velocity distribution. In the sheath region with parabolic confinement potential, ions travel at Bohm velocity $v_B = (k_B T_e / m_i)^{1/2}$ and are further accelerated (Tomme, Law, Annaratone, & Allen, 2000). As the ion streaming velocity exceeds that of thermal velocity of ions, the charge of dust grain will rise.

It is worth mention here that the charge of a dust grain is not a constant parameter but a time-varying stochastic variable itself. However, the typical charging time of a dust grain is in the order of microsecond, faster than the time scale of macroscopic particle movement. Therefore, it is reasonable to assume the particle charge to be constant as it responds to new plasma conditions almost instantaneously.

2.2.2 Particle mechanics

In a plasma discharge, ions and electrons stream due to either the influence of electric field in plasma sheath or the ambipolar diffusion in plasma bulk. Having a relatively larger mass, ions flow causes dragging effect on a dust grain. The force exerted by the ion streams on dust particle comes in two forms, one is by ion scattering (Coulomb force) and another is by direct impact on the dust surface (collection force). Ion drag force is associated with the void formation (Goree, Morfill, Tsytovich, & Vladimirov, 1999), wave phenomena and it also influences the stability of the dust structure (Fortov et al., 2005). Figure 2.2 shows a void formation in dusty plasma where there is an absence of dust grains at the center of the dust cloud.

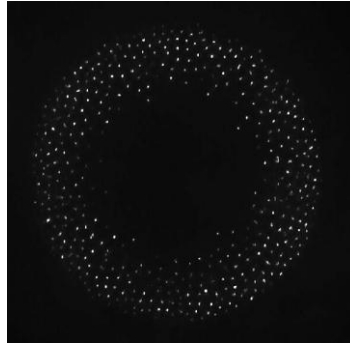


Figure 2.2 Void formation in polystyrene dust cloud.

Another type of important forces acting on a dust grain typically in ground based experiment is the gravitational force. For a dust grain with radius r_d , it experiences the gravitational force expressed as

$$F_g = m_d g = \frac{4}{3} \pi r_d^3 \rho_d g, \quad (2.5)$$

where g is the acceleration of gravity and ρ_d is the density of the grain material. Gravitational force is very dependent on the size of dust particle. It is significant for a micron-sized particle but less dominant for a nano-sized dust grain.

Electrostatic force plays an important role in dust particle confinement. The parabolic potential of confinement in the plasma sheath region exerted a horizontally inward and vertically upward directed electrostatic force on the dust grain. The electrostatic force balances the ion drag and gravitational force, consequently enables the dust grain to levitate above the confinement electrode. In uniform plasma, the electrostatic force is given by

$$F_e = Q_d E = -Q_d \nabla V, \quad (2.6)$$

where E denotes electric field.

Another significant force acting on dust grain is the neutral drag force which originates from the friction between neutral gas atoms and dust grains. Neutral gas atoms damp the dust grain, thereby lead to the dust cooling and contribute to the formation of ordered dusty plasma structures. Meanwhile, a streaming neutral gas will generate shear flows on the dust grains (Morfill & Ivlev, 2009). The neutral drag force is expressed as (Epstein, 1924)

$$F_{nd} = -\delta \frac{4}{3} \pi r_d^2 m_n n_n v_{Tn} (v_d - v_n), \quad (2.7)$$

in the limit of large Knudsen numbers $K_n = \lambda_n / r_d$ with λ_n as the mean free path for dust-neutral collisions, m_n , n_n , and v_{Tn} are the mass, number density, and thermal velocity of the neutrals, and $v_d - v_n$ is the relative velocity between dust component and neutrals. Parameter δ depends on the way neutral atoms are reflected by dust grain. For specular reflection (angle of incidence equals the angle of reflection), δ is equal to one.

Thermophoretic force originates from the temperature gradient presents in background gas in which the momentum transfers from the hotter to colder side. It is expressed by (Jellum, Daugherty, & Graves, 1991)

$$F_{Th} = -\frac{32}{15} \frac{r_d^2 \kappa_T}{v_{Tn}} \nabla T_n, \quad (2.8)$$

where κ_T and T_n are the thermal conductivity and the temperature of the gas. Thermophoretic has been manipulated to sustain micron-sized particle levitation and even forming three-dimensional dust structures (Arp, Block, Piel, & Melzer, 2004).

Dust grain also interacts with light that has high intensity such as a laser. There are two types of interactions between laser and dust grain. The first type is due to the radiation pressure of laser that pushes the dust grains along the beam direction (Ashkin, 1970). The magnitude of such force is expressed as

$$F_L = Y \frac{I_{laser}}{c} \pi r_d^2, \quad (2.9)$$

where I_{laser} is the laser intensity and Y is a coefficient describes the interaction of the photon with the grain surface ($Y=1$ for pure absorption and $Y=2$ for reflection). The second type of force is similar to thermophoretic force in which the laser heats the dust grain. When the dust grain is heated, neutral particles reflected on the hot side of the grain travel with higher velocity than on the cold side. Therefore, a net force is exerted on the particle along the beam direction.

So far, the external forces acting on the dust particle are briefly described; however, it is also important to mention the interactions between dust particles themselves. In isotropic plasma, dust particle shielded by the ambient plasma interacts with other dust particles through Debye-Huckel or Yukawa type potential

$$V(\Delta) = \frac{Q_d}{\Delta} \exp\left(-\frac{\Delta}{\lambda_D}\right), \quad (2.10)$$

where Δ is inter-particle distance and λ is Debye screening length. However, in an anisotropic plasma environment where a strong electric field is present and direct ion flow toward the electrode prevails, the geometry of grain potential is not symmetrical

anymore but showing an oscillating wake field with area of enhanced ion density downstream to the dust grain. It means that the shielding cloud around the dust grain is distorted downwards due to the ion streaming motion. Dust particles located lower in the sheath experience an attractive force by the upper layer particles, but the upper particles only experience a repulsive force from the lower. The manifestation of this effect is the vertical chain phenomena (see Figure 2.3) which is not a minimum energy configuration for purely repulsive particle interaction (Trottenberg, Melter, & Piel, 1995).



Figure 2.3 Vertical chains across several dusty plasma layers.

2.2.3 Collective behaviors

(a) Phases

Phase state of a system of particles interacting via the Yukawa potential is characterized by the coupling and screening parameter. Coupling parameter is defined as the ratio of the potential energy between two particles to the average thermal energy

$$\Gamma = \frac{Q_d^2}{4\pi\epsilon_0\Delta k_B T_d}, \quad (2.11)$$

where Δ is the average inter-particle distance. When the electrostatic interaction exceeded the thermal energy, i.e. $\Gamma > 1$, the system is said to be strongly coupled. The

screening parameter is defined as the ratio of inter-particle distance Δ and screening length λ_D

$$\kappa = \frac{\Delta}{\lambda_D}. \quad (2.12)$$

For a three-dimensional Yukawa system, the phase diagram in the Γ, κ plane has been found using numerical simulations as shown in Figure 2.4 (Hamaguchi, Farouki, & Dubin, 1997). The system exhibit body centered cubic and face centered cubic structures at strongly coupled solid phase. Meanwhile in weakly coupled system, fluid phase is observed. In dusty plasma experiment, hexagonal crystal structure of many layers is commonly found compared to other crystal structures.

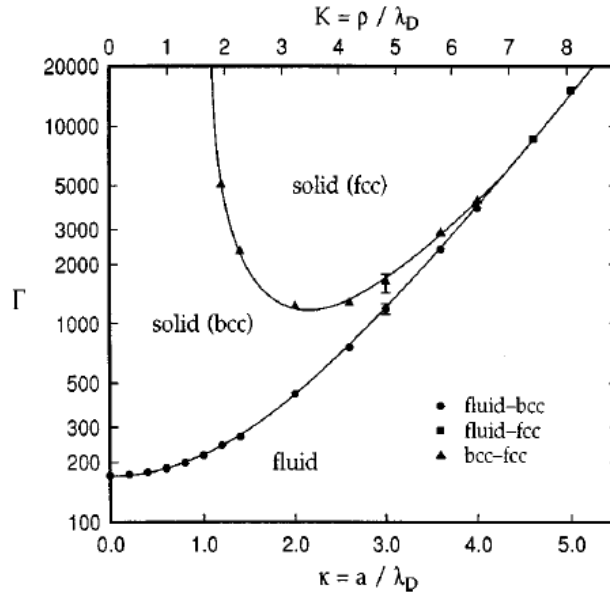


Figure 2.4 Phase diagram of Yukawa system in the (Γ, κ) plane, after (Hamaguchi et al., 1997).

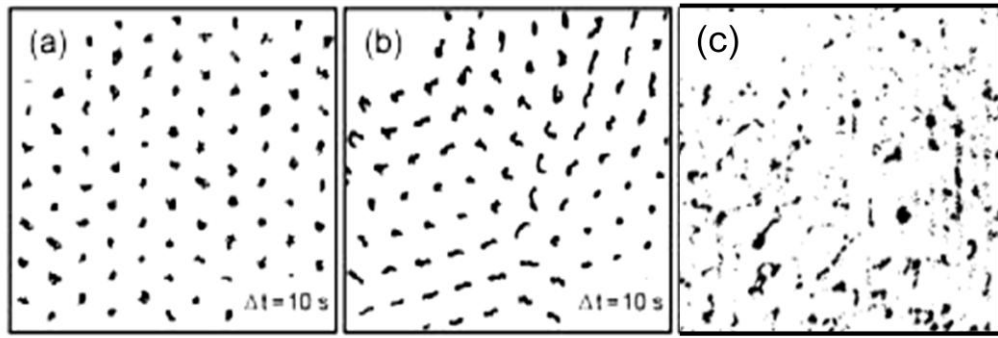


Figure 2.5 Dust particle trajectories at different structural states: (a) crystal, (b) melting, (c) disordered gas (Lai & I, 2002).

Figure 2.5 (a) shows the top view of a hexagonal dusty plasma crystal while the vertically particles are on top of each other due to ion wake effect. When heated, the crystal would be first melted into liquid state where particles oscillate and flow in the horizontal plane as depicted in Figure 2.5 (b). If the thermal energy of particles is further increased, particles move very fast in three-dimension and become disorder as shown in Figure 2.5 (c).

(b) Waves

Another collective behavior which can be observed in dusty plasmas is wave's excitation and propagation. Two types of wave which are commonly reported in dusty plasma experiments are the dust-acoustic wave (Rao, Shukla, & Yu, 1990) and dust lattice wave (Verheest, 2000). The dust-acoustic wave, driven by the electrons and ion pressure, travel with frequency lower than both ion and electron plasma frequency. On the other hand, dust lattice wave can be seen in crystal state and have different kind of modes that include compressional mode, shear mode or transverse mode depending on the particle motion relative to the wave motion (Verheest, 2000).

(c) Diffusion

Diffusion is one of the transport processes occurs in nature. It is used to describe the transfer of mass, momentum or heat in a physical system due to differences in concentration, energy or temperature. From an atomistic view point, diffusion is a result of random walk of diffusing particle. In 1827, Robert Brown observed random walk of small particles (pollen) in suspension in fluid and the phenomena was named Brownian motion.

Later in 1905, Einstein described the macroscopic transport in diffusive media using microscopic principles (Einstein, 2006). He assumed that in Brownian motion, each single particle motion is not influenced by the motion of other particles and its own motion at any previous time. With such assumption, Einstein found the Einstein relation, which stated that the mean of the squared displacement of a particle at a long time follows $\langle r_i^2(t) \rangle = \langle |r_i(t) - r_i(t_0)|^2 \rangle = 2Dt$, where $r_i(t)$ is the position of the i -th particle at time t and the angular bracket denotes ensemble average. Diffusion process that follows the Einstein relation is termed normal diffusion. However, there are diffusive processes in nature that do not obey the standard laws of diffusion. Such type of process is called anomalous diffusion as indicated by the nonlinear scaling of mean-square-displacement (MSD) by time, $\langle r^2 \rangle \propto t^\alpha$, where α is not equal to one. For $\alpha > 1$, the process is called superdiffusive and $\alpha < 1$ marks the subdiffusive behavior. Normal diffusion will have α equals to one while $\alpha = 2$ corresponds to ballistic motion and is described by the Newtonian kinematics equation.

Particle transport especially diffusion process in particularly, strongly coupled quasi-two dimensional dusty plasma state, is well-studied both experimentally and theoretically (Juan, Chen, & I, 2001; Juan & I, 1998; Lai & I, 2002; Ratynskaia, Knapek, Rypdal, Khrapak, & Morfill, 2005; Woon & I, 2004). These systems consist of several

layers of dust particles where the particles' motion are restricted horizontally, which is the reason why it is called quasi two-dimensional. In such system, it has been shown that anomalous diffusion occurs at a specific time scale and plasma environment. For example, subdiffusion is commonly observed at the small time scale in frozen dusty plasma state, where the dust particles in the lattice are bound due to the caging effect of neighbors (Juan & I, 1998; Nunomura, Samsonov, Zhdanov, & Morfill, 2006; R. Quinn & Goree, 2002). In melting and liquid state, Juan and I reported particles' correlated motion at small-time scale ($\text{MSD} < (0.2\Delta)^2$) (Juan & I, 1998).

On the other hand, superdiffusion is seen in melting state from short time scales up to 10-20s. The fast motion is related to the collective motion (vortex) and commence when the mean-square-displacement of a single particle exceeded $(0.2\Delta)^2$, where Δ is mean nearest particle separation (Juan & I, 1998). Besides that, cooperative fast particle cluster excitations (Lai & I, 2002) contribute to the superdiffusive motion as well. Ratynskaya et al. (Ratynskaia et al., 2005) have also reported superdiffusive particle transport at time scales in which the particle diffuses several inter-particle distances. The corresponded position increments were shown to be long-range dependent and follow Gaussian distribution, while the position distribution itself exhibited non-Gaussianity with exponential tails. Anomalous diffusion is thought to be a transient effect as at longer time scale, the process returns to normal diffusion. The transition occurs when the standard deviation of particle displacement approaches the mean inter-particle distance.

Along with experimental observations, extensive theoretical and simulation works have been conducted as well (Hou et al., 2009; Ott & Bonitz, 2009). The crucial factors that determine anomalous diffusion can be summarized as a function of background friction, coupling strength, and time of measurement (Ott & Bonitz, 2009). Among them, coupling shows great influence on the strength of superdiffusion.

Superdiffusion shows the strongest sign in medium coupling state where collective motions of particles contribute to the overall particles' motion. At higher coupling state, entrapment of particles in local minima hinders superdiffusion. At very low coupling state, particles' motion is dominated by binary collision. The lack of collective motion in such state results in non-superdiffusive behavior. On the other hand, by using simulation study, Ott et al. have shown that the anomalous-diffusion transition greatly depends on the type of particle confinement and also the formation of dust layers (Ott, Bonitz, Donkó, & Hartmann, 2008).

2.3 Diagnostic methods

There are various diagnostic techniques based on different physical principles used in dusty plasma research, such as probe measurement, emissive/absorptive spectroscopy, laser light scattering etc. Among them, laser light scattering is the most common technique due to its non-intrusive nature. There are four types of laser light scattering diagnostic (Garscadden, Ganguly, Haaland, & Williams, 1994): (1) visualization technique, in which the dusts are detected from its Mie scattering using broad area beam, (2) scattering depolarization using a polarized laser beam, (3) angular dependence of scattered light intensity, and (4) dynamic light scattering technique that measure temporal fluctuation of scattered light intensity. These optical diagnostic techniques are only valid for dust particles whose size is comparable with the incident wavelength range. In this work, direct visualization and dynamic light scattering techniques are used. In the following subsection, fundamental concepts of the used diagnostic technique are presented. Experimental details of the techniques are presented in the next chapter.

2.3.1 Dynamic light scattering

The basic geometry of a light scattering setup is shown in Figure 2.6. A coherent polarized light source enters a scattering medium is scattered in all directions.

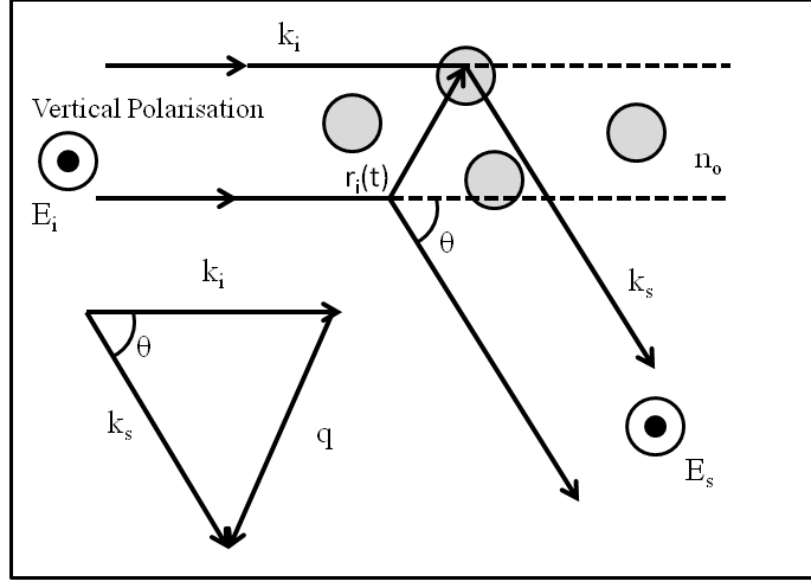


Figure 2.6 light scattering diagram.

The incident light is represented by its electric field component in the form of monochromatic plane wave,

$$E_i(r, t) = \hat{n}E_0 \exp(i(k_i \cdot r - \omega_0 t)) \quad (2.13)$$

where \hat{n} is the polarization vector of the electric field, E_0 is the amplitude of the field, ω_0 is the angular frequency and k_i is the incident wavevector with magnitude $|k_i| \equiv \frac{2\pi n_o}{\lambda}$ pointing at direction of wave propagation. By getting the difference between the incident and the scattered light wavevector, the scattering wavevector, $|q| \equiv |k_i - k_s|$ is obtained. In the case of quasi-elastic light scattering where little energy of incident light is absorbed or lost, one can use conservation of momentum and the law of cosines to find the magnitude of scattering wavevector which will be written as, $\frac{4\pi n_o}{\lambda} \sin(\frac{\theta}{2})$.

Now assume there are N scatterers with identical size and geometry, the instantaneous scattered field detected at an angle of θ from direction of transmitted light beam is equal to the sum of the individual field strength of i -th particle with position $r_i(t)$, field strength E_i and phase factor of $\exp[iq \cdot r_i(t)]$. Neglecting the scattering of fluid medium, the instantaneous scattered field is

$$E(t) = \sum_{i=1}^N E_i \exp(iq \cdot r_i(t)) \quad (2.14)$$

Considering that the field is a function of particles' position, it indicates particles' movement in the scattering volume will alter the phase of the scattered wave. Therefore, a time varying random interference pattern is detected and resulted in a random fluctuation of scattered light intensity. To characterize the fluctuation's behavior, it's useful to measure the similarity of the fluctuation at different times. This can be done by calculating the correlation function of the fluctuation with itself, which is also called auto-correlation.

Let $I(t)$ be the scattered light intensity measured at scattering angle θ at instantaneous time t . The intensity auto-correlation function with lag time τ is calculated taking the product of $I(t)$ and $I(t + \tau)$ and then average it over many such products that is

$$C_I(\tau) \equiv \langle I(t)I(t + \tau) \rangle = \lim_{T \rightarrow \infty} \frac{1}{T} \int_0^T I(t)I(t + \tau) dt. \quad (2.15)$$

$C_I(\tau)$ is independent of the starting time t and depends only on the lag time τ , given that $I(t)$ is stationary.

In discrete case, auto-correlation function is expressed as a function of lag time $\tau = j\Delta t$, that is

$$C_I(\tau) = \langle I(i)I(i+j) \rangle = \lim_{N \rightarrow \infty} \frac{1}{N-j} \sum_{i=1}^N I_i I_{i+j} \quad (2.16)$$

where j is a positive integer, and Δt is the time interval determined from the sampling time. The auto-correlation of a time series I with length N is obtained by averaging all products $I_i I_{i+j}$ from $I_1 I_{1+j}$ to $I_{N-j} I_N$. In data analysis, the intensity fluctuation is commonly demean and normalized by its own standard deviation so that the auto-correlation function decay from one to zero.

The scattered-field time auto-correlation function $C_E(t) \equiv \langle E(t)E(t+\tau) \rangle$ is related to the intensity auto-correlation function via the relation (Hurd & Ho, 1989)

$$C_I(t) \equiv I_0^2 + \chi [C_E(t)]^2, \quad (2.17)$$

where I_0 is a constant background and χ is a detector dependent constant. Using equation (2.14), the auto-correlation function of scattered field can be expressed as

$$\langle E(t)E(t+\tau) \rangle \sim \left\langle \sum_{i=1}^N (E_i)^2 \exp(iq \cdot [r_i(t) - r_i(t+\tau)]) \right\rangle. \quad (2.18)$$

Assume all the scatterers are statistically independent and identical, the resulting sum over i is $\langle N \rangle$ times the ensemble average of the phase factor difference for a single particle

$$\langle E(t)E(t+\tau) \rangle \sim \langle N \rangle (E_i)^2 \langle \exp(iq \cdot [r_i(t) - r_i(t+\tau)]) \rangle. \quad (2.19)$$

From that it can be seen that the field correlation function depends on three factors: (1) the mean number of scatterers in the scattering volume, (2) the amplitude of scattered field by each particle, E_i (which depend on the polarizability of the scatterer), and (3)

the positions of the particles. The ensemble average of the exponential term represents the integral of $\exp(iq \cdot \Delta r)$ over the conditional probability distribution $P(\Delta r, \tau | 0, 0)$

$$\begin{aligned} \langle \exp(iq \cdot [r_i(t) - r_i(t + \tau)]) \rangle &= \langle \exp(iq \cdot \Delta r) \rangle \\ &= \int_{-\infty}^{\infty} P(\Delta r, \tau | 0, 0) \exp(iq \cdot \Delta r) d^3 \Delta r. \end{aligned} \quad (2.20)$$

The conditional probability distribution describe the probability of a particle located at position r at time zero will be found at position $r + \Delta r$ at time τ later.

(a) Diffusive correlation model

For a Brownian particle undergoing random walk, the conditional probability distribution is a Gaussian function (Wang & Uhlenbeck, 1945)

$$P(r, t) = 4\pi Dt^{-\frac{3}{2}} \exp\left(-\frac{r^2}{4Dt}\right), \quad (2.21)$$

with diffusion coefficient, D . On substituting equation (2.21) into equation (2.19), the field auto-correlation function of scatterers undergo diffusive transport is obtained,

$$\langle E(t)E(t + \tau) \rangle \sim \langle N \rangle \langle E_i \rangle^2 \exp(-t/\tau_D). \quad (2.22)$$

The characteristic time, $\tau_D \sim (q^2 D)^{-1}$, denotes the time elapsed for any superposition of the phase changes into a new uncorrelated phase.

(b) Ballistic correlation model

For a particle undergoing ballistic motion, the mean free path Δr is proportional to $v_p \tau$, where v_p is the mean velocity of particle. In this case the field correlation function can be calculated using Maxwell-Boltzmann velocity distribution $P(v_p) = [m/2\pi k_B T]^{3/2} \exp[-mv_p^2/2k_B T]$ which will yield a Gaussian function (Chandrasekhar, 1943)

$$\begin{aligned} \langle E(t)E(t + \tau) \rangle &= (E_i)^2 \left\langle \sum_{i=1}^N \exp(iq \cdot \Delta r) \right\rangle = E_i^2 \langle \exp(iq \cdot v_p t) \rangle \quad (2.23) \\ &= E_i^2 \int_0^\infty P(v_p) \exp(iq \cdot v_p t) dv_p \\ &= E_i^2 \exp\left(-\left(\frac{1}{2}\right)q^2 \langle v_p^2 \rangle t^2\right) \sim \exp(-t^2/(2\tau_B^2)) \quad , \end{aligned}$$

where $\langle v_p^2 \rangle = k_B T/m$ is the mean square value of the velocity component along q , and $\tau_B = [q \langle v_p^2 \rangle^{1/2}]^{-1}$ is the characteristic time.

(c) Ballistic-diffusive correlation model

In the work of (Hurd & Ho, 1989), correlation function with crossover between kinetic and hydrodynamic behavior is obtained using standard Langevin equation for the motion of a particle in the presence of friction force $\xi \vec{u}$ and rapidly fluctuating force $\vec{\eta}(t)$

$$\dot{\vec{v}} + \xi \vec{v} = \vec{\eta}(t), \quad (2.24)$$

where \vec{v} is the velocity field. To solve the stochastic differential equation, Chandrasekhar (Chandrasekhar, 1943) first derived the probability $P(r, t | r_0, v_0)$ that a

particle is at position r at time t given an initial position r_0 and velocity v_0 to be in the form of

$$P(r, t | r_0, v_0) = P_0 \exp(-R^2/R_0^2) \quad (2.25)$$

where

$$R_0^2 = \frac{2k_B T}{m\xi^2} [2\xi t - 3 + 4 \exp(-\xi t) - \exp(-2\xi t)], \quad (2.26)$$

$$P_0 = \pi^{-3/2} R_0^{-3}, \text{ and } R = r - r_0 - f v_0$$

with $f = [1 - \exp(-\xi t)]/\xi$. Considering r_0 and v_0 to be a constant, the phase factor $\langle \exp[iq \cdot \Delta r] \rangle$ averaged over $P(r)$ is just $\exp(iq \cdot f v_0) \exp(-q^2 R_0^2/4)$ independent of r_0 . Assuming Maxwellian velocity distribution, the field correlation function with kinetic-hydrodynamic crossover is

$$C_E^{BD} \sim \exp \left(-q^2 \langle v_d^2 \rangle \xi^{-2} \varphi(\xi t) \right) \quad (2.27)$$

where $\varphi(x) = -1 + x + \exp[-x]$. One can easily note that $\varphi(x) \sim x$ for $x \gg 1$, and $\varphi(x) \sim x^2$ for $x \ll 1$. Hence, the correlation $C_E^{BD}(t)$ converges to $C_E^B(t)$ (ballistic) and $C_E^D(t)$ (diffusive) for time shorter and longer compared to persistence time β^{-1} , respectively. The mean-square-displacement $\langle \Delta r^2 \rangle$ can be obtained by averaging $|r - r_0|^2$ over $P(r)$, and is equal to $\langle v_d^2 \rangle t^2$ for $t \ll 1$ and $6Dt$ for $t \gg 1$ (Chandrasekhar, 1943).

(d) Polydispersity

The above mentioned correlation model assumes that the particles follow a uniform mass distribution and thus is not valid for particle with different sizes. By considering poly-disperse particle size, Hurd and Ho (Hurd & Ho, 1989) explored a model with

particles having mass distribution of mixed power-law and exponential distribution, $N(m) \sim m^{-\sigma} \exp[-m/m_0]$ where m_0 is the cutoff mass and σ is a scaling exponent. They have shown that the electric field correlation function in the kinetic limit is given by

$$C_E(t) \sim 2^{\sigma-2} \left(\frac{t}{t_0}\right)^{3-\sigma} K_{3-\sigma}\left(\frac{t}{t_0}\right), \quad (2.28)$$

where $K_v(z)$ is the v -th order modified Bessel function of second kind and $t_0 = m_0/q^2 k_B T$.

The correlation function which encompass both kinetic and hydrodynamical transport mechanisms for poly-disperse dust can be derived as

$$\begin{aligned} C_E^{BD*}(t) &= E_o'^2 \int_0^\infty m^{2-\sigma} \exp\left(-\frac{m}{m_o}\right) \exp\left(-\left(\frac{q^2}{2}\right)\left(\frac{k_B T}{2m}\right)(-1 + \xi t \right. \\ &\quad \left. + \exp(-\xi t))\xi^{-2}\right) dm, \\ &= 2^{\sigma-2} \{m_o^2 q^2 k_B T \exp(-\xi t) [1 + \exp(\xi t)(\xi t - 1)]\}^{(3-\sigma)/2} \\ &\quad \times K_{3-\sigma}(\{m_o^2 q^2 k_B T \exp(-\xi t) [1 + \exp(\xi t)(\xi t - 1)]\}^{1/2}). \end{aligned} \quad (2.29)$$

It can easily be shown that equation (2.29) reduces to the purely kinetic case in equation (2.23) when $t \ll 1$.

(e) Dynamic light scattering studies in dusty plasma

Hurd and Ho (Hurd & Ho, 1989) have studied Brownian particles of polydisperse size in rarefied environment of a glow discharge system using DLS. Using correlation analysis, they have tried different dynamical models that include the mono-disperse fully kinetic model, poly-disperse fully kinetic model and mono-disperse with kinetic-hydrodynamical model. The particles in the system are shown to be in kinetic-hydrodynamic cross over regime. Despite that, the mono-disperse model fits the data equally well which may be due to the striation of dusty plasma. DLS is also used by

Anderson and Radovanov (Anderson & Radovanov, 1995) to study nano-scaled particle generation and they have observed oscillation of 120-130 Hz in the auto-correlation function during liquid to crystal phase transition. The cause of that is speculated to be originated from the charge-density-wave motion (Hansen, Levesque, & Weis, 1979).

2.3.2 Visualization and particle tracking

Apart from the DLS method, another more direct diagnostic method used in dusty plasma system is the direct visualization of dust grains through the help of laser illumination. Typically, a flat laser sheet (of thickness of 100-300 μm) in visible wavelength generated using a cylindrical lens is used to illuminate the dust particles' ensemble. The scattered light by dust grains is then recorded using a CCD video camera. To get more accurate results, high-spatial-resolution lens and high-frame-rate camera is normally used. The recorded image sequences are then processed in order to obtain individual particles' position. From the particles coordinates for consecutive time, one can track the particles and obtain the trajectories provided the particles remained in the illuminated laser sheet throughout the video recording. Starting from the particle coordinates, tracking algorithm will search for the most probable particle location in the consecutive image frame based on the closest inter-particle distance. In the end, a time series of particles' trajectories in two-dimension are obtained.

Once the particle trajectory is determined, the velocity of each particle can be calculated. From the distribution function of velocity, kinetic temperature of dust particle can be determined using the equipartition theorem. To measure the average distance traveled by a randomly moving particle, the mean-square-displacement (MSD) generally defined as $\sigma^2(t) = \langle |r_i(t) - r_i(0)|^2 \rangle$ is used. Here, $r_i(t)-r_i(0)$ is the distance

travelled by particle i over some time interval of length t , and the square of that distance is averaged over many such time intervals or over all particles in the system.

2.3.3 Spatial correlation function

From the visualization technique, the two-dimensional image provides useful information regarding the spatial arrangement or orderliness of different dusty plasma states. One simple way to measure the degree of spatial orderliness is by using the Voronoi diagram. In two dimensions, Voronoi diagram is constructed by dividing any single plane of dust particles into a series of cells, of which the boundary is equidistance from two or more particles (Smith et al., 2004). From the Voronoi diagram, the average number of neighbors a cell has can serve as an indication of the overall orderliness in the system. For example, in a perfect hexagonal lattice, each hexagonal cell has six nearest neighbors.

For a more quantitative analysis of orderliness in dusty plasma system, three commonly used methods are the pair correlation function, the bond-orientational correlation function and the structure factor (Quinn, Cui, Goree, Pieper, Thomas, & Morfill, 1996). The pair correlation function $g(r)$ measures the translational order of the particle ensemble and its value represents the probability of finding two particles that are separated by a distance r .

While $g(r)$ is good in differentiating particle arrangement with different degree of orderliness, it performs poorly in determining different types of crystalline structures. For measuring orientational order like in crystal lattice, bond-orientational correlation function $g_6(r)$ is preferred. It is defined as $g_6(r) = \langle \exp((6i[\theta(r) - \theta(0)]) \rangle$ where θ is the nearest-neighbor bond angles and the average is taken over the entire particle

ensemble. For a perfect crystal at zero temperature, $g_6(r)$ is equal to unity while for other phases, it decays with increasing r . Another orderliness measure is the structure factor, usually obtained by light scattering experiment. Structure factor is the Fourier transform of the pair correlation function $S(k) = 1 + n_d \int dr [g(r) - 1] \exp(-ikr)$, where k is the scattering wave vector.

2.4 Stochastic models

One of the main purposes of this work is to model the particle dynamic including the anomalous diffusion process and DLS fluctuation signal using fractional stochastic process. Before introducing the fractional model, a brief description of stochastic process is given here. A stochastic process is a family of random variables $\{X(t)|t \in T\}$ defined on a given probability space, indexed by the time variable t , where t varies over an index set T (Trivedi, 1982). In the probability theory, diffusion process is considered to be a stochastic process because of its random nature. If all finite collections of a random process are jointly Gaussian random variable, it's called a Gaussian process. A Gaussian random process can be described by its statistical properties such as mean, correlation, variance, etc. If the mean and variance of a process is a constant throughout the entire process, the process is termed stationary. In a more accurate definition, stationarity requires all moments to remain constant. In other words, the distribution density of the values does not change with time.

Elements of a random process can be uncorrelated or correlated to each other. For example, the increments of Brownian motion (a White noise) are completely uncorrelated to each other (the present value is not influenced by the past values). To measure the statistical dependence of a stationary stochastic process $X(t)$, auto-covariance function $C(s) = E[X(t)X(t+s)]$ is normally used. By dividing the auto-

covariance by the variance $\langle X(t)^2 \rangle$, one get the auto-correlation function. Both quantities are identical if the data are demeaned and normalized by unit variance. For an uncorrelated process $X(t)$ such as white noise where every elements are independent of each other, $C(s)$ is equals to zero for $s > 0$. For short-range correlated process, $C(s)$ declines exponentially $C(s) \sim \exp(-s/d)$ with a characteristic decay time d . While for long-range correlated process, $C(s)$ decays slower and typically showing a power law behavior. Besides auto-correlation, there is another independent way to determine the correlation of a stochastic process that is by spectral analysis. The power spectrum $S(f)$ of a stationary process is related to the correlation function by Fourier Transform (Wiener-Kinchin theorem). The flat power spectrum indicates uncorrelated or short-range correlated process. In contrast, long-range correlated process is characterized by the power-law like spectrum $S(f) \sim f^{-\beta}$ where $0 < \beta < 2$. $S(f)$ with $\beta=0$ corresponds to white noise, $\beta=1$ corresponds to $1/f$ noise and $\beta=2$ indicates Wiener process, which is the integration of white noise. Note that for a long-range correlated process, correlation function and power spectrum both have power law type relation with the scale parameter (time scale and frequency). This type of scaling law is the main feature of fractal process, a process that is self-similar (magnification of a small part is statistically equivalent to the whole).

One subclass of stochastic processes that does not have any memory present is the Markov process. Its joint density function only depends on the most recent condition, for example, given the current state $X(t') = x'$, any knowledge of any values of the process earlier than t' does not enhance the prediction of $X(t)$ for any $t > t'$.

2.4.1 Fractional calculus

One characteristic of the stochastic process is its non-differentiability property; therefore it requires some special branch of calculus to formulate the differential equation describing the process. In this work, the stochastic model is formulated using the frame work of fractional differential equation which is a generalization of differential equation.

Fractional calculus is first addressed in 1695 when L'Hopital wrote to Leibniz asking him about a particular notation he had used in his publications for the n th-derivative of the linear function $f(x) = x$, $\frac{D^n x}{Dx^n}$ (Ross, 1977). The question posed by L'Hopital is what would be the result if the order of derivative is a fraction, for example $n=1/2$. The response from Leibniz's was: "An apparent paradox, from which one day useful consequences will be drawn." This is true as in the second half of twentieth century, fractional calculus has found its way in engineering and scientific application. Such application involves study of viscoelasticity (Bagley & Torvik, 1986), signal processing (Sabatier, Agrawal, & Machado, 2007), fluid mechanics (Kulish & Lage, 2002), bioengineering (Magin, 2004) and anomalous diffusion phenomena (Metzler & Klafter, 2000). After the first inquisition by L'Hopital and Leibniz, fractional calculus is further explored by Fourier, Euler, and Laplace (Podlubny, 1999b). Nowadays, the most popularized definitions of fractional calculus are the Riemann-Liouville and Grunwald-Letnikov definition. In this work, the Riemann-Liouville formalism is used to develop the stochastic model.

In fractional derivative, an n th time derivative is equivalent to the inverse operation of n -fold repeated integration

$$\int_{t_0}^t \int_{t_0}^{s_1} \cdots \int_{t_0}^{s_{n-1}} f(s_n) ds_n \cdots ds_1 = \frac{1}{(n-1)!} \int_{t_0}^t (t-s)^{n-1} f(s) ds. \quad (2.30)$$

By induction, fractional integral of arbitrary order $\alpha > 0$ of a function $f(t)$ is defined (Miller & Ross, 1993; Samko, Kilbas, & Marichev, 1993) as

$${}_{t_0}I_t^\alpha f(t) = \frac{1}{\Gamma(\alpha)} \int_{t_0}^t (t-s)^{\alpha-1} f(s) ds, \quad (2.31)$$

where $\Gamma()$ is the Gamma function. Generally, fractional derivative has the form of

$${}_{t_0}D_t^\alpha f(t) = \frac{1}{\Gamma(n-\alpha)} \left(\frac{d}{dt} \right)^n \int_{t_0}^t (t-s)^{n-\alpha-1} f(s) ds, \quad n-1 \leq \alpha < n. \quad (2.32)$$

If the lower limit of the integral is $-\infty$ $D_t^\alpha f(t)$, it's known as Weyl's fractional derivative and ${}_0D_t^\alpha f(t)$ is known as Riemann-Liouville fractional derivative (Miller & Ross, 1993; Samko et al., 1993). The shifted fractional derivative denoted by $({}_{t_0}D_t^\alpha + a)^\beta$ with real parameter $a > 0$ can be expressed in infinite series using binomial expression (Lim, Li, & Teo, 2008)

$$({}_{t_0}D_t^\alpha + a)^\beta f(t) = \sum_{j=0}^{\infty} \binom{\beta}{j} a^j {}_{t_0}D_t^{\alpha(\beta-j)} f(t), \quad (2.33)$$

$$n-1 \leq \alpha < n; \quad \beta > 0.$$

In this work, α is set to one, thus the fractional dynamics is characterized by the fractional index $\beta > 0$ which is connected to the fractional derivative through binomial expansion.

2.4.2 Ornstein-Uhlenbeck and fractional Ornstein-Uhlenbeck process

One of the stochastic processes used to model Brownian motion of a free particle in a fluid is the Ornstein-Uhlenbeck process, $X_{OU}(t)$ (Uhlenbeck & Ornstein, 1930). $X_{OU}(t)$

can be defined as a stationary solution of the Langevin equation (Coffey, Kalmykov, & Waldron, 2004; Uhlenbeck & Ornstein, 1930)

$$(-_{\infty}D_t^1 + a)X_{OU}(t) = \eta(t), \quad (2.34)$$

where η is the standard Gaussian white noise with zero mean and delta function as correlation function, i.e., $\langle \eta(t)\eta(s) \rangle = \delta(t - s)$ and $a > 0$ is a coefficient. The stationary solution can be written as

$$X_{OU}(t) = \int_{-\infty}^t \exp(-a(t - u))\eta(u)du, \quad (2.35)$$

with correlation function given by $C(\tau) = \langle X_{OU}(t)X_{OU}(t + \tau) \rangle = \exp(-\frac{a|\tau|}{2})$. It follows from this second-order property that the Ornstein-Uhlenbeck process is a Markovian process with short-range memory. Its spectral density takes the Lorentzian form, $S_{OU}(\omega) = (a^2 + \omega^2)^{-2}$.

One can generalize the ordinary Langevin equation using the fractional calculus as shown below (Lim & Muniandy, 2003),

$$(-_{\infty}D_t^1 + a)^{\beta}X_{\beta}(t) = \eta(t), \quad (2.36)$$

where β is the positive fractional index. The so-called nonstandard ‘fractional Langevin equation’ can be solved using the Green’s function technique. First, let $g_{\beta}(t)$ be the impulse response function

$$g(t) = \begin{cases} \frac{t^{H-1/2}}{\Gamma(H + 1/2)} & \text{for } t \geq 0 \\ 0 & \text{for } t < 0. \end{cases} \quad (2.37)$$

Hence we can write

$$({}_{-\infty}D_t^1 + a)^\beta g_\beta(t) = \delta(t). \quad (2.38)$$

By applying Fourier transform on both sides of equation (2.38), and noting the property of Fourier transform of fractional derivative (Podlubny, 1999a), namely, $\mathbf{F}[{}_{-\infty}D_t^\alpha g_\beta(t)] = (-i\omega)^\alpha \tilde{G}_\beta(\omega)$ and the corresponding shift theorem, we obtain (Li & Scalia, 2010; Lim & Muniandy, 2003)

$$\tilde{G}_\beta(\omega) = \mathbf{F}[g_\beta(t)] = \frac{1}{(a - i\omega)^\beta} \quad (2.39)$$

where $\mathbf{F}[\cdot]$ denotes the Fourier transform and $\mathbf{F}[\delta(t)] = 1$. Taking the inverse Fourier transform of equation (2.37), will give the response function for the fractional Ornstein-Uhlenbeck process $X_\beta(t)$,

$$g_\beta(t) = \begin{cases} \frac{t^{\beta-1} e^{-at}}{\Gamma(\beta)} & \text{for } t \geq 0 \\ 0 & \text{for } t < 0, \end{cases} \quad (2.40)$$

where $X_\beta(t) = g_\beta(t) * \eta(t)$. Lim et al (Lim et al., 2008) have shown that the solution of equation (2.36) permits a Fourier spectral representation for $\beta > 1/2$. Note that when $\beta = 1$, $X_\beta(t)$ reduces to the standard Ornstein-Uhlenbeck process, $X_{OU}(t)$. The solution of equation (2.36) can be written explicitly as

$$X_\beta(t) = c(a, \beta) \int_{-\infty}^t g_\beta(t - u) \eta(u) du, \quad (2.41)$$

with $c(a, \beta)$ as an arbitrary constant which can be determined by choosing $\beta = 1$. The correlation function of $X_\beta(t)$ is calculated as

$$\begin{aligned}
C_\beta(\tau) &= \langle X_\beta(t)X_\beta(t+\tau) \rangle \\
&= c'(a, \beta) \int_{-\infty}^t \int_{-\infty}^{t+\tau} g_\beta(t-u) g_\beta(t+\tau-v) \langle \eta(u)\eta(v) \rangle dudv, \\
&= \frac{a^{-2\nu}}{2^\nu \sqrt{\pi} \Gamma\left(\nu + \frac{1}{2}\right)} |a\tau|^\nu K_\nu(|a\tau|),
\end{aligned} \tag{2.42}$$

with $\nu = \beta - 1/2$ and K_ν is the modified Bessel function of the second kind (Erdelyi, Magnus, Oberhettinger, & Tricomi, 1995). It is interesting to note that the correlation function of fOU process shares the same form with the correlation function based on polydisperse mass distribution with kinetic transport as shown in equation (2.28).

The power-spectral density of $X_\beta(t)$ is given by $S_{X_\beta}(\omega) = |\tilde{G}_\beta(\omega)|^2 \sim (a^2 + \omega^2)^{-\beta}$. Moreover, the increments of fOU process satisfy the locally self-similarity property, namely, $\langle [X_\beta(t+\tau) - X_\beta(t)]^2 \rangle \sim |a\tau|^{2\nu}$. It is interesting to note that based on this local self-similarity property and the power-spectral density at high frequency limit (i.e., $\omega \gg a$), the fractional Ornstein-Uhlenbeck process and its increments converge to the well-known Hurst, $H (= \nu)$ -indexed fractional Brownian motion and fractional Gaussian noise, respectively (Lim & Sithi, 1995; Mandelbrot & Van Ness, 1968). Both fractional Brownian motion and fractional Gaussian noise will be discussed shortly in the next section. By having a second-order stationary property, fOU process is able to support memory. In fact, fOU process can be shown to be a non-Markovian process simply by verifying that $C_{X_\beta}(t_3 - t_1) \neq C_{X_\beta}(t_2 - t_1) \times C_{X_\beta}(t_3 - t_2)$, $t_1 < t_2 < t_3$ with short-memory, namely C_{X_β} decays slower than the standard exponential form of OU process.

2.4.3 Fractional Brownian motion

Standard diffusion theory is based on the finite value of velocity auto-correlation function, $\int_0^\infty \langle v(t)v(0) \rangle dt < \infty$. However, this excludes an important class of processes called fractional Gaussian noises, which leads to particle trajectories classified as fractional Brownian motion (Beran, 1994; Mandelbrot & Van Ness, 1968). A feature of this process is that the mean-square-displacement scales power law to time, $\propto t^{2H}$, where H is called Hurst exponent (Mandelbrot & Van Ness, 1968). The Hurst exponent represents the type of the diffusion, for example $H=1/2$ is normal diffusion, $H=1$ is ballistic transport, $H<1/2$ is subdiffusive, and $H>1/2$ is superdiffusive (Barkan et al., 1994; Beran, 1994). Standard diffusion theory fails when the velocity probability distribution function is non-Gaussian but has algebraic tails and diverging variance $\langle v(t)^2 \rangle$ (Lutz, 2001a, 2001b; Paul & Baschnagel, 1999). On the other hand, a Markovian velocity process is superdiffusive when very large velocities (Levy flight) are present.

Fractional Brownian motion (FBM) can be regarded as a natural generalization of Brownian motion from the perspective of the Langevin equation. Langevin equation with the following form

$$\frac{dX(t)}{dt} = F(X(t), t) + \eta(t) \quad (2.43)$$

has Brownian motion as the solution,

$$X(t) = \int_0^t \eta(\tau) d\tau, \quad (2.44)$$

provided that the external force is absent which means $[F(X,t)=0]$. Consider the fractional Langevin equation for a free particle,

$$\frac{d^\beta X(t)}{dt^\beta} = \eta(t), \quad (2.45)$$

where the fractional derivative can be defined in terms of the fractional integral ${}_a I_t^\beta$ (Samko, Kilbas, & Marichev, 1993),

$${}_a I_t^\beta f(t) = \frac{1}{\Gamma(\beta)} \int_a^t (t-u)^{\beta-1} f(u) du \quad \text{for } \beta > 0. \quad (2.46)$$

For $\gamma = -\beta > 0$, the fractional derivative ${}_a D_t^\gamma$ is defined as a fractional integral of order $n - \gamma$ (with $n - 1 < \gamma < n$) and an ordinary derivative of order n :

$${}_a D_t^\gamma f(t) = \left(\frac{d}{dt} \right)^n {}_a D_t^{\gamma-n} f(t) \quad (2.47)$$

For $a=0$, (2.46) and (2.47) are known, respectively, as the fractional integral and the fractional derivative of the Riemann-Liouville type; when $a=-\infty$, they are known as the Weyl type. FBM defined by the Weyl fractional integral alone is divergent and can be regarded as the sum of two independent Gaussian process: a process that represents a history of infinite past and a part that begins at time $t=0$ with no memory of the past. The second part can be defined using Riemann-Liouville type fractional derivative and inverting equation (2.45), we will obtain the Riemann-Liouville type fractional Brownian motion (RL-FBM) (Barnes & Allan, 1966):

$$X_H(t) = \frac{1}{\Gamma\left(H + \frac{1}{2}\right)} \int_0^t (t-\tau)^{H-\frac{1}{2}} \eta(\tau) d\tau \quad (2.48)$$

RL-FBM is a self-similar Gaussian process with zero starting point, zero mean, and a rather complicated correlation function that is

$$R(t, s) = \frac{t^{H+\frac{1}{2}} s^{H-\frac{1}{2}}}{\left(H + \frac{1}{2}\right) \Gamma\left(H + \frac{1}{2}\right)^2} {}_2F_1\left(\frac{1}{2} - H, 1, H + \frac{1}{2}, \frac{t}{s}\right) \quad (2.49)$$

where $s > t$ and ${}_2F_1$ denotes the Gauss hypergeometric function. The variance is given by $\sigma^2 = Ct^{2H}$ where $C = (2H\Gamma(H+1/2)^2)^{-1}$. This important feature allows RL-FBM to model anomalous diffusion process. However, due to the fact that the process starts from the origin, RL-FBM does not have stationary increments for transient time. However, at large time limit, this desired property is recovered, and hence one can still define the power-law type power spectral density. On the other hand, RL-FBM does not satisfy the Markov property.

Chapter 3

Experiments

In order to investigate the particle dynamic in dusty plasma system, a capacitively coupled radio frequency plasma system with dust dispenser and dust confinement is setup. Two types of optical diagnostic system: 1) dynamic light scattering (DLS) and 2) particle visualization technique (using video CCD camera) are installed after the plasma system is established. Signal acquired from DLS experiment is processed using Matlab before the correlation analysis. Similarly, image sequences captured by CCD camera are processed and enhanced before pair correlation and particle tracking analysis are performed.

3.1 Capacitively coupled radio frequency plasma system

(a) Plasma chamber

The dusty plasma experiment is carried out in a ready build capacitively coupled radio-frequency gas discharge system as shown in Figure 3.1 and Figure 3.2. The chamber [1] is a cylindrical stainless steel vacuum chamber (inner diameter=355 mm, inner height =153 mm) with six ports installed on the wall each separated by 60 degrees apart as shown in Figure 3.3. Three of the ports are mounted with quartz window, another two with electrical feed-through and one connected to the pumping arm. A brass plate [2] with a circular opening at the center is used as the top cover. The circular opening is sealed with a Perspex glass [3] and allows a top view of the chamber. Inside the chamber, a pair of circular brass plates is used as electrodes.

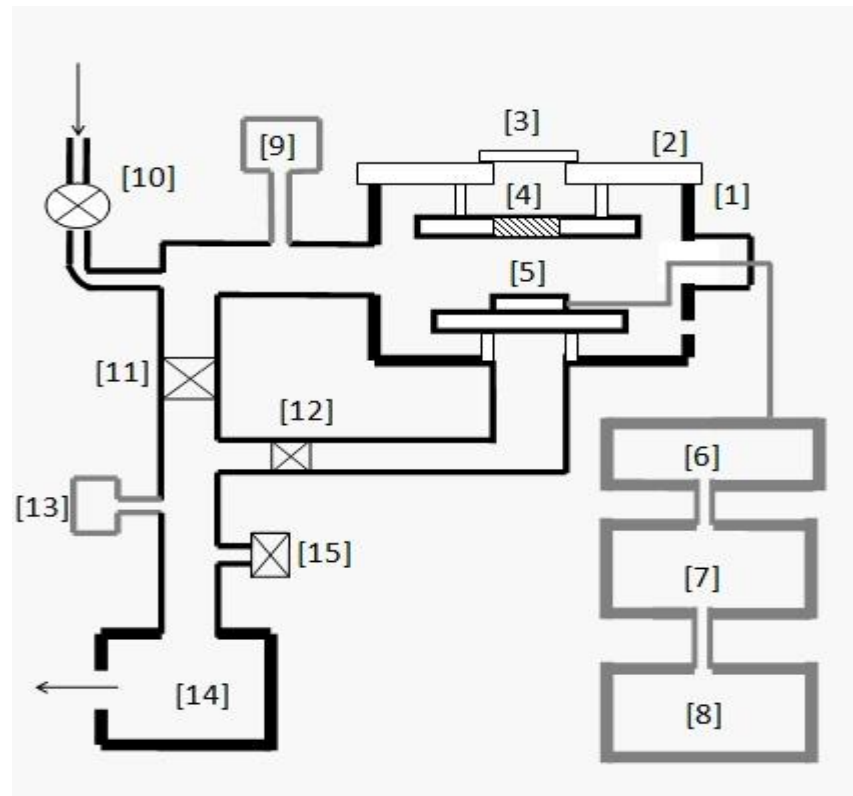


Figure 3.1 Schematic diagram of capacitively coupled radio frequency plasma system.

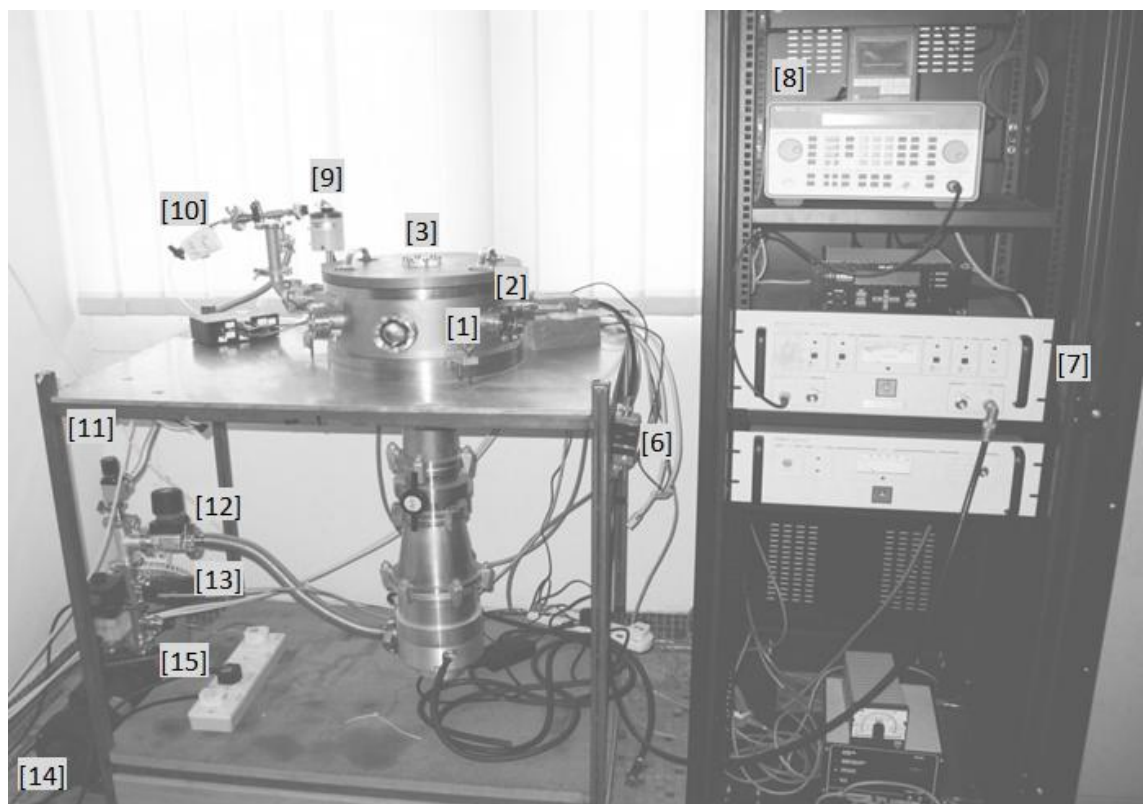


Figure 3.2 Photo of the capacitively coupled radio frequency plasma system

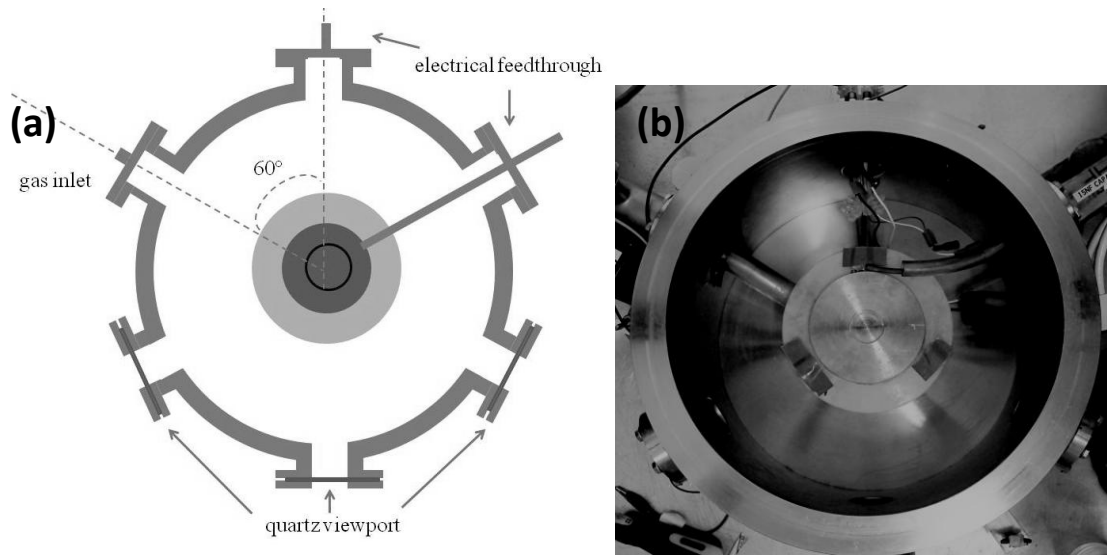


Figure 3.3 (a) Sketch schematic diagram of a cross-sectional top view of plasma chamber and (b) its photo.

The top electrode [4] which is mounted on the grounded top plate has a diameter of 130 mm and a circular opening at the center as seen in Figure 3.4. While the 100 mm-long bottom electrode [5] is insulated from the chamber wall, the bottom electrode plate is connected to a matching unit [6] located outside the chamber through an electrical feed-through. The cable that connects the bottom electrode and electrical feed-through is shielded by a hollow glass tube and PVC tube for isolation from the chamber's wall.

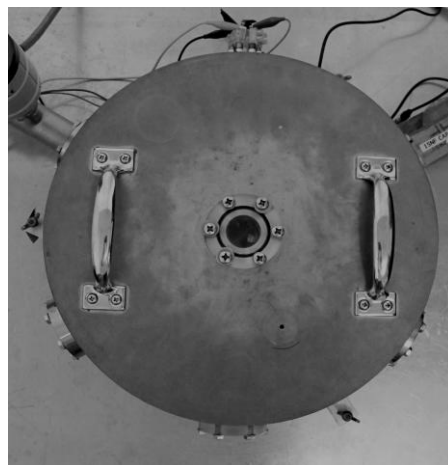


Figure 3.4 Vacuum chamber covered by top plate with viewing window at the center.

(b) Pumping system

The pumping system consists of a rotary pump [14], a gas inlet (Argon gas) [10], two pressure gauge [9, 13], three valves [11, 12, 15] and several fittings. The Leybold trivac D16E rotary vane pump is capable of evacuating the chamber up to 1×10^{-2} mbar. Argon gas is used for gas discharge and is injected into the chamber through a needle valve controller located at [10]. A pressure transducer [9] (MKS 622 Baratron[®] Absolute Capacitance Manometers) and a Pirani gauge [13] are used to monitor the chamber pressure. In each experiment, the chamber is first pumped down to 0.06 mbar followed by the closing of valve [11]. Valve [12] is kept opened throughout the experiment. The gas is then injected into the chamber until the required dynamical balanced pressure is achieved.

(c) Power supply

The power-supply unit consists of a signal generator [8], a RF amplifier [7] and a matching unit [6]. The signal generator (Hewlett-Packard 8647A) can generate sinusoidal signal ranged from 250 kHz to 1000 MHz with peak-to-peak voltage up to one Volt. The signal generated is amplified using a wide-band RF amplifier (RLA500V) which has a maximum output of 500W within 10 to 100 MHz. During the experiment, 13.56 MHz signal with amplitude of 600 mV is fed to the RF amplifier. The maximum forward output power from the amplifier is about 100W with reflected power 41W. The amplified current is injected to the matching unit consisting of capacitors and inductor as shown in Figure 3.5. The inductance of the inductor, L_M is 4.5 μH . Three 4.7 μF capacitors are connected in parallel and have a total capacitance, C_M of 14.1 μF . R_T is the resistance of the power-line cable while C_p and R_p represent the capacitance and resistance of the plasma respectively.

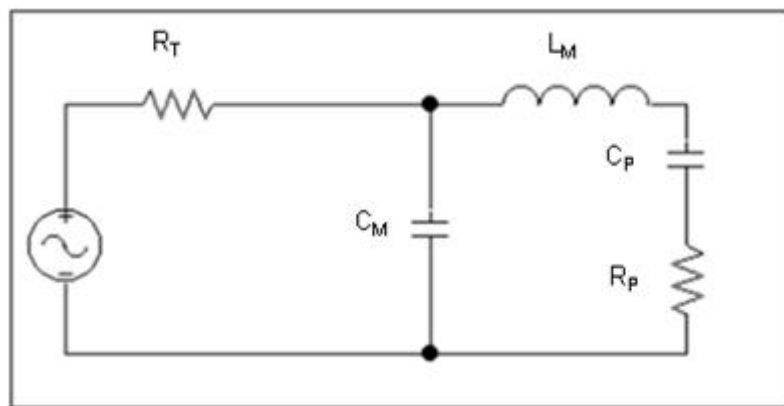


Figure 3.5 Circuit of matching network.

(d) Dust dispenser

Dust particles are introduced into the inter-electrode gap using a mechanical dust dispenser system located above the top electrode as shown in Figure 3.6. The dust powder is stored inside a small container that has a number of milimetre-sized openings at the bottom side. The container is attached onto a rotatable aluminum plate controlled by a DC motor as shown in Figure 3.6. Once the dust dispenser system is turned on, the aluminum plate will rotate towards the opening of the top electrode until it is stopped by a vibrator that will shake the whole aluminum plate and sprinkle down the dust particles. After sprinkling the dust, the polarity of the DC motor is reversed. That will move the aluminum plate away from the electrode opening, leaving an unobstructed view from the top window of the chamber plate.

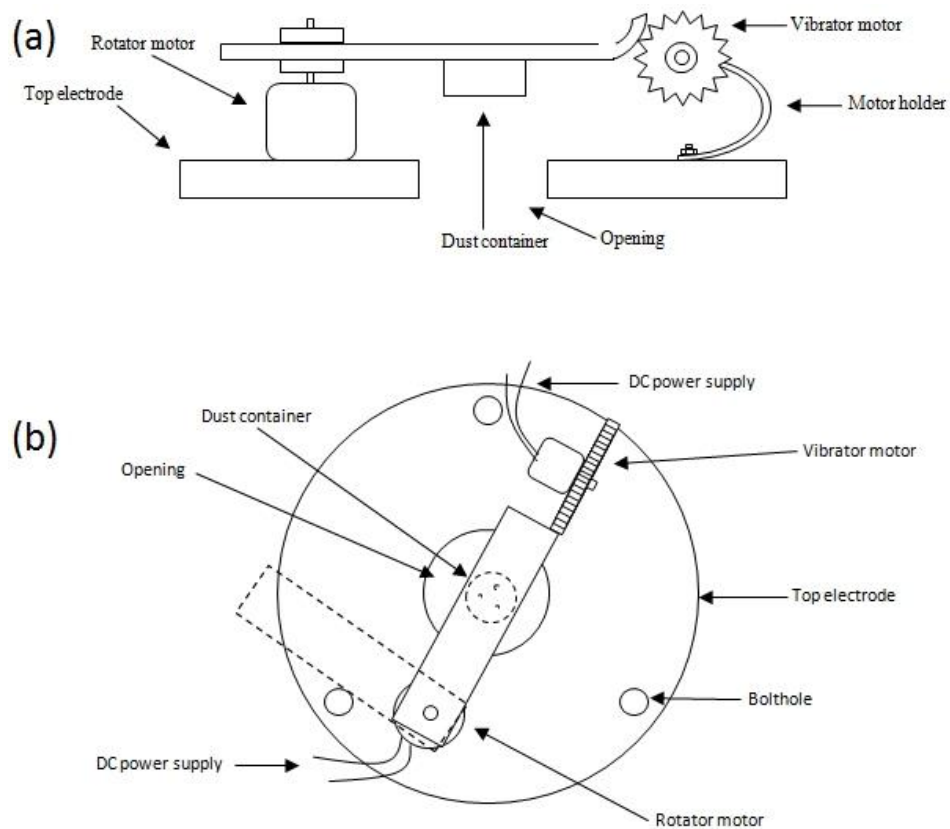


Figure 3.6 (a) Side view and (b) top view of dust dispenser system

(e) Dust particles

Poly-disperse titanium dioxide particles with mean size smaller than 1 μm are used in this work (see Figure 3.7).

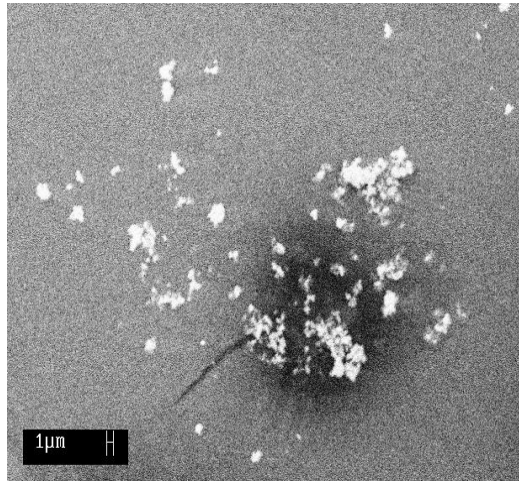


Figure 3.7 SEM images of poly-disperse titanium dioxide particles.

(f) Confinement electrode

On the surface of the bottom electrode, there is a 0.35 mm deep and 3 cm wide cylindrical depression designed for particle confinement as seen in Figure 3.8. The depression creates a parabolic shape electrical potential well which traps the charged dust particles inside. Depending on the charge and weight, dust grains introduced into the plasma levitate at various heights as shown in Figure 3.9.



Figure 3.8 Cylindrical depression on the bottom electrode.

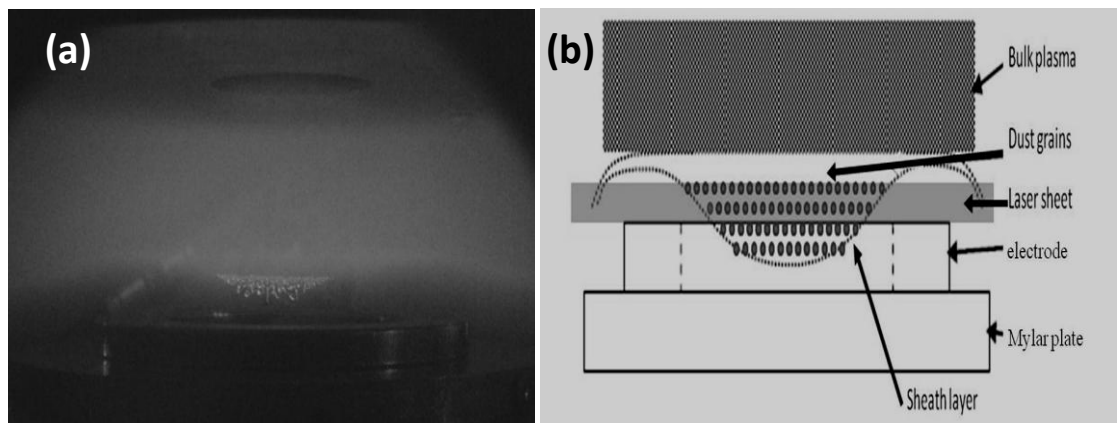


Figure 3.9 (a) Side view of the bottom electrode with dust particles levitating at the sheath region, (b) Position of levitating dust particles in plasma.

3.2 Visualization system

3.2.1 Experiment setup

The visualization system is basically a means to illuminate the dust particles levitating inside the plasma chamber using a laser. A thin laser sheet with thickness approximately 1mm is generated using a continuous 1.5 mW 635 nm He-Ne laser diode attached with a cylindrical lens. The laser sheet which is transmitted in a parallel manner to the electrode and through the quartz window illuminated the dust cloud as shown in Figure 3.10. Illuminated dust particles are viewed from the top of the chamber using an EoSens CL high-speed-CMOS video camera that operates at 100 frames per second and is equipped with a macro lens. A narrow band-pass interference filter (636 ± 10 nm) that selects only the laser wavelength is placed before the camera to increase the image contrast. To obtain the ratio of image's pixel to real length, the real and pixel dimensions of the cylindrical depression on the bottom electrode are calculated.

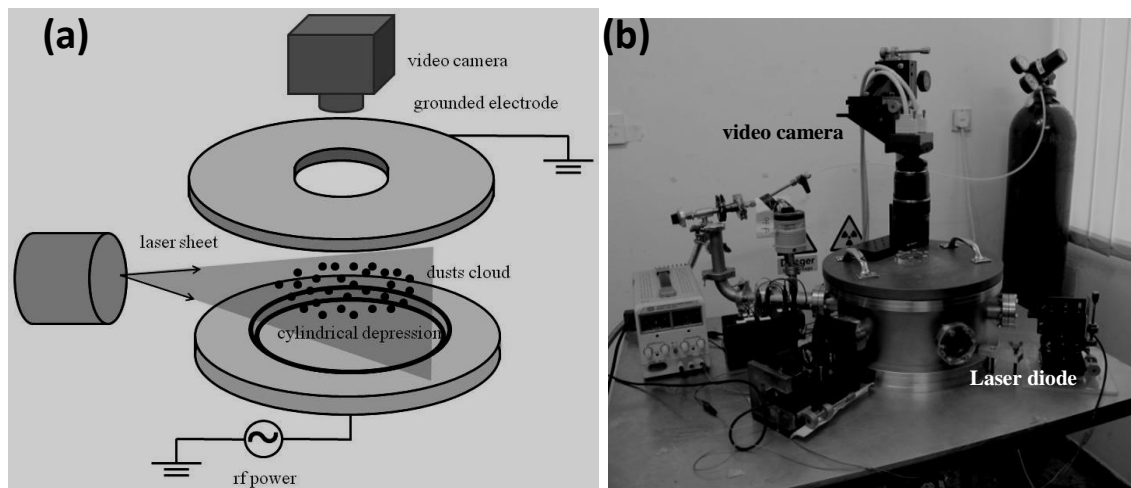


Figure 3.10 (a) A schematic diagram and (b) photo of the particle visualization setup.

3.2.2 Image processing

Raw video captured from the experiment contained an abundance of information as well as noises. Therefore the image sequences are processed and enhanced before further analysis is carried out. The image processing in this work is carried out mostly in Virtualdub and Matlab (see appendix B2). First, the raw video saved in the MPEG-2 format is cropped and deinterlaced. Subsequently, the video is converted into binary image sequence and saved in .bmp format with fixed aspect ratio. Following that, the image sequence is band-pass filtered to suppress pixel noise and long-wavelength image variations while retaining information of particle size. The band-pass filtering is performed based on an algorithm developed by J. C. Crocker and D. G. Grier (Crocker & Grier, 1996) and was translated into mfile (Matlab) by Daniel Blair and Eric Dufresne (Blair & Dufresne). From the processed images, the positions of each particle are determined by using the pkfnd.m algorithm (Blair & Dufresne). Before the pkdfnd.m algorithm is executed, parameters that include particle diameter and the minimum brightness of a pixel (that might be the local maximum) are defined. From the estimated particle position and window diameter, cntrd.m (Blair & Dufresne) is used to calculate the centroid of the bright spot up to sub pixel accuracy. The centroids are used to represent the position of each dust particle.

3.2.3 Pair correlation

Pair correlation function $g(r)$ as described earlier in section 2.3.3 is often used as a measure of orderliness in dusty plasma. The algorithm used in this work starts by measuring the distances r between one particular particle and other particles. Next, the number of particles with inter-particle distance that falls between r to $r+\Delta r$ is calculated. The calculation is repeated for every particle to obtain an average value of $g(r)$. After that, the average number of particles is normalized by dividing the annular area between r and $r+\Delta r$, and a factor that enables the asymptotic value of $g(r)$ to converge to one (Quinn et al., 1996). Note that in the $g(r)$ plot, the x-axis represents the inter-particle distance divided by the closest inter-particle distance, r/IPD . Theoretically, the $g(r)$ of a perfect crystal consists of a series of peaks whose position and height depend on the type of crystal structure. In a liquid-like state, the $g(r)$ is characterized by a primary peak followed by shorter second or third peak. While in the gas-like state, the uncorrelated particle arrangement gives rise to $g(r)$ that equals to one with no distinctive peaks.

Before the pair correlation algorithm (see section 2.3.3) is implemented, it is benchmarked using three different images that represent different orderliness of dusty plasma: 1) ordered hexagonal crystal lattice (Figure 3.11(a)), 2) ordered dusty plasma liquid (Figure 3.12(a)) and 3) disordered gas state (Figure 3.13(a)). In the crystal state, $g(r)$ is a series of delta functions as shown in Figure 3.11(b). Whereas in liquid state, $g(r)$ is characterized by a primary peak followed by smaller second or third peak as shown in Figure 3.12(b). For disordered gas state, an image of randomly distributed dots is used to simulate uncorrelated spatial distribution. It is found that $g(r)$ is equals to one with no distinctive peaks as examined in Figure 3.13(b).

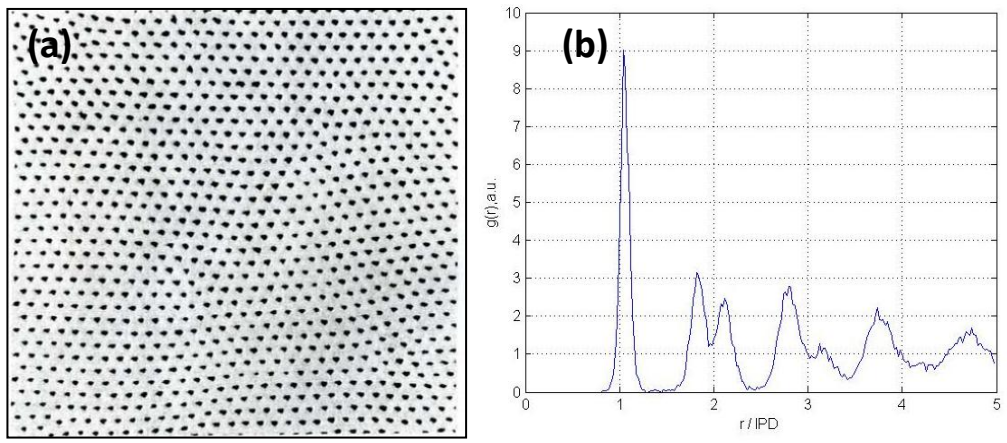


Figure 3.11(a) Two-dimensional hexagonal crystal lattice (Pieper, Goree, & Quinn, 1996) and (b) its estimated pair correlation function.

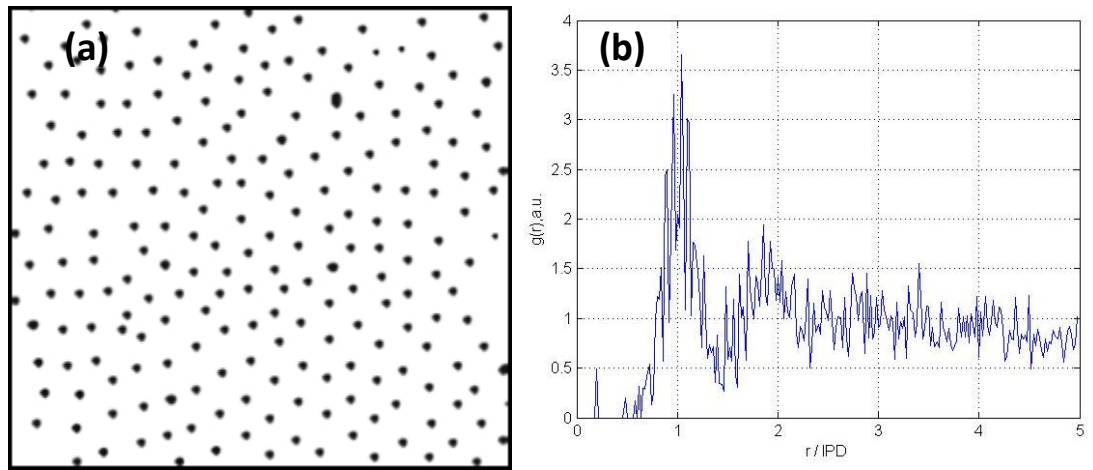


Figure 3.12 (a) Dusty plasma ordered liquid (Boesse, 2005) and (b) its estimated pair correlation function.

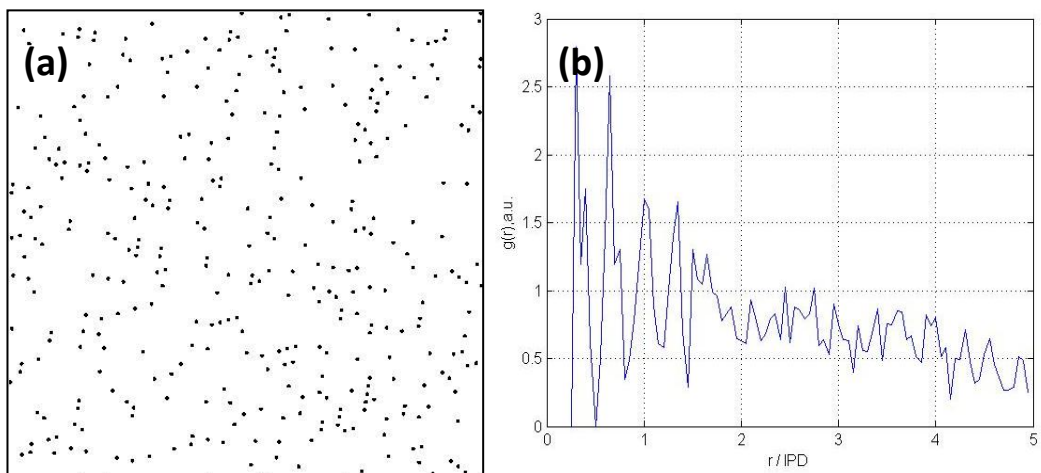


Figure 3.13 (a) Randomly distributed dots and (b) its estimated pair correlation function.

3.2.4 Particle tracking

In particle tracking analysis, the algorithm `track.m` developed by (Blair & Dufresne) which constructs a 2-D trajectory from a scrambled list of particle coordinates is used. The trajectory is a list of particle's position in successive time frame sorted according to individual particle with specific ID. From the trajectories, squared displacement in both x and y component started from different time origins are calculated according to $(\Delta x(\tau))^2 = [x(t + \tau) - x(\tau)]^2$ and $(\Delta y(\tau))^2 = [y(t + \tau) - y(\tau)]^2$, where τ is a positive integer range from one to predefined value τ_m . The total squared displacement is equal to $(\Delta r(\tau))^2 = (\Delta x(\tau))^2 + (\Delta y(\tau))^2$ and is averaged for every τ to give the time averaged mean-square-displacement $MSD_i(t) = \frac{1}{\tau_m} \sum_{\tau=1}^{\tau_m} (\Delta r(\tau))^2$. The same calculation is performed on all the trajectories and is then averaged to give the ensemble mean-square-displacement $MSD(t) = \frac{1}{N} \sum_{i=1}^N (MSD_i(t))^2$, where N is the number of particles. Finally, the scaling exponent α is determined from the slope of MSD versus time plot in log-log scale.

3.3 Dynamic light scattering system

3.3.1 Experiment setup

The same He-Ne polarized laser beam as used in the particle visualization system is transmitted through the dusty plasma cloud via the side quartz windows as shown in the schematic diagram in Figure 3.14. The polarization direction of the laser is perpendicular to the bottom electrode. Due to the limitation of chamber construction, the measurement of scattered light could only be done at an angle of 60° from the primary beam axis. The scattered light passed through a band-pass interference filter ($636 \pm 5\text{nm}$) and is focused using an aspherical lens ($f=26.2\text{mm}$) onto a photodetector. The registered current signal is recorded using a Newport 1936-C single channel optical power meter at a data sampling rate of 10 kHz.

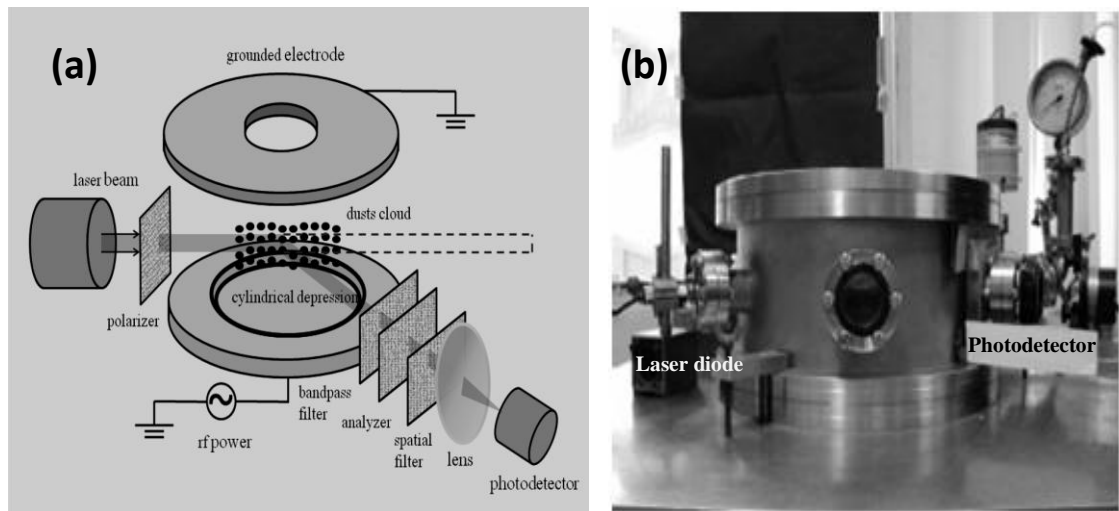


Figure 3.14 (a) The schematic diagram and (b) photo of dynamic light scattering setup.

3.3.2 Signal processing

In order to remove the contamination of deterministic (caused by power-line interference) and random thermal noise in the raw signal, band-stop filter is applied. On the other hand, the high-frequency white noise-like fluctuation is removed by applying a low-pass filter. To obtain zero-mean intensity fluctuation, the intensity time series is subtracted with its mean value. The time series is then normalized by dividing it with its standard deviation. Intensity data preprocessing procedures are performed using the signal processing toolbox in MATLAB (see appendix B1).

3.3.3 Correlation models

Correlation analysis is carried out once the intensity signals are preprocessed. The intensity auto-correlation function by definition is $C_I(\tau) = \langle I(i)I(i + \tau) \rangle = \lim_{k \rightarrow \infty} \frac{1}{k} \sum_{i=1}^k I_i I_{i+\tau}$ with positive integer k and τ . The correlation at each lag time is obtained by taking the average of all products from $I_1 I_{1+\tau}$ to $I_{N-\tau} I_N$, with N is the data length. In the signal preprocessing step, the intensity fluctuation is demeaned and normalized by its own standard deviation thus the auto-correlation function will decay from one to zero. The empirical intensity correlation function is then fitted by the four theoretical models as mentioned in chapter two. Note that the intensity correlation is related to electric field correlation function through $C_I(\tau) \propto [C_E(\tau)]^2$, hence from the equations (2.22), (2.23), (2.27) and (2.42) we obtain $C_I^B(\tau) = c_2 \exp(-\tau^2/\tau_B^2)$ for ballistic transport, $C_I^D(\tau) = c_1 \exp(-2t/\tau_D)$ for diffusive transport, $C_I^{BD}(\tau) = c_3 \exp([-c(-1 + \xi t + \exp(-\xi t))])$ for hybrid ballistic-diffusion transport, and the fractional dynamic correlation function based on fractional Ornstein-Uhlenbeck process, $C_I^F(\tau) = [2^{1-\nu} |a\tau|^\nu K_\nu(|a\tau|)/\Gamma(\nu)]^2$. Note that $C_E^F(\tau) \equiv C_\beta(\tau)$ with $\nu = \beta - 1/2$. All the correlation models are normalized such that $C_I(0) = 1$, thus $c_1=c_2=c_3=1$. The fitting

of empirical correlation function with theoretical model is done using nonlinear regression technique of curve fitting toolbox in Matlab (see appendix B1).

Chapter 4

Results and Discussions

This chapter presents the experimental and modeling results of the two diagnostic methods used: 1) dynamic light scattering and 2) particle tracking. First, the dusty plasma phases being investigated are described using the pair correlation function and particles' speed distribution. Following that the time series of DLS experiment and the calculated empirical auto-correlation functions fitted by theoretical models are shown. Finally, the results of particle tracking and MSD analysis are presented and a discussion of the type of transport present is also embedded.

4.1 Structural states of dusty plasma

In the experiment, dusty plasma of distinct physical states is observed when the neutral gas pressure is changed. Figure 4.1 shows three snapshots of different physical states taken at 0.1, 0.3 and 0.5 mbar with fixed power. At 0.5 mbar, several layers of dust particles can be seen levitating above the electrode. In each of these layers, dust particles are separated in a uniform manner. Particles' motion in these layers is restricted to the plane that is without any vertical migration. In contrast, particles at 0.1 and 0.3 mbar move freely in both vertical and horizontal directions.



Figure 4.1 Snapshots of dusty plasma at different neutral gas pressures: (a) 0.1 mbar, (b) 0.3 mbar, and (c) 0.5 mbar.

As a measure of translational ordering in the particles' arrangement, pair correlation function $g(r)$ is calculated and is presented in Figure 4.2. It is obvious that at 0.1 and 0.3 mbar, there is no distinctive feature in the pair correlation plot which suggests the presence of dusty plasma gaseous state at 0.1 and 0.3 mbar. While at 0.5 mbar, there is a peak at the closest neighbor distance, $r/ipd=1$, which is a sign of short-range orderliness that indicates the formation of dusty plasma disordered liquid state at 0.5 mbar.

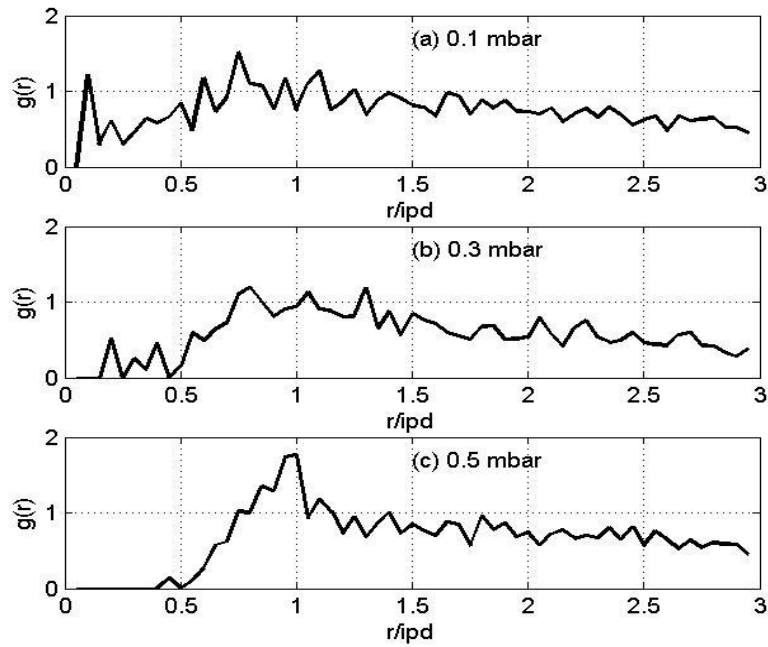


Figure 4.2 Pair correlation functions of dusty plasma at different pressures. Radial distance is normalized by nearest inter-particle distance.

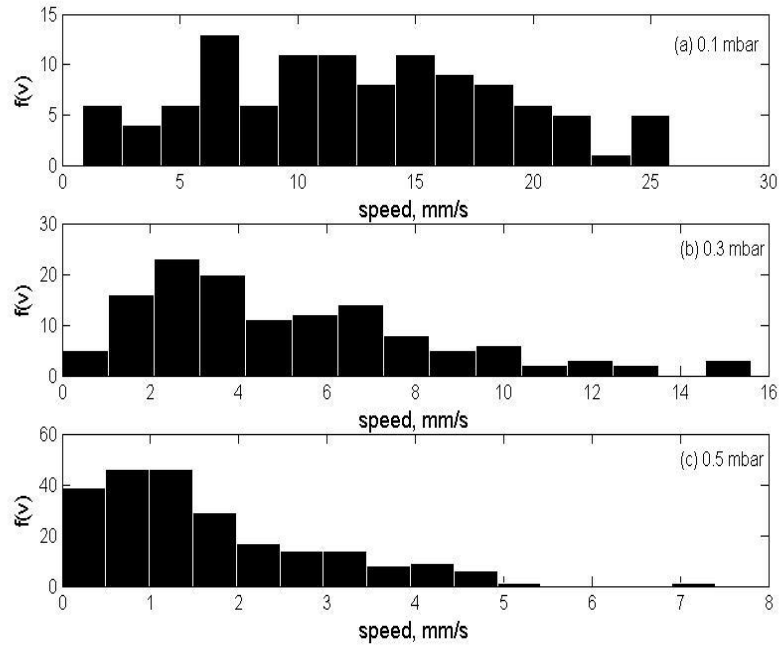


Figure 4.3 Distributions of particles' speed at different pressures.

To get a sense of particles' kinetic energy, one can notice the length difference of the light streaks as shown previously in Figure 4.1 . Particles that move faster than the camera frame rate (such as at the low-pressure state) will be captured as a line of dots/ streak. From the particle trajectories, the particle speed distribution is calculated and is shown in Figure 4.3. Dust particles at 0.1 mbar have the highest mode speed that is 13 mm/s, followed by 5 mm/s at 0.3 mbar and 2mm/s at 0.5 mbar respectively.

In short, two different physical states of dusty plasma are observed as the neutral gas pressure is changed. At low pressure (0.1 and 0.3 mbar), disordered gaseous state as indicated by the random-liked pair correlation function and high particle speed is observed. While at higher pressure (0.5 mbar), particles' speed is slowed down and spatial arrangement shows short range ordering, which is a feature of dusty plasma disordered liquid. The balance between electrostatic potential and thermal energy of dust particle is responsible for the phase transition with varying pressures. At a higher pressure, the formation of ordered structure due to ion wake effect (Trottenberg et al.,

1995) is relatively stable because the energy transfer from ion flow to particles is effectively dissipated through friction with neutral gas. As the neutral gas density decreases, the energy of dust particle cannot be dissipated totally, and that has led to the onset of characteristic horizontal oscillation of dust particles (Schweigert, Schweigert, Melzer, Homann, & Piel, 1998). At the same time, electron temperature in plasma will reduce (Godyak & Piejak, 1990) and results in a lower dust charge. As a result, the ratio of electrostatic potential to thermal energy has reduced, and hence the transition from ordered to disordered state.

4.2 Dynamic light scattering experiment

4.2.1 Intensity fluctuation at different pressures

The intensity fluctuation signals at different gas pressures recorded in the dynamic light scattering experiment are shown in Figure 4.4. The signals are acquired at 10 kHz for 13 s. As a reference signal, the intensity signal without the presence of dust particles (dust off) is shown at the bottom of the figure as well.

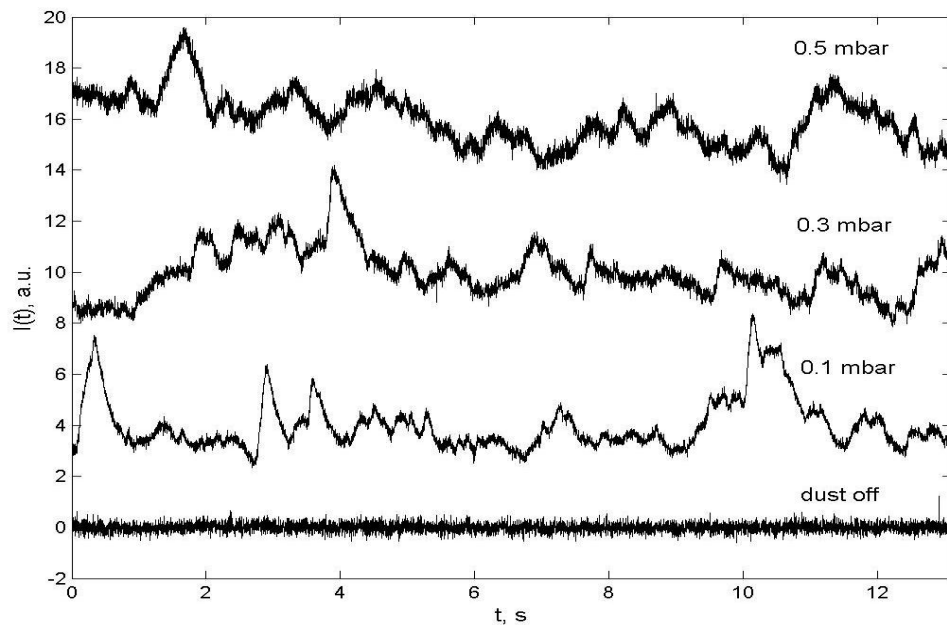


Figure 4.4 Intensity fluctuations of dynamic light scattering signal at different gas pressures and absence of dust.

4.2.2 Correlation analysis and model fitting

From the intensity fluctuations, the empirical auto-correlation function is calculated and is shown in Figure 4.5. It is apparent that the correlation function at 0.5 mbar decays fastest to zero as compared with others. In other words, it decorrelates faster. The decaying part of the correlation function is then fitted by the four correlation models, namely,

$$\text{Ballistic model, } C_I^B(\tau) = c_2 \exp(-\tau^2/\tau_B^2),$$

$$\text{Diffusive model, } C_I^D(\tau) = c_1 \exp(-2t/\tau_D),$$

$$\text{Ballistic-diffusive model, } C_I^{BD}(\tau) = c_3 \exp([-c(-1 + \xi t + \exp(-\xi t))]) \text{ and}$$

$$\text{Fractional Ornstein-Uhlenbeck model, } C_I^F(\tau) = [2^{1-\nu} |a\tau|^\nu K_\nu(|a\tau|)/\Gamma(\nu)]^2.$$

Note that the bumps at the decaying tail due to non-stationary (see Figure 4.5 (a) and (b)) are excluded in the model fitting.

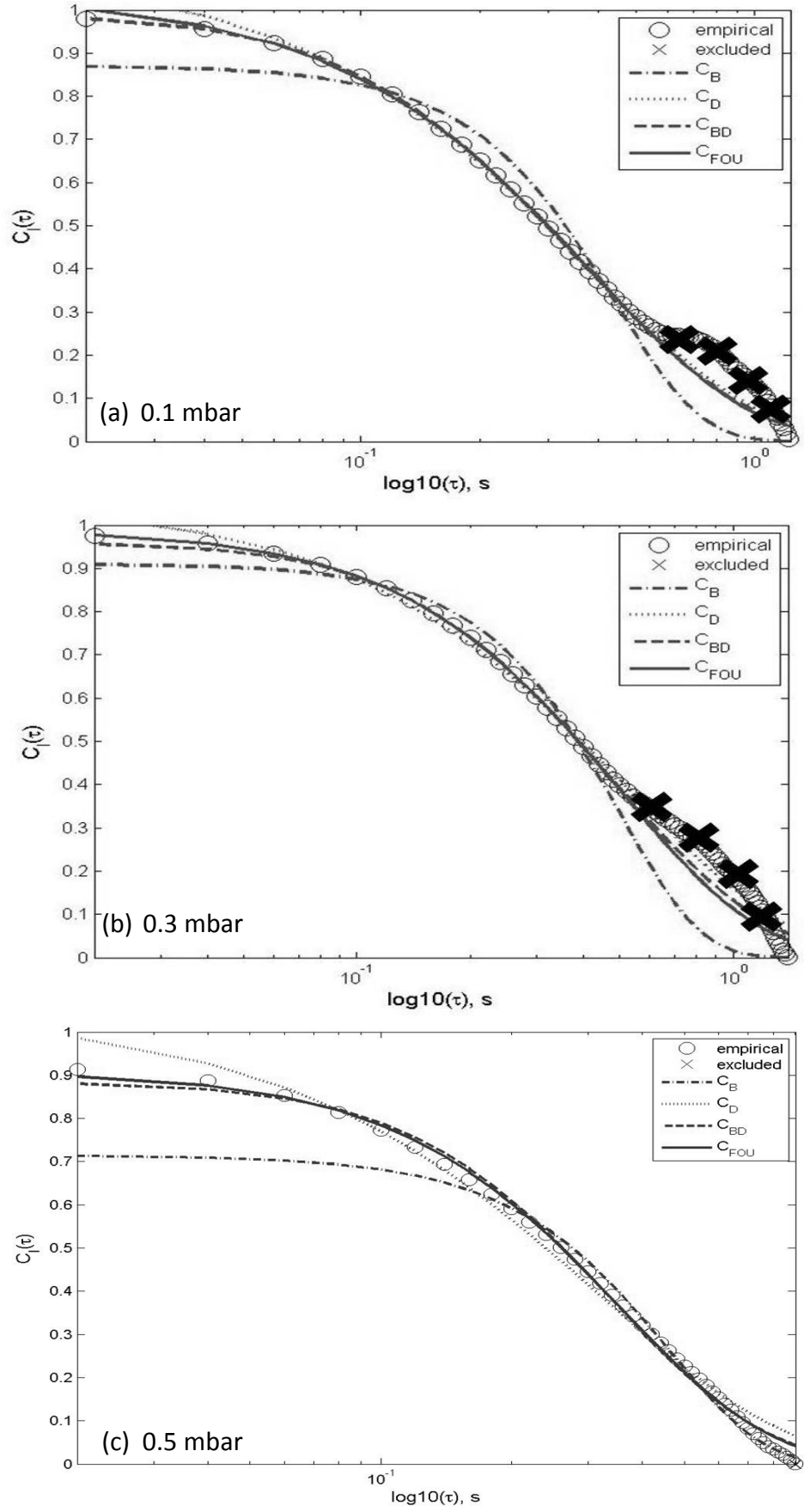


Figure 4.5 Empirical auto-correlation functions of intensity fluctuation at (a) 0.1 mbar, (b) 0.3 mbar, and (c) 0.5 mbar fitted with ballistic, diffusive, ballistic-diffusive and fractional dynamical model.

The fitting parameters and fitting errors of different correlation models are summarized in Table 4.1. Among the existing models, the ballistic-diffusive model provides the best fit with the smallest root-mean-square (rms) fitting error than the other two. It is observed that the persistence time ζ^I increases as the pressure increases. On the other hand, the new model based on fractional dynamic has fitted the empirical data equally well with comparable rms error. Parameter a , which is analogous to friction coefficient ζ in the standard Langevin equation for the velocity field, shows a sudden increase at 0.5 mbar. The other fractional parameter, ν rises with increasing pressure as well.

In summary, correlation model based on ballistic-diffusive transport provides a better fit than the purely ballistic and purely diffusive model. This agrees with previous work done by (Hurd & Ho, 1989) and suggests that particles in the gaseous and disordered liquid state of dusty plasma follow the ballistic type motion at short time scale and transit to diffusive behavior for longer time scale. The ballistic-diffusive transition time, namely the persistence time ζ^I , shows an increasing trend with increasing pressure.

Table 4.1 Fitting parameters of ballistic, diffusive, ballistic and fractional Ornstein-Uhlenbeck correlation model.

Correlation Pressure (mbar)	$C_I^B(t) \quad \tau_B$ (s) (rms error)	$C_I^D(t) \quad \tau_D$ (s) (rms error)	$C_I^{BD}(t) \quad c, \zeta$ (s ⁻¹) (rms error)	$C_I^{FOU}(t) \quad a$ (s ⁻¹), ν (rms error)
0.1	0.626±0.003 (0.062)	0.754±0.001 (0.008)	0.1410±0.0004 19.78±0.04 (0.001)	1.568±0.005 0.609±0.002 (0.006)
0.3	0.704±0.002 (0.037)	1.055±0.003 (0.014)	0.1933±0.0003 11.26±0.02 (0.001)	1.470±0.001 0.759±0.001 (0.001)
0.5	0.653±0.001 (0.098)	0.646±0.002 (0.036)	0.536±0.014 7.24±0.14 (0.022)	2.521±0.018 0.960±0.009 (0.018)

This suggests that at low pressure, the friction coefficient ζ is much higher than at high pressure. That is because at low pressure, diffusion is strongly suppressed due to the small number of neutral gas atoms. Strong interactions between particles such as dust-dust collision have increased the friction resistance, thus the friction coefficient is large. The friction reduces as the pressure increases, as there is a sufficient amount of neutral species that enhance the particle diffusion (Petrov, Nefedov, & Fortov, 2001; Vaulina & Vladimirov, 2002).

The fOU model that describes the experimental data equally well shows an increasing trend in the fractional parameter ν as the pressure increases. As mentioned in chapter two, parameter ν is related to the polydispersity of the power-law mass distribution $N(m) \sim m^{-\sigma}$ through $\nu = 3 - \sigma$. From that, small value of ν will have a larger σ exponent, corresponding to a faster decay in particle mass distribution. In other words, the model suggests that at low neutral gas pressure (in which the ν values from model fitting show the smallest value) the particles size distribution would be less polydisperse. The other fractional parameter, a shows a sharp rise between the transition from liquid state (0.5 mbar) to gaseous state (0.3 mbar). However, its physical interpretation is still unclear.

4.3 Particle tracking analysis

4.3.1 Particle trajectories

In particle tracking analysis, tracking duration and frame rate differ at different pressures due to different dynamical behaviors involved. At 0.1 mbar, the fast-moving particles are tracked at 100 Hz for 0.59 s before the particles disappeared from the laser sheet. At 0.3 mbar, tracking is done at 100 Hz for 2.5 s, while at 0.5 mbar, 56 Hz is used to track the relatively slower moving particles for 7 s. For illustration purpose, particle trajectories with equal tracking duration (0.6 s) are plotted in Figure 4.6 with the same spatial scale.

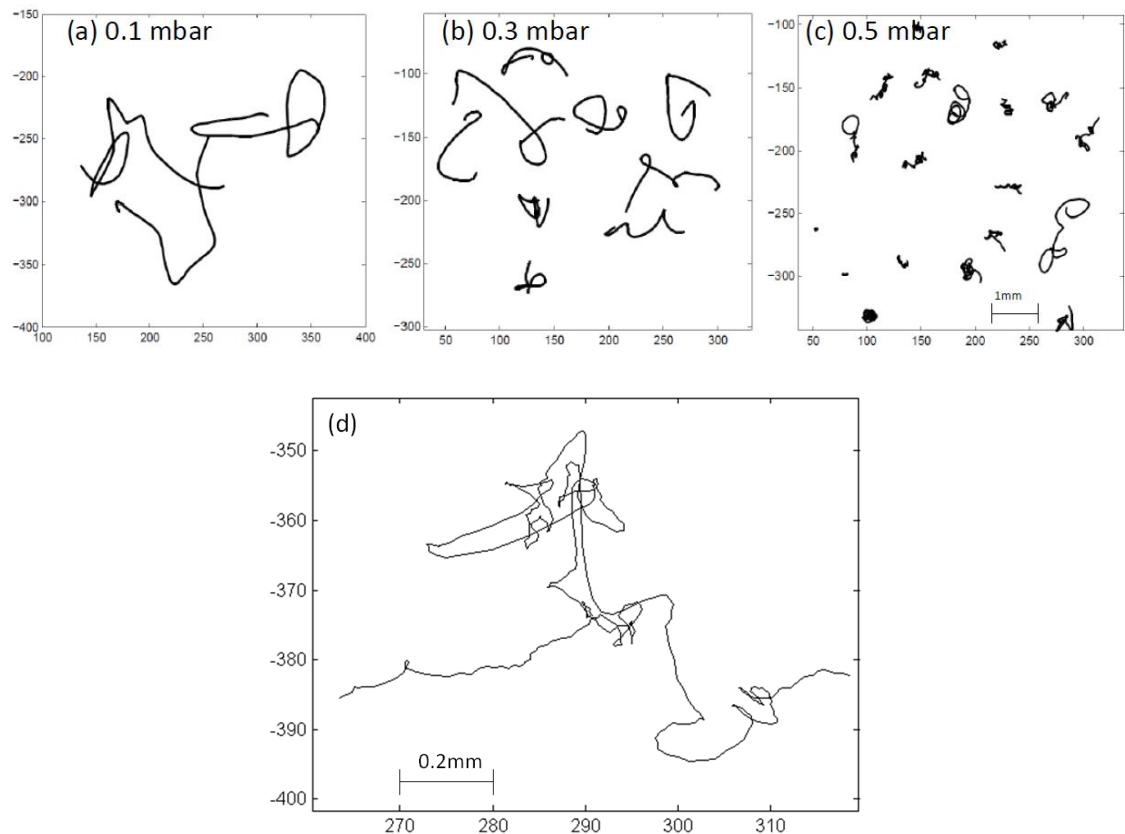


Figure 4.6 Selected particle trajectories at (a) 0.1 mbar, (b) 0.3 mbar, and (c) 0.5 mbar with the same time duration (0.6 s) and spatial scale, (d) magnified single particle trajectory at 0.5 mbar with duration of 0.6 s.

Particle trajectories in gaseous state at 0.1 and 0.3 mbar show similar behavior in which the particles travel linearly for long distance before changing their direction. However, at 0.3 mbar, such straight path is shorter. This trend persists until 0.5 mbar (disordered liquid state) where particles reverse their direction in much shorter length scale and tend to diffuse around their initial position as can be seen in Figure 4.6 (c). Figure 4.6 (d) shows a single particle trajectory at 0.5 mbar moving in a zigzag manner.

4.3.2 Mean-square-displacement (MSD)

In order to determine the type of transport followed by the dust particles, MSD calculation using the algorithm described in chapter three is performed. The time and ensemble averaged mean-square-displacement is calculated from few particle trajectories of different gas pressures. At 0.1 mbar, 52 trajectories are calculated and maximum lag time of MSD is $\tau_m=10$. At 0.3 mbar, 43 trajectories are calculated with $\tau_m=100$. At 0.8 mbar, 32 trajectories are calculated with $\tau_m=100$. The MSD scaling exponent α is obtained from the slope of log-log plot of MSD versus time (Figure 4.7) using linear least square fitting. The scaling exponents of different time regimes are tabulated in Table 4.2.

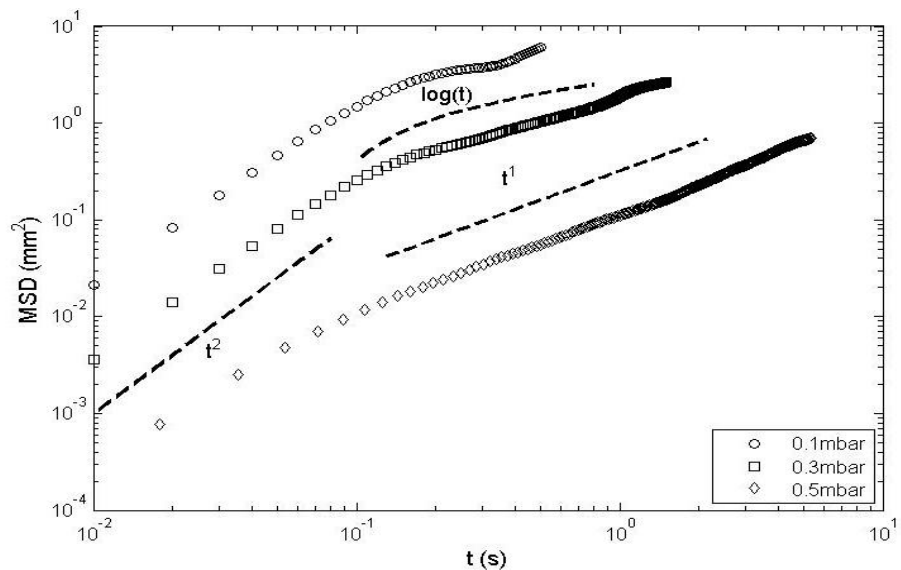


Figure 4.7 Particles' mean-square-displacement at different pressures.

Table 4.2 Scaling exponents of mean-square-displacement at different pressures and time regimes.

Pressure (mbar)	MSD scaling exponent, α		
	Regime I (0.01-0.13s)	Regime II (0.13-1.63s)	Regime III (1.63-5s)
0.1	1.864 \pm 0.020	0.668 \pm 0.019	-
0.3	1.852 \pm 0.025	0.727 \pm 0.002	-
0.5	1.515 \pm 0.049	0.979 \pm 0.003	1.175 \pm 0.003

Generally, it is found that the magnitude of MSD at the lower pressure is larger than those at the higher pressure. The greater magnitude of displacement at the low pressure is found to be consistent with the longer straight trajectories as seen in previous section. It is also observed that the type of particle transport is changing throughout the whole duration. At times shorter than 0.13 s, the scaling exponents of MSD at all pressures are close to two, a sign of ballistic transport. After 0.13 s, MSD exponent of gaseous state has changed to ~ 0.7 , a value that indicates subdiffusion transport. Further investigation suggests that the MSD scaling behaviour in gaseous state at that time regime is better described by the logarithmic function of time, $\log(t)$, which turns out to be the characteristic of binary uncorrelated transport (Pöschel & Luding, 2001; Schofield, Marcus, & Rice, 1996). On the other hand, at 0.5 mbar, normal diffusion ($\alpha=1$) occurs at the intermediate time regime. The higher concentration of neutral particles might be the reason that hinders the binary uncorrelated collision. As a result, dust particles' motion is damped and diffuses normally as depicted by the zigzag trajectory in Figure 4.6 (d).

For a much longer time scale (regime III), the normal diffusion has ceased and transits to superdiffusion as indicated by $\alpha > 1$. To investigate the cause of superdiffusion, the increments of particle trajectories are computed and subjected to correlation analysis. Figure 4.8 shows the results of auto-correlation function calculated at three different pressures. It is interesting that both auto-correlation functions at 0.1 and 0.3 mbar decay

quickly to zero while the auto-correlation at 0.5 mbar has the longest decay time. This is a sign of long memory effect, which is present in the particle trajectory from 0.5 mbar and that contributes to the superdiffusive behavior observed. This finding is similar to the work of Ratynskaia et al., (2005), in which they have found long-range dependence in particle position increments that are responsible to the observed superdiffusive particle transport. The non-linear MSD scaling behavior and long-range dependence displayed in the particle trajectory can be modeled using the Riemann-Liouville fractional Brownian motion (RL-FBM) with time scaling Hurst exponent larger than 0.5.

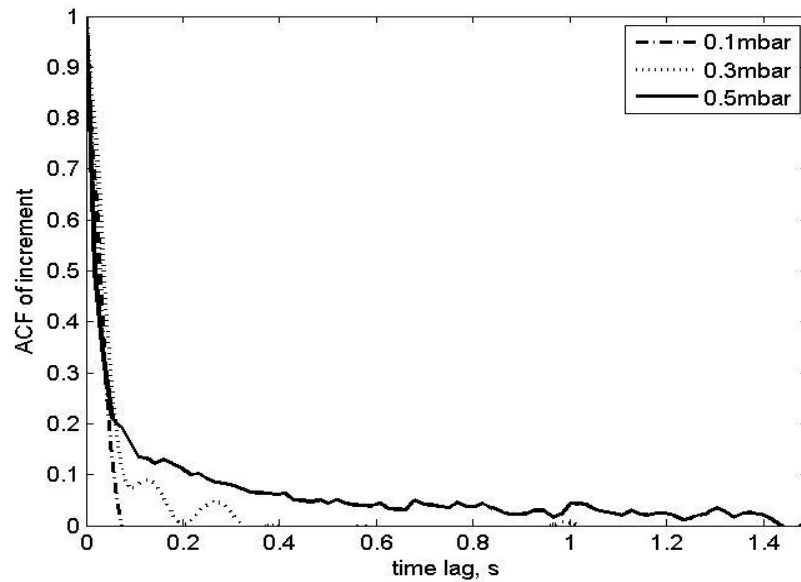


Figure 4.8 Auto-correlation function of trajectories' increments at different pressures.

Chapter 5

Conclusions

In this work, two types of optical diagnostic techniques based on dynamic light scattering (DLS) and particle visualization are setup to study the particle dynamics in dusty plasma system. Scattered laser intensity fluctuation in dusty plasma has been investigated using different stationary correlation models that are derived based on purely ballistic, purely diffusive, and hybrid ballistic-diffusive transport mechanisms with the assumption of monodisperse particles. It is found that the empirical correlation function is best fitted by the hybrid ballistic-diffusive transport model instead of the purely ballistic or purely diffusive model. It is worth to mention that the persistence time parameter in the DLS hybrid correlation model shows a high value at the disordered liquid state, indicating persistence behavior in the particle movement. This persistence behavior in particle motion is confirmed later in the particle tracking experiment. While the existing hybrid correlation model provides a good fit on the experimental data, the proposed fractional dynamical model fitted the data equally well. In addition, the fractional dynamical model derived from the fractional Langevin equation with shifted fractional derivative operator is shown to have the same form of correlation model as the purely ballistic model for particle with polydisperse size proposed by Hurd and Ho (Hurd & Ho, 1989). The solution of the fractional stochastic differential equation is the fractional Ornstein-Uhlenbeck process, which have a stationary correlation function parameterized by a generalized friction coefficient a and fractional index β . The empirical fractional index β in the fractional dynamical model suggests that, in the disordered liquid state, dust particles are more polydisperse than it is in the disordered gas state. The issue whether the empirical particle size distribution follows the polydispersity as predicted by the fractional Ornstein-Uhlenbeck model is not yet confirmed experimentally and requires further investigations.

In particle visualization and tracking experiment, time dependent scaling in particles mean-square-displacement with time is observed. This is consistent with the result in DLS experiment that shows dust particles undergo fast ballistic transport at short time scale and slow dynamic at later time duration. Interestingly, the slower dynamic varies with the state of dusty plasma. For example, in a disordered gas state, particle transport is dominated by uncorrelated binary collision at longer time scale. While in the disordered liquid state, ballistic transport at early time scale has eventually changed to normal diffusion. However, the normal diffusion does not last long, as the sign of anomalous diffusion is observed for much longer observation time. The anomalous diffusion observed in the disordered liquid state is found to possess long-range correlated increments. Such long-range correlation property does not exist in the traditional diffusion model based on Brownian motion. Hence, a Gaussian model formulated using fractional calculus, Riemann-Liouville fractional Brownian motion (RL-FBM) with time scaling exponent is proposed as a candidate model for the observed anomalous transport.

As for future study, it would be interesting to determine if there is a theoretical connection between the RL-FBM (describes individual particle motion) and the fOU model (describes the scattered light intensity fluctuation). In addition, one maybe investigate the anomalous transport behavior of charged Brownian particles using other fractional dynamical frameworks such as the fractional diffusion equation or the fractional Langevin equation with dynamic memory function (del-Castillo-Negrete, Carreras, & Lynch, 2004). Apart from that, the assumption that dust particles only interact with other particles from the same plane is weak. It is because the inter-particle interaction is not only limited to particles in the same layer but also involves coupling of other particles located above or below such layer through the ion wakes effect. Therefore, it would be interesting to study such particles systems with inter-layer

coupling and explore other fractional dynamical models such as fractional Langevin equation. This work here also leads to a new research direction, which is the study of anomalous diffusion in one dimensional charged particle system such as a dusty plasma ring (see the proceeding paper in appendix A1).

References

- Allen, J. E. (1992). Probe theory - the orbital motion approach. *Physica Scripta*, 45(5), 497-503.
- Anderson, H. M., & Radovanov, S. B. (1995). Dusty plasma studies in the gaseous electronics conference reference cell. *Journal of Research of the National Institute of Standards and Technology*, 100(4), 449-462.
- Arp, O., Block, D., Piel, A., & Melzer, A. (2004). Dust coulomb balls: three-dimensional plasma crystals. *Physical Review Letters*, 93(16), 165004,1-4.
- Ashkin, A. (1970). Acceleration and trapping of particles by radiation pressure. *Physical Review Letters*, 24(4), 156-159.
- Bagley, R. L., & Torvik, P. J. (1986). On the fractional calculus model of viscoelastic behavior. *Journal of Rheology*, 30(1), 133-155.
- Barkan, A., Dangelo, N., & Merlino, R. L. (1994). Charging of dust grains in a plasma. *Physical Review Letters*, 73(23), 3093-3096.
- Barnes, J., & Allan, D. (1966). A Statistical Model of Flicker Noise. *Proceedings of the IEEE*, 54(2), 176-178.
- Beran, J. (1994). *Statistics for long-memory processes*. New York: Chapman & Hall.
- Blair, D., & Dufresne, E. The Matlab Particle Tracking Code Repository, from <http://physics.georgetown.edu/matlab/index.html>
- Boesse, C. M. (2005). *Development of a digital optical diagnostic system for the CASPER*. PhD, Baylor University, United States.
- Bouchaud, J. P., & Georges, A. (1990). Anomalous diffusion in disordered media: statistical mechanisms, models and physical applications. *Physics Reports*, 195(4), 127-293.
- Boufendi, L., & Bouchoule, A. (2002). Industrial developments of scientific insights in dusty plasmas. *Plasma Sources Science and Technology*, 11, A211-A218.
- Chandrasekhar, S. (1943). Stochastic Problems in Physics and Astronomy. *Reviews of Modern Physics*, 15(1), 1-89.

- Coffey, W., Kalmykov, Y. P., & Waldron, J. T. (2004). *The Langevin equation: with applications to stochastic problems in physics, chemistry, and electrical engineering*. Singapore: World Scientific.
- Crocker, J. C., & Grier, D. G. (1996). Methods of digital video microscopy for colloidal studies. *Journal of Colloid and Interface Science*, 179(1), 298-310.
- del-Castillo-Negrete, D., Carreras, B., & Lynch, V. (2004). Fractional diffusion in plasma turbulence. *Physics of Plasmas*, 11, 3854-3864.
- Einstein, A. (2006). Über die von der molekularkinetischen Theorie der Wärme geforderte Bewegung von in ruhenden Flüssigkeiten suspendierten Teilchen. *Annalen der Physik*, 322(8), 549-560.
- Epstein, P. S. (1924). On the resistance experienced by spheres in their motion through gases. *Physical Review*, 23(6), 710-733.
- Erdelyi, A., Magnus, W., Oberhettinger, F., & Tricomi, F. G. (1995). *Higher transcendental functions*. New York: McGraw-Hill.
- Fortov, V. E., Ivlev, A. V., Khrapak, S. A., Khrapak, A. G., & Morfill, G. E. (2005). Complex (dusty) plasmas: Current status, open issues, perspectives. *Physics Reports-Review Section of Physics Letters*, 421(1-2), 1-103.
- Garscadden, A., Ganguly, B. N., Haaland, P. D., & Williams, J. (1994). Overview of growth and behaviour of clusters and particles in plasmas. *Plasma Sources Science & Technology*, 3(3), 239-245.
- Godyak, V., & Piejak, R. (1990). Abnormally low electron energy and heating-mode transition in a low-pressure argon rf discharge at 13.56 MHz. *Physical Review Letters*, 65(8), 996-999.
- Goertz, C. K. (1989). Dusty Plasmas in the Solar-System. *Reviews of Geophysics*, 27(2), 271-292.
- Goree, J. (1994). Charging of particles in a plasma. *Plasma Sources Science & Technology*, 3(3), 400-406.
- Goree, J., Morfill, G. E., Tsytovich, V. N., & Vladimirov, S. V. (1999). Theory of dust voids in plasmas. *Physical Review E*, 59(6), 7055-7067.
- Hamaguchi, S., Farouki, R. T., & Dubin, D. H. E. (1997). Triple point of Yukawa systems. *Physical Review E*, 56(4), 4671-4682.

- Hansen, J. P., Levesque, D., & Weis, J. J. (1979). Self-Diffusion in the Two-Dimensional, Classical Electron Gas. *Physical Review A*, 43(14), 979-982.
- Hou, L.-J., Piel, A., & Shukla, P. K. (2009). Self-Diffusion in 2D Dusty-Plasma Liquids: Numerical-Simulation Results. *Physical Review Letters*, 102(8), 5002, 1-4.
- Hurd, A. J., & Ho, P. (1989). Velocity Persistence of Brownian Particles Generated in a Glow-Discharge. *Physical Review Letters*, 62(26), 3034-3037.
- Hutchinson, I. H. (2005). Ion collection by a sphere in a flowing plasma: 3. Floating potential and drag force. *Plasma Physics and Controlled Fusion*, 47(1), 71-87.
- Jellum, G. M., Daugherty, J. E., & Graves, D. B. (1991). Particle Thermophoresis in Low-Pressure Glow-Discharges. *Journal of Applied Physics*, 69(10), 6923-6934.
- Juan, W. T., Chen, M. H., & I, L. (2001). Nonlinear transports and microvortex excitations in sheared quasi-two-dimensional dust Coulomb liquids. *Physical Review E*, 64(1), 6402, 1-5.
- Juan, W. T., & I, L. (1998). Anomalous diffusion in strongly coupled quasi-2D dusty plasmas. *Physical Review Letters*, 80(14), 3073-3076.
- Kulish, V. V., & Lage, J. L. (2002). Application of fractional calculus to fluid mechanics. *Journal of Fluids Engineering*, 124(3), 803-806.
- Lai, Y. J., & I, L. (2002). Avalanche excitations of fast particles in quasi-2D cold dusty-plasma liquids. *Physical Review Letters*, 89(15), 5002, 1-4.
- Lampe, M., Goswami, R., Sternovsky, Z., Robertson, S., Gavrishchaka, V., Ganguli, G., & Joyce, G. (2003). Trapped ion effect on shielding, current flow, and charging of a small object in a plasma. *Physics of Plasmas*, 10(5), 1500-1513.
- Li, M., & Scalia, M. (2010). Fractal time series—a tutorial review. *Mathematical Problems in Engineering*, 112.
- Lim, S., Li, M., & Teo, L. (2008). Langevin equation with two fractional orders. *Physics Letters A*, 372(42), 6309-6320.
- Lim, S., & Muniandy, S. (2003). Generalized Ornstein–Uhlenbeck processes and associated self-similar processes. *Journal of Physics A: Mathematical and General*, 36, 3961-3982.

- Lim, S., & Sithi, V. (1995). Asymptotic properties of the fractional Brownian motion of Riemann-Liouville type. *Physics Letters A*, 206(5-6), 311-317.
- Lutz, E. (2001a). Fractional Langevin equation. *Physical Review E*, 64(5), 051106, 1-4.
- Lutz, E. (2001b). Fractional transport equations for Lévy stable processes. *Physical Review Letters*, 86(11), 2208-2211.
- Magin, R. L. (2004). Fractional calculus in bioengineering. *Critical Reviews in Biomedical Engineering*, 32(1), 1.
- Mandelbrot, B. B., & Van Ness, J. W. (1968). Fractional Brownian motions, fractional noises and applications. *SIAM Review*, 10(4), 422-437.
- Metzler, R., & Klafter, J. (2000). The random walk's guide to anomalous diffusion: a fractional dynamics approach. *Physics Reports*, 339(1), 1-77.
- Miller, K., & Ross, B. (1993). *An introduction to fractional calculus and fractional differential equations*. New York: Wiley.
- Morfill, G. E., & Ivlev, A. V. (2009). Complex plasmas: An interdisciplinary research field. *Reviews of Modern Physics*, 81(4), 1353-1404.
- Nunomura, S., Samsonov, D., Zhdanov, S., & Morfill, G. (2006). Self-diffusion in a liquid complex plasma. *Physical Review Letters*, 96(1), 15003, 1-4.
- Ott, T., & Bonitz, M. (2009). Is diffusion anomalous in two-dimensional Yukawa liquids? *Physical Review Letters*, 103(19), 5001, 1-5.
- Ott, T., Bonitz, M., Donkó Z., & Hartmann, P. (2008). Superdiffusion in quasi-two-dimensional Yukawa liquids. *Physical Review E*, 78(2), 6409, 1-6.
- Paul, W., & Baschnagel, J. (1999). *Stochastic processes: from physics to finance*. Berlin: Springer-Verlag.
- Petrov, O., Nefedov, A., & Fortov, V. (2001). Thermal dusty plasmas: diagnostics and results of investigations. *Physica Scripta*, 2001, 25-28.
- Pieper, J., Goree, J., & Quinn, R. (1996). Experimental studies of two-dimensional and three-dimensional structure in a crystallized dusty plasma. *Journal of Vacuum Science & Technology A: Vacuum, Surfaces, and Films*, 14(2), 519-524.

- Podlubny, I. (1999a). *Fractional Differential Equations*. San Diego: Academic Press.
- Podlubny, I. (1999b). *Fractional differential equations: an introduction to fractional derivatives, fractional differential equations, to methods of their solution and some of their applications*. San Diego: Academic Press.
- Pöschel, T., & Luding, S. (2001). *Granular gases*. Berlin: Springer-Verlag.
- Quinn, R., & Goree, J. (2002). Particle interaction measurements in a Coulomb crystal using caged-particle motion. *Physical Review Letters*, 88(19), 195001, 1-4.
- Quinn, R. A., Cui, C., Goree, J., Pieper, J. B., Thomas, H., & Morfill, G. E. (1996). Structural analysis of a Coulomb lattice in a dusty plasma. *Physical Review E*, 53(3), 2049-2052.
- Rao, N. N., Shukla, P. K., & Yu, M. Y. (1990). Dust-acoustic waves in dusty plasmas. *Planetary and Space Science*, 38(4), 543-546.
- Ratynskaia, S., Knappek, C., Rypdal, K., Khrapak, S., & Morfill, G. (2005). Statistics of particle transport in a two-dimensional dusty plasma cluster. *Physics of Plasmas*, 12(2), 2302, 1-11.
- Ross, B. (1977). Fractional calculus. *Mathematics Magazine*, 50(3), 115-122.
- Sabatier, J., Agrawal, O. P., & Machado, J. (2007). *Advances in fractional calculus: Theoretical developments and applications in physics and engineering*. Dordrecht: Springer.
- Samko, S. G., Kilbas, A. A., & Marichev, O. I. (1993). *Fractional integrals and derivatives: theory and applications*. Yverdon: Gordon and Breach Science Publishers.
- Schofield, J., Marcus, A. H., & Rice, S. A. (1996). Dynamics of quasi two-dimensional colloidal systems. *The Journal of Physical Chemistry*, 100(49), 18950-18961.
- Schweigert, V., Schweigert, I., Melzer, A., Homann, A., & Piel, A. (1998). Plasma crystal melting: a nonequilibrium phase transition. *Physical Review Letters*, 80(24), 5345-5348.
- Shukla, P. K., & Mamun, A. (2002). *Introduction to dusty plasma physics*. London: Taylor & Francis.

- Smith, B., Vasut, J., Hyde, T., Matthews, L., Reay, J., Cook, M., & Schmoke, J. (2004). Dusty plasma correlation function experiment. *Scientific Exploration, Planetary Protection, Active Experiments and Dusty Plasmas*, 34(11), 2379-2383.
- Smith, B. A., Soderblom, L., Batson, R., Bridges, P., Inge, J., Masursky, H., Suomi, V. E. (1982). A new look at the Saturn system - the Voyager-2 images. *Science*, 215, 504-537.
- Tomme, E. B., Law, D. A., Annaratone, B. M., & Allen, J. E. (2000). Parabolic plasma sheath potentials and their implications for the charge on levitated dust particles. *Physical Review Letters*, 85(12), 2518-2521.
- Trivedi, K. S. (1982). *Probability and statistics with reliability, queuing, and computer science applications*. Englewood Cliffs: Prentice-hall.
- Trottenberg, T., Melter, A., & Piel, A. (1995). Measurement of the electric charge on particulates forming coulomb crystals in the sheath of a radiofrequency plasma. *Plasma Sources Science & Technology*, 4(3), 450-458.
- Uhlenbeck, G. E., & Ornstein, L. S. (1930). On the theory of the Brownian motion. *Physical Review*, 36(5), 823-841.
- Vaulina, O., & Vladimirov, S. (2002). Diffusion and dynamics of macro-particles in a complex plasma. *Physics of Plasmas*, 9, 835-840.
- Verheest, F. (2000). *Waves in dusty space plasmas*. Dordrecht: Kluwer Academic Publishers.
- Wang, M. C., & Uhlenbeck, G. (1945). On the Theory of the Brownian Motion II. *Reviews of Modern Physics*, 17(2-3), 323-342.
- Woon, W. Y., & I, L. (2004). Defect turbulence in quasi-2D creeping dusty-plasma liquids. *Physical Review Letters*, 92(6), 5003,1-4.

Appendix A: Research outputs

A1: Published paper in journal

Fractional dynamics in the light scattering intensity fluctuation in dusty plasma

S. V. Muniandy,^{a)} W. X. Chew, and C. S. Wong

Department of Physics, Plasma Research Laboratory, University of Malaya, 50603 Kuala Lumpur, Malaysia

(Received 3 September 2010; accepted 15 December 2010; published online 3 January 2011)

Light scattering intensity fluctuation in dusty plasma system is studied. The scattered electric field of the laser light is treated as a stationary stochastic process. A nonstandard form of fractional Langevin equation is solved using Green's function approach to obtain the so-called fractional Ornstein–Uhlenbeck process. The empirical correlation function of light intensity fluctuation is fitted with four model correlation functions which are representative of different mechanisms for monodisperse particle transport, namely, the kinetic (ballistic) model, the hydrodynamical (diffusive) model, the hybrid kinetic-hydrodynamic model, and the fractional kinetic model for polydisperse particles. The shifted fractional derivative index is found to be related to power-law exponent of polydisperse dust mass distribution. It is shown that the correlation model based on fractional Ornstein–Uhlenbeck process may provide a novel insight into the complex transport behaviors in dusty plasma. © 2011 American Institute of Physics. [doi:10.1063/1.3533905]

I. INTRODUCTION

Dusty plasma can be considered as a complex colloidal system composed of massive charged dust immersed in electron-ion plasma.^{1,2} These dust particles can be charged either negatively or positively depending on their surrounding plasma environment and the charging mechanisms. Dusty plasmas are known to support diverse phenomena such as stochastic charge fluctuation, anomalous diffusion, linear and nonlinear waves, and structural phase transition from disordered gas phase to ordered plasma crystals.^{3,4}

There are various techniques to measure the space and time variation of plasma and dust parameters based on different physical principles.³ Light scattering has been one of the most commonly used techniques for detecting particles in gases and liquids.⁵ Moreover, dynamics light scattering from particulate suspensions is a powerful way to probe of the dynamics of neutral or charged particles based on Brownian motion framework. Light scattering experiments in plasma essentially examine the spatiotemporal variation of the laser light intensity (usually of visible range) that is directed at the plasma/sheath interface region, in sheet ray form parallel to the electrode. Forward directed elastic scattering or the Mie scattering often occurs when laser light incident on particles of size is comparable to the wavelength of the light. In fact, Mie scattering has a complicated dependence on the particle size, number density, and refractive index of particles. It is also strongly angular dependent.⁵ For particles of smaller sizes, a more isotropic scattering occurs, also known as the Rayleigh scattering.

Laser light scattering technique was used to demonstrate the role of dust contaminant in plasma processing⁶ which also served as the impetus for the increasing number of studies on charged particle dynamics in dusty plasmas. *In situ* light scattering studies of particle synthesis, particle aggre-

gation, size effect, and particle dynamics have been reported by many authors.^{7–9} Among the interesting charged particle dynamics in dusty plasmas are the formation of spatially ordered structures similar to those existing in liquids and solids,^{10–13} wave motion,^{14,15} and collective particle transports.^{16,17} Phase transitions in dusty plasmas have also been the subject of intense study over the past decade. If the ratio of the interparticle potential energy to the average kinetic energy is high enough, the particle will form either a “liquid” structure with short-range ordering or a crystalline structure with long-range ordering. Optical diagnostics of particle dynamics in dusty plasma may utilize digital imaging techniques for particle tracking and trajectory analysis or the direct light scattering data. In this study, we consider the dynamic light scattering technique based on correlation function approach. The temporal variation of fluctuation of the scattered intensity contains useful information regarding the particle dynamics.^{7,18,19} The particles are treated as charged Brownian particles and we investigate the transport mechanism based the correlation functions. The main contribution of this study is the introduction of the fractional Ornstein–Uhlenbeck (fOU) process²⁰ using nonstandard generalization of the Langevin equation^{21,22} using fractional calculus^{23–25} for studying charged Brownian motion in dusty plasma. We show that the scattered electric-field correlation model based on fractional Ornstein–Uhlenbeck process reproduces the qualitative features of the purely kinetic (ballistic) transport model proposed by Hurd and Ho¹⁸ for polydisperse particles.

In fact, this study demonstrates for the first time the direct link between power-law exponent of the dust particle mass distribution and the fractional derivative index. The performance of our correlation model is compared with the correlation functions corresponding to diffusive, ballistic (Gaussian), hybrid kinetic—hydrodynamics models using light scattering data from capacitively coupled radio-frequency dusty plasma system.

^{a)} Author to whom correspondence should be addressed. Electronic mail: msithi@um.edu.my. Telephone: +603-79674292. Fax: +603-79674146.

II. INTENSITY FLUCTUATION CORRELATION FUNCTION FOR KINETIC AND HYDRODYNAMICS TRANSPORT MECHANISMS

Consider the scattered intensity $I(t)$ measured at a given scattering angle θ as a stationary stochastic process with correlation function

$$C_I(t) \equiv \langle I(0)I(t) \rangle = \int_0^t I(t')I(t'+t)dt'. \quad (1)$$

The intensity fluctuation correlation function in Eq. (1) is related to that of the scattered electric field $C_E(t) = \langle E(0)E(t) \rangle$ through the relation $C_I(t) = I_o^2 + \kappa[C_E(t)]^2$, where I_o is the constant background and κ is detector dependent constant.¹⁸ Assuming there are N scatterers, the instantaneous scattered electric field $\vec{E}(t)$ is the sum of the individual strength of the scattering from j th particle located at position $\vec{r}_j(t)$ with a phase factor, $\exp[i\vec{q} \cdot \vec{r}_j(t)]$. The scattering wavevector in the unit direction \hat{n} is $\vec{q} = (4\pi/\lambda)\sin(\theta/2)\hat{n}$ with λ as wavelength of the incident light. Fluctuation in the intensity is due to temporal variation in the interference condition as a result of particle movements. Hence, useful information regarding the particle dynamics can be deduced from the intensity fluctuation analysis. If the mean intensity is subtracted from the scattered intensity fluctuation, then $C_I(t) \propto [C_E(t)]^2$.

Calculation of the correlation function of the electric-field fluctuation $C_E(t)$ depends on the assumptions regarding the size/mass distribution of the particles (whether monodispersed or polydispersed) and the nature of the transport mechanisms, namely, whether it is diffusive (hydrodynamics) or ballistic (kinetic).¹⁸ In this section, we recall some results on the correlation properties of the scattering intensity for monodisperse and polydisperse particles (see Refs. 7 and 18 for the details). Consider the correlation function of the electric field as

$$C_E(t) \equiv \langle E(0)E(t) \rangle = E_o^2 \left\langle \sum_{j=1}^N \exp[i\vec{q} \cdot \Delta\vec{r}_j] \right\rangle, \quad (2)$$

where $\Delta\vec{r}_j(t)$ is the displacement vector of the j th particle. If the particle is diffusive, the characteristic time $\tau_D \approx \Delta r^2/D$, where D is the diffusion constant. On the other hand, for ballistic motion, the characteristic time $\tau_B \approx \Delta r/u$, where u is the mean velocity of the particles. For the case of ballistic motion, $C_E(t)$ has been calculated using the Maxwell velocity distribution,²⁶ $P(u) = [m/2\pi k_B T]^{3/2} \exp[-mu^2/2k_B T]$. This results in the Gaussian type correlation function $C_E^B(t) \sim \exp[-t^2/(2\tau_B^2)]$ in contrast to the exponentially decaying correlation $C_E^D(t) \sim \exp[-t/(2\tau_D)]$ for diffusive dynamics. The superscripts B and D refer to ballistic and diffusive dynamics, respectively. The cross-over between the hydrodynamics and kinetic behaviors has been described in Ref. 18 using the standard Langevin equation, namely, $\ddot{u} + \xi\dot{u} = \tilde{\gamma}(t)$, where \vec{u} is the velocity field, ξ is the friction coefficient, and $\tilde{\gamma}(t)$ is the rapidly fluctuating force. The corresponding electric-field correlation with the Maxwellian assumption for velocity distribution is shown to be $C_E^{BD}(t) \sim \exp[-q^2\langle u_z^2 \rangle \xi^{-2} \varphi(\xi t)]$, where $\langle u_z^2 \rangle$ is the mean square value

of velocity component in the direction of \vec{q} and $\varphi(x) = -1 + x + \exp[-x]$. One can easily note that $\varphi(x) \sim x$ for $x \gg 1$, and $\varphi(x) \sim x^2$ for $x \ll 1$. Hence, the correlation $C_E^{BD}(t)$ converges to $C_E^B(t)$ (ballistic) and $C_E^D(t)$ (diffusive) for short time and long time, respectively. The mean square displacements for ballistic transport are $\langle \Delta r^2 \rangle = \langle u_z^2 \rangle t^2$ for $t \ll \xi^{-1}$ and for diffusive transport are $\langle \Delta r^2 \rangle = 6D_s t$ for $t \gg \xi^{-1}$ and D_s is self-diffusion coefficient.

The above derivation of the correlation function can be described more intuitively using the Van Hove autocorrelation function^{27,28} $G_s(\vec{r}, t) = \langle n(0, 0)n(\vec{r}, t) \rangle_{V, \Gamma}$, which measures the probability of finding a given scattering particle at position \vec{r} at time t given it was at position $\vec{0}$ at time $t=0$. The particle density at position \vec{r} and time t is denoted by $n(\vec{r}, t)$ and the average $\langle \rangle$ is taken both over the whole scattering volume V and the total measurement time Γ . The Van Hove autocorrelation function is related to dynamic structure factor $F_s(\vec{q}, t)$ through the three dimensional Fourier transform

$$F_s(\vec{q}, t) = \int_V G_s(\vec{r}, t) e^{i\vec{q} \cdot \vec{r}} d\vec{r}. \quad (3)$$

The dynamic structure factor in turn is related to the correlation function of electric-field fluctuation through the Siegert relation,²⁹ namely, $F_s(\vec{q}, \tau) = \langle E(\vec{q}, t)E(\vec{q}, t+\tau) \rangle$. Using the Gaussian approximation initially proposed by Vineyard³⁰ for nearly classical fluids model, the dynamic structure factor takes the form $F(\vec{q}, t) = \exp[-q^2\varphi(t)/6]$ with the so-called time-dependent width function $\varphi(t)$ analogous to the one defined above. Hence, the Van Hove autocorrelation function now takes the familiar Gaussian form

$$G_s(r, t) = \left(\frac{2}{3} \pi \varphi(t) \right)^{-3/2} \exp\left(-\frac{3}{2} \frac{r^2}{\varphi(t)} \right), \quad (4)$$

where the time-dependent width function $\varphi(t)$ is actually proportional to the variance or the mean square displacement of a Gaussian process, namely,

$$\varphi(t) \equiv \langle \Delta r^2 \rangle = \int_{R^3} r^2 G_s(\vec{r}, t) d^3r. \quad (5)$$

One can now write explicitly the expression for $\varphi(t)$ earlier in this section as $\varphi(t) = [6k_B T / (\xi^2 m)] [\xi t - 1 + \exp(-\xi t)]$ for $t > 0$ and deduce the two limits of ballistic transport ($t \ll \xi^{-1}$) and diffusive transport ($t \gg \xi^{-1}$). It is interesting to see how the Van Hove autocorrelation function or the dynamic structure factor would change if one is to consider anomalous diffusion transport with mean square displacement law satisfying a power-law such as $\varphi_H(t) \equiv \langle \Delta r^2 \rangle \sim t^\gamma$, where the scaling exponent $0 < \gamma < 2$. If we set $\gamma = 2H$, where $0 < H < 1$ is the Hurst exponent, then the two limiting cases described above are obtained, namely, the standard diffusion process (i.e., Brownian motion) when $H = 1/2$ and the ballistic transport when $H = 1$. The fractional Brownian motion^{31,32} is an example of a fractal Gaussian stochastic process which has the similar mean square displacement (or variance), but lacks time-shift invariance. Another example is the stationary Gaussian stochastic process characterized by correlation function in the form of stretched exponent

$C(t) \sim \exp[-(t/\tau)^\gamma]$, where τ is the characteristic time.²⁰ For both examples, concrete dynamical equations in the form of stochastic differential equations are not available.

So far, we have assumed that the particles' mass is uniform. For polydisperse samples with size distribution $p(R)$ with corresponding self-diffusion $p(D_s)$, the dynamic structure factor is not a simple monotonically decaying exponential function, but a superposition of several exponential functions implicitly dependent on D_s , given by³³

$$F_s(\vec{q}, \tau) = \int_0^\infty p(D_s) e^{-q^2 \tau \varphi(D_s)/6} dD_s. \quad (6)$$

The determination of the $p(D_s)$ is a challenging task and a practical way to estimate the calculate dynamic structure factor for polydisperse particles is to use cumulant analysis³⁴ in which $F_s(\vec{q}, t)$ is expanded as

$$\ln F_s(q, \tau) \approx -\kappa_1 \tau + \frac{1}{2!} \kappa_2 \tau^2 - \frac{1}{3!} \kappa_3 \tau^3 + \dots, \quad (7)$$

where the first cumulant $\kappa_1 = \bar{D} q^2$ yields the average diffusion coefficient \bar{D} and the second cumulant $\kappa_2 = [\bar{D}^2 - (\bar{D})^2] q^4$, which measures the polydispersity of the diffusion coefficient via $\sigma_D = (\kappa_2 / \kappa_1)^{1/2}$. It should be mentioned that the cumulant expansion is only strictly valid for small size polydispersities ($< 20\%$). Accurate estimation of the dynamic structure factor is further complicated by detailed knowledge of particle topology and form factor, particle concentration, and q -dependence.³⁴

Here, we adopt the generalization to the case of polydisperse mass distribution based on the study by Hurd and Ho.¹⁸ Assuming a mixed power-law and exponential distribution for particle mass in the form of $N(m) \sim m^{-\sigma} \exp[-m/m_o]$, with a cutoff mass m_o and scaling exponent σ , they showed that the electric-field correlation function in the kinetic limit is given by

$$C_E(t) \sim 2^{\sigma-2} \left(\frac{t}{t_o}\right)^{3-\sigma} K_{3-\sigma} \left(\frac{t}{t_o}\right), \quad (8)$$

where $K_\nu(z)$ is the ν th order modified Bessel function of second kind and $t_o = m_o / q^2 k_B T$. The correlation function which encompass both kinetic and hydrodynamical transport mechanisms for polydisperse dust can be derived as

$$\begin{aligned} C_E^{BD*}(t) &= E_o'^2 \int_0^\infty m^{2-\sigma} e^{-m/m_o} e^{-(q^2/2)(k_B T/2m)(-1+\xi t + e^{-\xi t})\xi^{-2}} dm, \\ &= 2^{\sigma-2} \{m_o^2 q^2 k_B T e^{-\xi t} [1 + e^{\xi t}(\xi t - 1)]\}^{(3-\sigma)/2} \\ &\quad \times K_{3-\sigma}(\{m_o^2 q^2 k_B T e^{-\xi t} [1 + e^{\xi t}(\xi t - 1)]\}^{1/2}). \end{aligned} \quad (9)$$

It can easily be shown that Eq. (9) reduces to the purely kinetic case equation (8) when $t \ll 1$.

In Sec. III, we introduce a generalization of the Langevin equation to a nonstandard form using fractional calculus.^{23,24} The resulting process denoted by $X_\beta(t)$ is called the fractional Ornstein–Uhlenbeck process. Our generalization preserves the stationary property of the original Ornstein–Uhlenbeck process,²¹ which is crucial for a time-

translational invariance property of the correlation function used to model the light scattering intensity fluctuation.

III. FRACTIONAL ORNSTEIN–UHLENBECK PROCESS

An intuitive way of introducing the fractional derivative is by noting that the n th derivative is basically an operation inverse to n -fold repeated integration,

$$\begin{aligned} \int_{t_o}^t \int_{t_o}^{s_1} \cdots \int_{t_o}^{s_{n-1}} f(s_n) ds_n \cdots ds_1 \\ = \frac{1}{(n-1)!} \int_{t_o}^t (t-s)^{n-1} f(s) ds. \end{aligned} \quad (10)$$

By induction, fractional integral of arbitrary order $\alpha > 0$ of a function $f(t)$ is defined as^{23,24}

$${}_o I_t^\alpha f(t) = \frac{1}{\Gamma(\alpha)} \int_{t_o}^t (t-s)^{\alpha-1} f(s) ds. \quad (11)$$

A version of fractional derivative denoted as ${}_o D_t^\alpha f(t)$ is defined as

$$\begin{aligned} {}_o D_t^\alpha f(t) &= \frac{1}{\Gamma(n-\alpha)} \left(\frac{d}{dt}\right)^n \\ &\quad \times \int_{t_o}^t (t-s)^{n-\alpha-1} f(s) ds, \quad n-1 \leq \alpha < n. \end{aligned} \quad (12)$$

Depending on the lower limit of the integral, $_{-\infty} D_t^\alpha f(t)$ is known as Weyl's fractional derivative and ${}_o D_t^\alpha f(t)$ is known as Riemann–Liouville fractional derivative.^{23,24} The shifted fractional derivative denoted by $({}_o D_t^\alpha + a)^\beta$ with real parameter $a > 0$ can be expressed in infinite series using binomial expression³⁵

$$\begin{aligned} ({}_o D_t^\alpha + a)^\beta f(t) &= \sum_{j=0}^\infty \binom{\beta}{j} a^j {}_o D_t^{\alpha(\beta-j)} f(t), \\ n-1 \leq \alpha < n; \quad \beta > 0. \end{aligned} \quad (13)$$

In this study, we let $\alpha=1$ but the fractional dynamics is characterized by the fractional index $\beta > 0$ which connected to the fractional derivative through binomial expansion. The general definition of the shifted fractional derivative with dual (α, β) fractional indices has been investigated by Lim *et al.*³⁵ A direct application of the Riemann–Liouville fractional integral to a Gaussian white noise would realize a fractional filtered process known in the literature as the one-sided fractional Brownian motion or the Levy-type fractional Brownian motion, defined as^{31,32}

$$\begin{aligned} B_H(t) &\equiv {}_o I_t^{H+1/2} \eta(t) \\ &= \frac{1}{\Gamma(H+1/2)} \int_0^t (t-s)^{H-1/2} \eta(s) ds \\ &= g_{B_H}(t) * \eta(t), \end{aligned} \quad (14)$$

where $*$ denotes convolution of the white noise $\eta(t)$ with a fractional response function

$$g_{B_H}(t) = \begin{cases} \frac{t^{H-1/2}}{\Gamma(H+1/2)} & \text{for } t \geq 0 \\ 0 & \text{for } t < 0. \end{cases} \quad (15)$$

The inverse operation of the fractional filtering of the white noise is the fractional derivative of fractional Brownian motion denoted by ${}_0D_t^{-(H+1/2)}B_H(t) = \eta(t)$. This form of fractional differential equation can be solved using the Green's function method.

The ordinary Ornstein–Uhlenbeck process $X_{OU}(t)$ is the stationary solution of the Langevin equation^{21,22}

$$(-\infty D_t^1 + a)X_{OU}(t) = \eta(t), \quad (16)$$

where $\eta(\cdot)$ is the standard Gaussian white noise with mean zero and delta function as correlation function, i.e., $\langle \eta(t)\eta(s) \rangle = \delta(t-s)$ and $a > 0$ is a coefficient. The stationary solution can be written as

$$X_{OU}(t) = \int_{-\infty}^t e^{-a(t-u)} \eta(u) du, \quad (17)$$

with correlation function given by $C(\tau) = \langle X_{OU}(t)X_{OU}(t+\tau) \rangle = \exp[-a|\tau|]/(2a)$. It follows from this second-order property that the Ornstein–Uhlenbeck process is a Markovian process with short-range memory. Its spectral density takes the Lorentzian form, $S_{OU}(\omega) = (a^2 + \omega^2)^{-2}$. Next, we describe the main result of the study by introducing a nonstandard generalization of the ordinary Langevin equation using the fractional calculus as shown below,²⁰

$$(-\infty D_t^1 + a)^\beta X_\beta(t) = \eta(t), \quad (18)$$

with fractional index $\beta > 0$. As we will see later, the fractional index can be related to the scaling exponent of the power-law mass distribution of the dust particles. The so-called nonstandard “fractional Langevin equation” can be solved using Green's function technique. Let $g_\beta(t)$ be the impulse response function of the system described in Eq. (18), hence we write

$$(-\infty D_t^1 + a)^\beta g_\beta(t) = \delta(t). \quad (19)$$

By applying Fourier transform on both sides of Eq. (19), and noting the property of Fourier transform of fractional derivative,²⁵ namely, $F[-\infty D_t^\alpha g_\beta(t)] = (-i\omega)^\alpha \tilde{G}_\beta(\omega)$ and the corresponding shift theorem, we obtain^{20,36}

$$\tilde{G}_\beta(\omega) = F[g_\beta(t)] = \frac{1}{(a - i\omega)^\beta}, \quad (20)$$

where $F[\cdot]$ denotes the Fourier transform and $F[\delta(t)] = 1$. Taking the inverse Fourier transform of Eq. (15) gives the response function for the fractional Ornstein–Uhlenbeck processes $X_\beta(t)$, namely,

$$g_\beta(t) = \begin{cases} \frac{t^{\beta-1} e^{-at}}{\Gamma(\beta)} & \text{for } t \geq 0 \\ 0 & \text{for } t < 0, \end{cases} \quad (21)$$

where $X_\beta(t) = g_\beta(t) * \eta(t)$. Lim *et al.*³⁵ showed that the

solution of Eq. (18) permits a Fourier spectral representation for $\beta > 1/2$. Note that when $\beta = 1$, $X_\beta(t)$ reduces to the standard Ornstein–Uhlenbeck process, $X_{OU}(t)$. The solution of Eq. (18) can be written explicitly as

$$X_\beta(t) = c(a, \beta) \int_{-\infty}^t g_\beta(t-u) \eta(u) du, \quad (22)$$

with $c(a, \beta)$ as an arbitrary constant which can be determined by choosing $\beta = 1$. The correlation function of $X_\beta(t)$ is calculated as

$$\begin{aligned} C_\beta(\tau) &= \langle X_\beta(t)X_\beta(t+\tau) \rangle, \\ &= c'(a, \beta) \int_{-\infty}^t \int_{-\infty}^{t+\tau} g_\beta(t-u) g_\beta(t+\tau-v) \\ &\quad \times \langle \eta(u)\eta(v) \rangle du dv, \\ &= \frac{a^{-2\nu}}{2^\nu \sqrt{\pi} \Gamma(\nu + 1/2)} |a\tau|^\nu K_\nu(|a\tau|), \end{aligned} \quad (23)$$

with $\nu = \beta - 1/2$ and K_ν is the modified Bessel function of the second kind.³⁷ The power-spectral density of $X_\beta(t)$ is given by $S_{X_\beta}(\omega) = |\tilde{G}_\beta(\omega)|^2 \sim (a^2 + \omega^2)^{-\beta}$. Moreover, the increments of fOU process also satisfy the locally self-similarity property, namely, $\langle [X_\beta(t+\tau) - X_\beta(t)]^2 \rangle \sim |a\tau|^{2\nu}$. It is interesting to note that based on this local self-similarity property and the power-spectral density at high frequency limit (i.e., $\omega \gg a$), the fractional Ornstein–Uhlenbeck process and its increments converge to the well-known Hurst, $H (= \nu)$ -indexed fractional Brownian motion and fractional Gaussian noise, respectively.^{31,32} Another advantage of fOU process having second-order stationary property is the possibility of describing the memory of the process through

$$\phi = \int_0^\infty C(t) dt. \quad (24)$$

A process is said to have a short-memory if ϕ is finite and long-memory if ϕ diverges. The fractional Ornstein–Uhlenbeck process can be shown to be a non-Markovian process simply by verifying that $C_{X_\beta}(t_3 - t_1) \neq C_{X_\beta}(t_2 - t_1) \times C_{X_\beta}(t_3 - t_2)$, $t_1 < t_2 < t_3$ with short-memory, namely, $C_{X_\beta}(t)$ decays slower than the standard exponential form of Ornstein–Uhlenbeck process. There are a number of generalizations of the standard Langevin equation using fractional calculus approach.^{38–46} Here, we mention one common form that may be considered as the standard fractional Langevin equation as given below,²⁰

$${}_t D_t^\beta Y(t) + aY(t) = \eta(t), \quad \beta > 0. \quad (25)$$

Equation (25) can be solved using the method of Laplace transform to give the general solution,

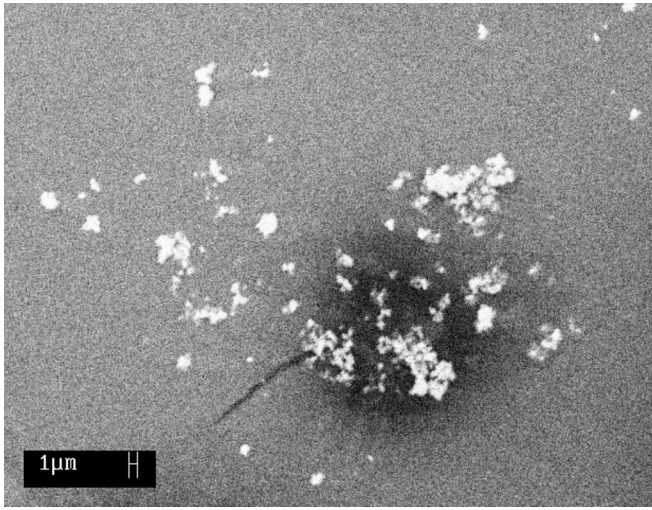


FIG. 1. Scanning electron micrograph of titanium dioxide dust particles used in dynamic light scattering experiment.

$$Y(t) = \sum_{j=1}^n Y_{j-1}^0 t^{j-1} E_{\beta,j}(-at^\beta) + \int_0^t (t-u)^{\beta-1} E_{\beta,\beta}[-a(t-u)^\beta] \eta(u) du, \quad (26)$$

where $E_{\alpha,\beta}$ is the generalized Mittag-Leffler function³⁷ and the boundary conditions Y_j^0 , $j=0, 1, \dots, n$ with $n-1 < \beta < n$ are assumed. Moreover, it has been shown that the correlation function of the process shown in Eq. (26) does not possess second-order stationarity,²⁰

$$C_Y(t_1, t_2) = \sum_{j,k=1}^{\infty} \frac{(-a)^{j+k-2}}{\Gamma(\beta j + 1) \Gamma(\beta k)} t_1^{\beta j} t_2^{\beta k-1} \times {}_2F_1(1, 1 - \beta k, 1 + \beta j, t_1/t_2), \neq f(t_1 - t_2), \quad (27)$$

where ${}_2F_1(\cdot)$ is the Gauss hypergeometric function. Despite its wide usage for modeling fractional dynamics in anomalous diffusion,⁴⁵⁻⁴⁷ the solution of the standard fractional Langevin equation lacks the key properties needed for modeling of the light intensity scattering fluctuation.

IV. LIGHT SCATTERING EXPERIMENT AND RESULTS

The light scattering experiment is conducted using a capacitively coupled 13.56 MHz radio-frequency (rf) plasma generator with argon gas operated at three different pressures, namely, 0.1, 0.5, and 0.8 mbar. First, the vacuum chamber is thoroughly cleaned and pumped to a pressure about 0.09 mbar. Argon gas is then injected into the chamber to a pressure not exceeding 1 mbar and then pumped down to the desired pressure and maintained at a constant value by adjusting the gas flow control valve. The gas is discharged with 100 W forward rf power and the plasma is generated. Light scattering measurement is carried out first without the presence of dust. Dusty plasma is then created by dispensing small amount of titanium dioxide dust particles into the

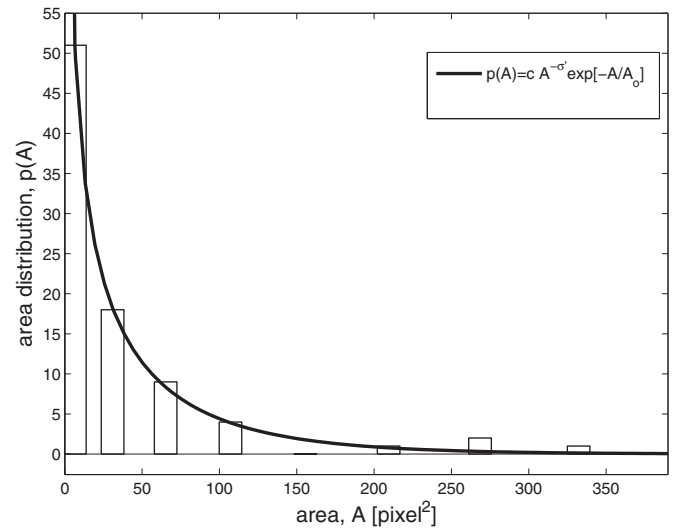


FIG. 2. Particles area distribution fitted with mixed exponential and power-law function.

chamber using a mechanical sprinkler system. As the dust particles acquire charges by mainly capturing electrons from the plasma, a cloud of suspended charged dust is formed above the lower electrode. By placing a copper ring on the lower electrode, the dust particles are confined to a finite region. Figure 1 shows the scanning electron micrograph (SEM) of the titanium dioxide dust particles used for this experiment. It is obvious that the particle size, hence the mass, is not monodisperse as indirectly verified by the particle area distribution shown in Fig. 2. If one chooses the particle area distribution $p(A)$ in the form of $p(A) = cA^{-\sigma'} \exp[-A/A_0]$, where A denotes areas, A_0 is the cut-off area, c is a constant, σ' is scaling exponent analogous to the mass distribution defined above for polydisperse particles, then the use of correlation model given by Eq. (23) is justified with respect to kinetic transport described by Eq. (8). The empirical fitting parameter estimates are $c = 132 \pm 24$, $\sigma' = 0.46 \pm 0.11$, and $A_0 = 76.92 \pm 29$ pixel². The value of σ' obtained from particle analysis based on two-dimensional

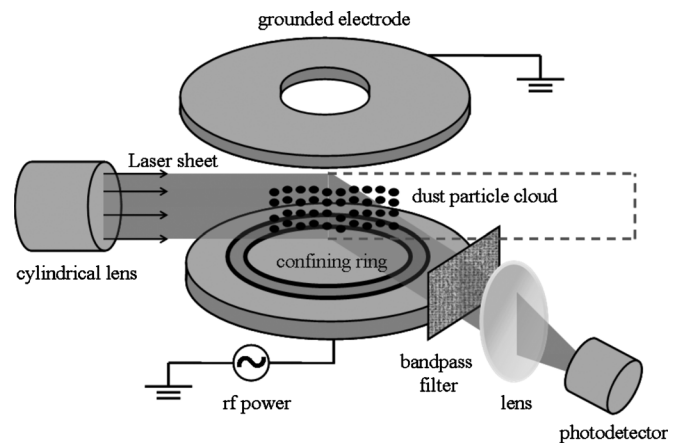


FIG. 3. Experimental setup for laser light scattering measurement in dusty plasma system.

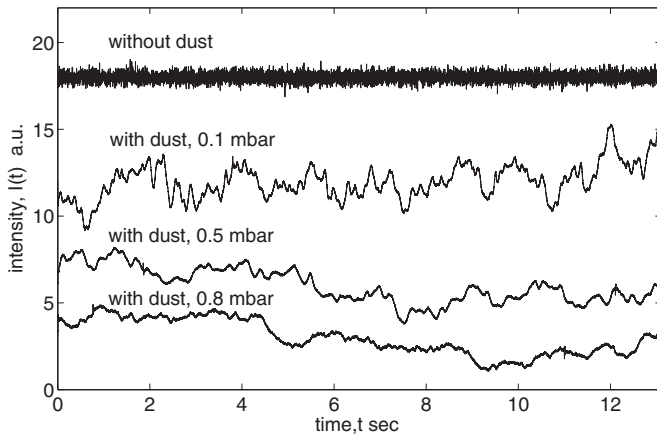


FIG. 4. Normalized light intensity fluctuations (arbitrary unit) in the absence of dust and with dust at discharge chamber pressure of 0.1, 0.5, and 0.8 mbar.

SEM micrograph is only indirectly related to the power-law exponent for mass distribution since the real mass would be very difficult to calculate.

The He–Ne laser beam with wavelength $\lambda=636.5$ nm is converted to a sheet beam using a cylindrical lens and transmitted through the plasma via the quartz windows, parallel to the electrodes. The schematic diagram of the experimental setup is shown in Fig. 3. Due to the construction limitation of the viewing windows of the discharge chamber, the measurement could only be done at an angle of 30° from the primary beam axis. The scattered light intensity is recorded using Newport 1936-C single channel optical power meter at data sampling rate of 10 kHz. The light intensity fluctuations in the absence of dust and with an argon gas pressure of 0.1, 0.5, and 0.8 mbar are shown in Fig. 4. High-frequency fluctuation that originates from the background plasma scattering is removed by applying a low-pass filter on the intensity time series. By subtracting the intensity time series with its mean value, one obtains the mean-zero intensity fluctuation. The time series is then normalized by dividing it with its standard deviation. These procedures form the intensity data preprocessing done using signal processing toolbox in MATLAB.

The empirical correlation of a discrete sequence of length N is calculated using

$$C_X(t) = \frac{1}{N} \sum_{s=1}^{N-t} X(s)X(s+t), \quad t=0,1,2,\dots,N-1. \quad (23')$$

The empirical correlation for the light intensity scattering fluctuation in dusty plasma at three aforementioned pressures will be fitted with four intensity correlation models based on different transport mechanisms. By noting that $C_I(t) \propto [C_E(t)]^2$, we use $C_I^B(t) = c_2 \exp(-2t^2/\tau_B^2)$ for ballistic transport, $C_I^D(t) = c_1 \exp(-2t/\tau_D)$ for diffusive transport, $C_I^{BD}(t) = c_3 \exp[-c(-1+\xi t + e^{-\xi t})]$ for hybrid ballistic-diffusion transport, and our fractional dynamics correlation function

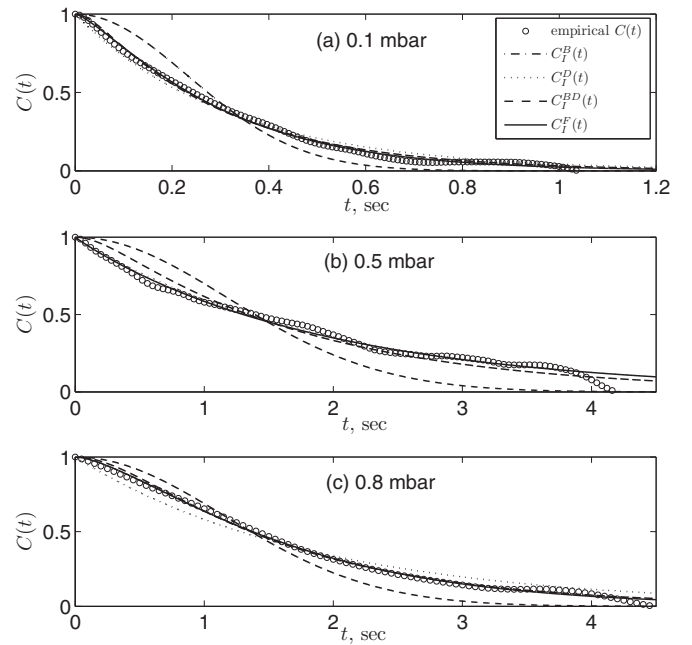


FIG. 5. Empirical correlation of intensity scattering fluctuation fitted with four different correlation functions at pressure (a) 0.1 mbar, (b) 0.5 mbar, and (c) 0.8 mbar.

based on fractional Ornstein–Uhlenbeck process, $C_I^F(t) = [2^{1-\nu} |at|^\nu K_\nu(|at|) / \Gamma(\nu)]^2$. Note that $C_E^F(t) \equiv C_\beta(t)$ with $\nu = \beta - 1/2$. All the model correlation functions are normalized such that $C_I(0)=1$, so we can set $c_1=c_2=c_3=1$.

The results of the correlation model fitting on the empirical correlation using nonlinear regression technique are shown in Figs. 5(a)–5(c) for three different argon gas pressures. The best fit model parameters for correlation functions $C_I^B(t)$, $C_I^D(t)$, $C_I^{BD}(t)$, and $C_I^F(t)$ are summarized in Table I with their respective root mean square error (RMSE).

V. DISCUSSIONS

Our correlation model based fOU process produced the best fit of the experimental data with the least error for pressure 0.1 and 0.8 mbar. For 0.5 mbar, the fit accuracy of fOU process is comparable with that of the hybrid kinetic-hydrodynamics model. The advantage of the fOU based correlation model may rest on the phenomenological origin of the fitting parameters a and ν (or $\beta = \nu + 1/2$). Parameter a is analogous to the friction coefficient ξ in the standard Langevin equation for the velocity field, hence a^{-1} may be seen as the persistence time or braking time of the fluctuations. Parameter ν is related to the polydispersity of the power-law mass distribution with exponent σ through $\nu = 3 - \sigma$ (or terms of shifted fractional derivative index $\beta = 7/2 - \sigma$). As noted earlier, the function $\varphi(x) = -1 + x + \exp[-x]$ which was introduced in an *ad hoc* manner to describe the cross-over between kinetic and hydrodynamical regimes in two opposite time limits does not seem to give a clear physical justification. Better insight into the relationship between the temporal variations of the scattered electric field and particle dynamics is obtained by considering the Van Hove autocorrelation function²⁷ together with the Vineyard's Gaussian approx-

TABLE I. Summary of best fit model parameters for different correlation functions.

Correlation\Pressure (mbar)	$C_I^B(t)$ τ_B (s) (rms error)	$C_I^D(t)$ τ_D (s) (rms error)	$C_I^{BD}(t)$ c, ξ (s^{-1}) (rms error)	$C_I^F(t)$ a (s^{-1}), ν (rms error)
0.1	0.465 ± 0.002 (0.079)	0.638 ± 0.002 (0.035)	$0.125 \pm 0.03,$ 28.49 ± 0.75 (0.022)	$2.246 \pm 0.010,$ 0.701 ± 0.003 (0.016)
0.5	2.315 ± 0.007 (0.116)	3.876 ± 0.003 (0.023)	0.138 ± 0.001 4.50 ± 0.12 (0.048)	0.251 ± 0.001 0.480 ± 0.001 (0.026)
0.8	2.312 ± 0.004 (0.053)	3.690 ± 0.007 (0.050)	0.301 ± 0.002 2.40 ± 0.02 (0.017)	0.479 ± 0.001 0.861 ± 0.002 (0.015)

imation³⁰ for the dynamic structure factor. Hence, one could identify the role of the mean square displacement (or the variance of particle position) in determining the types of transport mechanisms. We have also reasoned why the Gaussian models such as the fractional Brownian motion that is widely used for describing anomalous diffusion characterized by $\langle \Delta r^2 \rangle \sim t^{2H}$ would not serve as a plausible covariance model, despite encompassing both limiting cases for $H=1$ (ballistic) and $H=1/2$ (diffusive). Moreover, the dynamic structure factor for polydisperse particles is rather difficult to estimate using the Gaussian approximation and distribution for diffusion coefficients $p(D_s)$. Thus, we chose the non-standard fractional Langevin equation as the phenomenological model that gave a correlation function analogous to the result obtained by Hurd and Ho¹⁸ for polydisperse particles. In this respect, the fractional calculus approach gives one possible interpretation of the complex scaling behavior of the light intensity correlation function.

Overall, the correlation function based on purely ballistic transport mechanism does not seem to fit the experimental data for all three argon gas pressures. The RMSE for the data fitting is the largest among the four models considered here. At pressure 0.1 mbar, the dust particles were seen to be moving more erratically. The hybrid and the fractional correlation models seem to describe the empirical correlation data well. All models except the Gaussian type correlation model represent the empirical correlation data well for pressure 0.5 mbar. Finally, for the case of 0.8 mbar, only the hybrid correlation model and the fractional correlation model give satisfactory results. The persistence time (ξ^{-1}) is found to increase as the chamber pressure is increased from 0.1 to 0.8 mbar. On the other hand, we notice that the fractional index ν shows intricate dependence on the pressure with compensation coming from parameter a as well. Further study is needed to relate the fractional index ν (or β) to fractional oscillator characteristic of the charged dust particles. It is also remarked that all the correlation models are presumably associated to different Gaussian stochastic processes. The Gaussian nature of the intensity fluctuation is verified by plotting the empirical probability density function (pdf) as shown in Fig. 6.

VI. CONCLUSIONS

Dynamical laser intensity scattering in dusty plasma has been investigated using different stationary correlation models that are derived based on purely ballistic, purely diffusive, and hybrid ballistic-diffusive transport mechanisms with the assumption of monodisperse particles. Our main result is concerned about polydispersity of the dust mass distribution in which the original correlation model proposed by Hurd and Ho¹⁸ is reproduced using a completely different route, namely, the fractional Langevin equation with shifted fractional derivative operator. The solution of this fractional stochastic differential equation is the fractional Ornstein–Uhlenbeck process. It has a stationary correlation function parametrized by generalized friction coefficient a and fractional index β . In addition, the study also described for the first time a phenomenological link between power-law behavior in the particle polydispersity characterized by σ with fractional index β of dynamic light scattering fluctuation. Yet, more studies are needed to understand the origin of fractional dynamics from first principles. It would be interesting to investigate the anomalous transport properties of charged Brownian particles using the fractional diffusion equation⁴⁸ or the fractional Langevin equation with dynamic memory

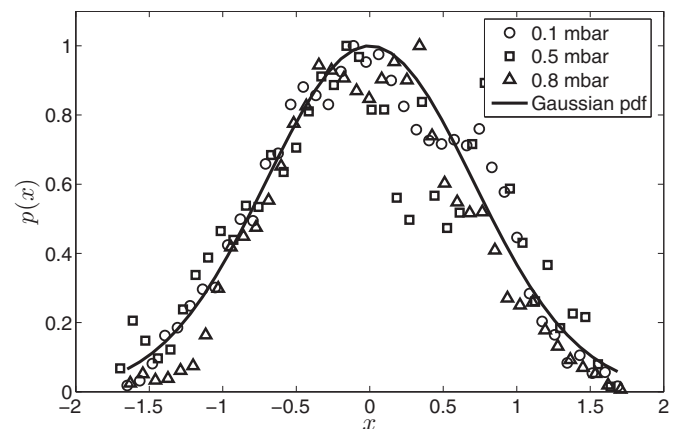


FIG. 6. Normalized empirical probability density function of the light intensity fluctuation fitted with normalized Gaussian probability density function.

A2: Published papers in proceedings

Diffusion Dynamics of Charged Dust Particles in Capacitively Coupled RF Discharge System

W.X. Chew, S.V. Muniandy, C.S. Wong, S.L. Yap, and K.S. Tan

*Plasma Research Laboratory, Department of Physics, University of Malaya,
50603 Kuala Lumpur, Malaysia*

Abstract. Dusty plasma is loosely defined as electron-ion plasma with additional charged components of micron-sized dust particles. In this study, we developed a particle diagnostic technique based on light scattering and particle tracking velocimetry to investigate the dynamics of micron-sized titanium oxide particles in Argon gas capacitively coupled rf-discharge. The particle trajectories are constructed from sequence of image frames and treated as sample paths of charged Brownian motion. At specific sets of plasma parameters, disordered liquid-like dust particle configuration are observed. Mean-square-displacement of the particle trajectories are determined to characterize the transport dynamics. We showed that the dust particles in disordered liquid phase exhibit anomalous diffusion with different scaling exponents for short and large time scales, indicating the presence of slow and fast modes which can be related to caging effect and dispersive transport, respectively.

Keywords: dusty plasma, transport process, brownian motion

PACS: 52.27.Lw

INTRODUCTION

Dusty or complex plasma are plasma containing charged micron-sized dust particle [1]. Dusty plasma are found in interstellar clouds, tokamaks and plasma reactor [1]. The charged particles experience various types of forces which include electrostatic force, gravitational force, ion drag force, thermophoresis force, neutral drag force and radiation pressure force. The many-body interaction of charged particles with the surrounding electrons and ions have give rise to many interesting phenomena such as crystal structures, ordered and disordered phases, linear and nonlinear waves, vortices, dust void, and Coulomb ball [1]. The dust-dust interaction in dusty plasma is described by Coulomb coupling parameter Γ_c , which is defined as the ratio of the electrostatic energy of neighboring particles and their thermal energy [2]. A system is said to be strongly coupled when the electrostatic interaction exceeds the thermal energy, i.e. when $\Gamma_c > 1$. By controlling the dust particle charge or dust temperature, highly-ordered crystal-like structure can be formed from a disordered gas-like or liquid-like dust configuration of states [3].

Kinetic description the dust particles in these disordered states have been investigated in a number of studies. Among the common framework used is the theory of Brownian motion that can model diverse

diffusion phenomena [4]. Diffusion process is characterized by the mean square displacement (MSD) of the Brownian particle defined as

$$\sigma^2(t) = \langle |r_i(t) - r_i(0)|^2 \rangle. \quad (1)$$

Here $r_i(t)$ is the position of the i -th particle at time t and the angular bracket denotes ensemble average. For normal or Fickian diffusion process, the MSD scales linear with time, namely $\sigma^2(t) \sim t$ and the diffusion coefficient D is determined through the Einstein relation, $D = \lim_{t \rightarrow \infty} \sigma^2(t)/(4t)$. Anomalous diffusion refers to nonlinear behavior of MSD [5], i.e. $\sigma^2(t) \sim t^\alpha$ with scaling exponent $\alpha \neq 1$. The system is said to undergo slow or sub-diffusion when $0 < \alpha < 1$, and fast or super-diffusion when $1 < \alpha < 2$. Normal diffusion or Brownian motion corresponds to $\alpha = 1$, and $\alpha = 2$ characterizes ballistic transport. Anomalous diffusion can be modeled using a version of fractional Brownian motion defined using Riemann-Liouville (RL) fractional integral [6],

$$X_H(t) = \frac{1}{\Gamma(H + \frac{1}{2})} \int_0^t (t - \tau)^{H - \frac{1}{2}} \eta(\tau) d\tau \quad (2)$$

where Γ is gamma function, $\eta(\tau)$ is the Gaussian, delta-correlated white noise and $H > 0$ is the Hurst exponent. The standard definition of FBM is based on modified Weyl fractional integral introduced by Mandelbrot and van Ness [7]. Here, the RL-FBM, $X_H(t)$ is the solution of the Langevin equation in which random force is the Riemann-Liouville derivative of Gaussian noise. RL-FBM is a Gaussian process characterized by zero starting point, zero mean, correlation function [6]:

$$R(t, s) = \frac{t^{H+\frac{1}{2}} s^{H-\frac{1}{2}}}{(H+\frac{1}{2})\Gamma(H+\frac{1}{2})^2} {}_2F_1(\frac{1}{2}-H, 1, H+\frac{1}{2}, \frac{t}{s}) \quad (3)$$

where $s > t$ and ${}_2F_1$ denotes the Gauss hypergeometric function, and the variance given by $\sigma^2 = Ct^{2H}$, where $C = (2H\Gamma(H+1/2)^2)^{-1}$. It is clear that the variance (or the MSD) of RL-FBM satisfies the required power-law scaling with $\alpha = 2H$. Moreover, the RL-FBM is also a self-similar process, namely $\{X_H(at)\} \equiv \{a^H X_H(t)\}$, for $a > 0$ and the equivalence is in the statistical properties. However, due to the fact that the process starts from the origin, RL-FBM does not have stationary increments for transient time. However, at large time limit, this much desired property is recovered and hence one can define the power spectral density of power-law type and the fractal dimension is then given by $D_H = 2 - H$.

Anomalous diffusion of dust particles in strongly coupled quasi-2D and 2D ordered dusty plasma have been reported in a number of experiments. Sub-diffusion was observed at small time scale in frozen dusty plasma state, where the dust particles experience caging effect of neighboring particles [8-10]. Meanwhile super-diffusion have been observed on time scales up to 10 - 20 seconds due to collective (vortex) motion in melting state of quasi-2D dusty plasma [9,11] or due to cooperative fast particle excitations in cold quasi 2D dusty plasma [11]. Normal diffusion was observed at longer time scale in these experiments. Ratynskaia et al. [12] had reported non-Gaussian position distribution with exponential tails in super-diffusive particle transport. Liu et al. [13] use laser power to heat the dust suspension to create a 2D nonequilibrium driven-dissipative system. Non-Gaussian statistics and super-diffusion were found in the experiment. To explain the wide range of diffusion scaling exponents reported in experimental data, several theoretical investigations using Langevin dynamics simulation have been carried [14,15]. From the numerical analysis, super-diffusion is observed in weak neutral gas damping rate and weakly coupled system. Meanwhile, sub-diffusion occurred at large neutral gas damping rate and strongly coupled system. Also, anomalous diffusion is shown to be a transient behavior, which converges into normal diffusion at

long time limit. It is remarked that these models are only applicable to stationary equilibrium states. On the contrary, most reported cases of super-diffusion behavior are observed in systems that were not in equilibrium. This applies to the experiment of Ratynskaia et al. [12,16], where super-diffusion was observed in viscoelastic vertical dust fluid and to those of Liu and Goree [12], which was carried out in driven dissipative system.

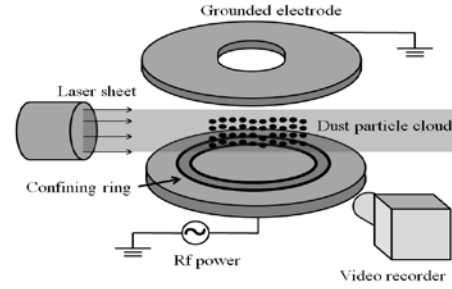


FIGURE 1. 3D configuration of rf capacitively coupled dusty plasma system.

EXPERIMENT SETUP

The experiment is conducted in a cylindrical symmetric rf dusty plasma system as shown in Fig. 1. It consists of a top grounded electrode, and a bottom electrode coupled to a 13.56 MHz rf power amplifier. The system is vacuumed using a rotary pump and filled with Argon gas at 0.1-0.9 mbar. Plasma is generated using 100W forward power with 43W reflected power. Polydispersed titanium oxide particles with mean size of 3 micron are introduced. The particles are negatively charged and thus suspended in the region of sheath boundary. The particles are confined using metallic confining ring placed on the lower electrode. A digital video recording system with 25 frame rate is used to capture the dust particles motion with the help of illumination by a He-Ne laser.

DATA ANALYSIS AND DISCUSSION

We observed an ordered dust configuration at pressure of 0.8 mbar compared to the disordered gas-like structure at 0.1 mbar as shown in Fig. 2 (a) and Fig. 2(b), respectively. Due to the limited frame rate of video recorder and viewing angle, we choose to analyze the relatively slower dust dynamics at 0.8 mbar. The spatial resolution of the video is approximately $\sim 38.7\mu\text{m}$. The average inter-particle spacing is estimated to be around 0.855mm.



FIGURE 2(a). Disordered dust configuration at pressure 0.1 mbar, **(b).** Ordered structure at 0.8 mbar.

Trajectories of particles are calculated as follows. Video is digitized to yield the coordinates of all the particles in a single field. Trajectories of individual particle is found using a computer algorithm that link a particle in one field to the most probable closest particle in the next field with the distance travel less than inter-particle spacing. Figure 3 shows the particle trajectories as they evolve in time (as indicated by gray-scale time mapping). Particle displacements at time t from initial positions are calculated for an ensemble of similarly behaving particles. The MSD is then calculated using Eq.(1) and plotted versus time in log-log scale as shown in Fig. 4. The slope of log-log plot gives the scaling exponent of the diffusion process. At small time scale (0.04 – 2 sec), the scaling exponent is close to one, indicating normal diffusion. At later time (after 2 sec), a slight change in the slope which points towards sign of anomalous transport behavior is observed. This shows the presence of slow and fast modes which can be related to caging effect and dispersive transport, respectively.

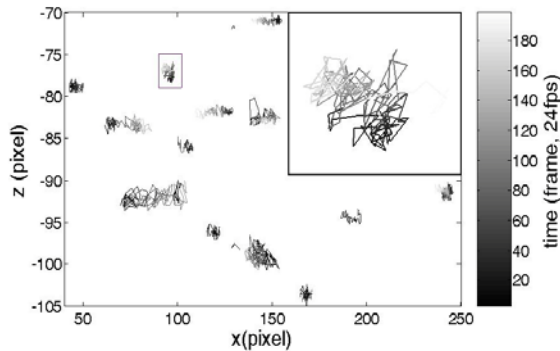


FIGURE 3. Evolution of particle trajectories with grayscale time mapping.

CONCLUSION

Scaling behavior of the MSD is used to characterize the transport dynamics of charged particles in dusty plasma. It is found that dust particles in disordered liquid-like phase exhibit anomalous diffusion with different scaling exponents for short time and long time scales.

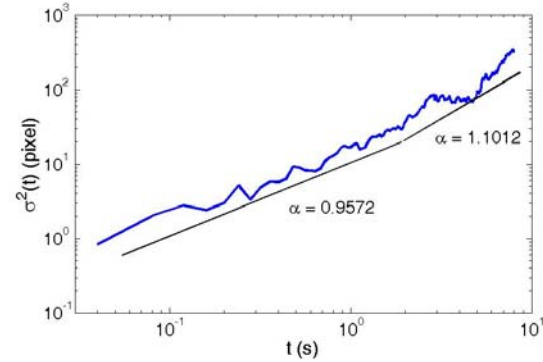


FIGURE 4. Log-log plot of MSD versus time showing slope $\alpha \sim 1$ at short time (0.04 – 2 sec) and slope $\alpha > 1$ after 2 sec.

ACKNOWLEDGMENTS

The authors thank Professor P.W. Smith (Oxford University) and Jasbir Singh for technical assistance in setting up the dusty plasma system. This work is supported under the University of Malaya Research Grant (RG062/09 AFR).

REFERENCES

1. P. K. Shukla and A. A. Mamun, *Introduction to Dusty Plasma*, IOP press: Bristol, 2002.
2. H. Ikezi, *Phys. Fluids* **29**, 1764-1766 (1986).
3. R. A. Quinn, C. Cui, J. Goree, J. B. Pieper, H. Thomas and G. E. Morfill, *Phys. Rev. E* **53**, R2049- R2052 (1996).
4. E. Cussler, *Diffusion: Mass Transfer in Fluid Systems*, Cambridge University Press: Cambridge, 1997.
5. J. P. Bouchaud and A. Georges, *Phys. Rep.* **195**, 127-293 (1990).
6. V.M. Sithi and S. C. Lim, *J. Phys. A: Math. Gen.* **28**, 2995-3003 (1995).
7. B. B. Mandelbrot and J. W. van Ness, *SIAM Rev.* **10**, 422 (1968).
8. S. Nunomura, D. Samsonov, S. Zhdanov and G. Morfill, *Phys. Rev. Lett.* **96**, 015003 (2006).
9. W. T. Juan and L. I., *Phys. Rev. Lett.* **80**, 3073-3076 (1998).
10. R. A. Quinn and J. Goree, *Phys. Rev. Lett.* **88**, 195001 (2002).
11. Y. J. Lai and L. I., *Phys. Rev. Lett.* **89**, 155002 (2002).
12. S. Ratynskaia, C. Knapek, K. Rypdal, S. Khrapak and G. Morfill, *Phys. Plasmas* **12**, 022302 (2005).
13. B. Liu and J. Goree, *Phys. Rev. Lett.* **100**, 055003 (2008).
14. L. J. Hou, A. Piel and P. K. Shukla, *Phys. Rev. Lett.* **102**, 085002 (2009).
15. T. Ott and M. Bonitz, *Phys. Rev. Lett.* **103**, 195001 (2009).
16. S. Ratynskaia, K. Rypdal, C. Knapek, S. Khrapak, A. V. Milovanov, A. Ivlev, J. J. Rasmussen and G. E. Morfill, *Phys. Rev. Lett.* **96**, 105010 (2006).

Fractional Dynamics of Single File Diffusion in Dusty Plasma Ring

S.V. Muniandy^a, W.X. Chew^a, H. Asgari^a, C.S. Wong^a and S.C. Lim^b

^aPlasma Technology Research Center, Department of Physics, University of Malaya
50603 Kuala Lumpur, Malaysia.

^bFaculty of Engineering, Multimedia University, 63100 Cyberjaya, Selangor, Malaysia

Abstract. Single file diffusion (SFD) refers to the constrained motion of particles in quasi-one-dimensional channel such that the particles are unable to pass each other. Possible SFD of charged dust confined in biharmonic annular potential well with screened Coulomb interaction is investigated. Transition from normal diffusion to anomalous sub-diffusion behaviors is observed. Deviation from SFD's mean square displacement scaling behavior of 1/2-exponent may occur in strongly interacting systems. A phenomenological model based on fractional Langevin equation is proposed to account for the anomalous SFD behavior in dusty plasma ring.

Keywords: Yukawa liquid. Dusty plasma ring. Anomalous diffusion. Fractional calculus.

PACS: 52.27 .Lw; 52.25 Fi; 52.27 .Gr.

ANOMALOUS DIFFUSION IN DUSTY PLASMAS

Anomalous diffusion refers to nonlinear scaling of the mean square displacement (MSD) of the particles with respect to time, namely $R^2(t) \sim t^\alpha$, where $\alpha \neq 1$ [1]. Subdiffusion occurs when $0 < \alpha < 1$ and super-diffusion when $1 < \alpha < 2$. Ordinary diffusion is seen when $\alpha = 1$. Single file diffusion (SFD) is an interesting type of subdiffusive ($\alpha = 1/2$) transport, in which the particles are constrained from passing each other in a narrow channel or potential confinement [2]. The possibility of observing SFD in dusty plasma ring was reported in [3,4]. Following a similar experimental setup as described in [4], we obtained the dusty plasma ring as shown in Figure 1(a) with samples of particle trajectories (Figure 1(b)). The MSD of an ensemble of almost identical particles is depicted in Figure 1(c) showing transition from diffusion to sub-diffusion and later to complicated scaling with oscillations.

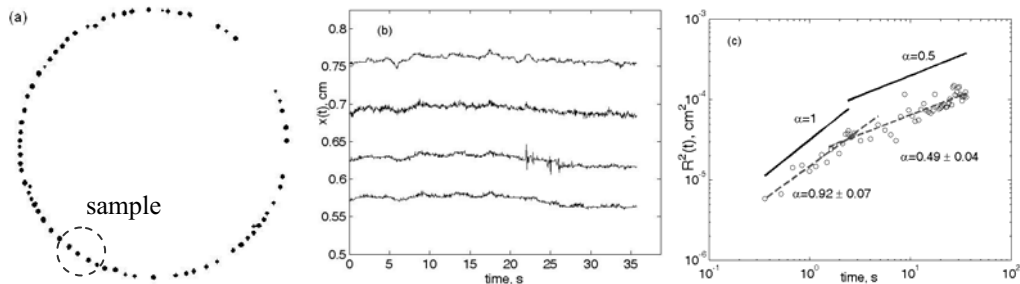


FIGURE 1. (a) Snapshot of strongly correlated dust particles in quasi-1D dusty plasma ring, (b) selected particles trajectories and (c) averaged mean square displacement.

FRACTIONAL LANGEVIN DYNAMICS

The microscopic dynamics of a tagged dust particle (assuming unit mass) in a single file system can be modeled using generalized fractional Langevin equations [5]:

$${}_0D_t^\beta x(t) = v(t), \quad 0 < \beta \leq 1, \quad (1)$$

$${}_0D_t^\alpha v(t) + \lambda v(t) + \int_0^t \gamma(t-s)v(s)ds = \xi(t), \quad 0 < \alpha \leq 1 \quad (2)$$

where ${}_0D_t^\beta$ and ${}_0D_t^\alpha$ are the Caputo fractional derivatives, $\gamma(t) = 2\lambda\delta(t) + t^{\zeta-1}/\Gamma(\zeta)$ is the fractional kernel, λ is the dissipation parameter and $0 \leq \zeta < 1$. Here, we simplify the model by assuming $\alpha=\beta=1$. The second term in $\gamma(t)$ is responsible for the correlated effect due to confinement [6]. Dust-plasma interaction is described via the correlated Gaussian noise $\xi(t)$ term such that $\langle \xi \rangle = 0$ and it satisfies the generalized fluctuation dissipation relation $\langle \xi(t)\xi(0) \rangle = k_B T \gamma(t)$, where k_B is the Boltzmann constant, T is temperature. Using the method of Laplace transform, the particle position is given by

$$x(t) = x(0) + \int_0^t \psi(t-s)\xi(s)ds + v(0)\psi(t), \quad (3)$$

where $\psi(t)$ is related to the mobility $\mu(t)$, i.e. $d\psi(t)/dt = \mu(t)$ and noting that $\tilde{\psi}(s) = (s^2 + \gamma s + s^{1-\zeta})^{-1}$ is the inverse Laplace transform of $\psi(t)$. The MSD of the tagged particle is given by

$$R^2(t) = 2k_B T \int_0^t \int_0^{t'} \psi(s)\gamma(t'-s)\psi(t')dsdt' + v^2(0)(\psi(t))^2, \quad (4)$$

with the long-time behavior $R^2(t) \sim t^{1-\zeta}$. Initial transient behavior of this system was shown to be ballistic with $R^2(t) \sim t^2$ before changing to normal diffusion ($\zeta=0$) and later to SFD (with $\zeta=1/2$) [6]. Our model is able to describe the anomalous SFD in dusty plasma ring with exponent ζ which may be different from 1/2. This may occur in strongly correlated Yukawa liquid, systems with inhomogeneous dust, internal degree of freedom such as particle rotation and complex dust-plasma interactions.

ACKNOWLEDGMENTS

This research was partly supported by the University of Malaya Research Grant (RG062/09AFR) and the Fundamental Research Grant Scheme (FP003/2010B) under the Malaysian Ministry of Higher Education.

REFERENCES

1. R. Metzler and J. Klafter, *Phys. Rep.* **339**, 1-77 (2000)
2. T.E. Harris, *J. Appl. Prob.* **2**, 323-338 (1965).
3. T.E. Sheridan, *Phys. Scr.* **80**, 065502 (2009).
4. T.E. Sheridan and J.C. Gallagher, *arXiv*:1004.1148 (April 2010).
5. S.C. Lim and L.P. Teo, *J. Stat. Mech.* P08015 (2009).
6. A. Taloni and M. A. Lomholt, *Phys. Rev. E* **78**, 051116 (2008).

Fractal analysis of dynamics light scattering intensity fluctuation in disordered dusty plasmas

W.X. Chew, S.S. Safaai, S.V. Muniandy*, S.L. Yap, C.S. Wong
*Plasma Technology Research Centre, Department Of Physics
University of Malaya, 50603, Kuala Lumpur, Malaysia*

Abstract. Dynamic light scattering (DLS) technique is a simple and powerful technique for characterizing particle properties and dynamics in complex liquids and gases, including dusty plasmas. In this study, fractal characteristics of DLS time series are analyzed using wavelet scalogram approach. Wavelet based scale decomposition approach is used to separate non-scaling background noise (without dust) from scaling intensity fluctuation from dusty plasma. The Hurst exponents for light intensity fluctuation in dusty plasma at different neutral gas pressures are determined. At low pressures, weaker damping of dust motions via collisions with neutral gases result in stronger persistent behaviors in the fluctuation of DLS time series. The fractal scaling Hurst exponent is demonstrated to be useful for characterizing structural phases in complex disordered dusty plasma, especially when particle configuration or sizes are highly inhomogenous, making the standard pair-correlation function difficult to interpret. The results from fractal analysis are verified using an alternative interpretation of disorder based on approximate entropy.

Keywords: *Dynamic light scattering; Dusty plasmas; Fractal analysis*

PACS: 52.25.Os; 52.27.Lw; 64.60.al

A4: Abstract of presentations

National Conference on Physics (PERFIK2010)

28th-30th October 2010

Swiss-Garden Golf Resort & Spa Damai Laut, Perak, Malaysia.

Diffusion Dynamics of Charged Dust Particles in Capacitively Coupled RF Discharge System.

W.X. Chew, S.V. Muniandy, C.S. Wong, S.L. Yap, and K.S. Tan

*Plasma Research Laboratory, Department of Physics, University of Malaya,
50603 Kuala Lumpur, Malaysia*

Abstract. Dusty plasma is loosely defined as electron-ion plasma with additional charged components of micron-sized dust particles. In this study, we developed a particle diagnostic technique based on light scattering and particle tracking velocimetry to investigate the dynamics of micron-sized titanium oxide particles in Argon gas capacitively coupled rf-discharge. The particle trajectories are constructed from sequence of image frames and treated as sample paths of charged Brownian motion. At specific sets of plasma parameters, disordered liquid-like dust particle configuration are observed. Mean-square-displacement of the particle trajectories are determined to characterize the transport dynamics. We showed that the dust particles in disordered liquid phase exhibit anomalous diffusion with different scaling exponents for short and large time scales, indicating the presence of slow and fast modes which can be related to caging effect and dispersive transport, respectively.

Keywords: Dusty plasma, transport process, Brownian motion.

PACS: 52.27.Lw

The 6th Mathematics and Physical Sciences Graduates Congress
13 - 15th December 2010
Faculty of Science, University of Malaya.

Stochastic Dynamics of Charged Dust Particles in Capacitively Coupled RF Discharge System

W.X. Chew, S.V. Muniandy and C.S. Wong

*Plasma Research Laboratory, Department of Physics, University of Malaya,
50603 Kuala Lumpur, Malaysia*

Abstract. Dusty plasma is loosely defined as electron-ion plasma with additional charged components of micron-sized dust particles. In this study, we developed a particle diagnostic technique based on particle tracking velocimetry to investigate the dynamics of micron-sized titanium oxide particles in Argon gas capacitively coupled rf-discharge. The particle trajectories are constructed from sequence of image frames and treated as sample paths of charged Brownian motion. At specific sets of plasma parameters, disordered liquid-like dust particle configuration are observed. Mean-square-displacement of the particle trajectories are determined to characterize the transport dynamics. We showed that the dust particles in disordered liquid phase exhibit anomalous diffusion with different scaling exponents for short and large time scales, indicating the presence of slow and fast modes which can be related to caging effect and dispersive transport, respectively. A Gaussian model with varying scaling exponent is proposed as candidate model for observed anomalous transport.

Keywords: Dusty plasma, transport process, Brownian motion.

Diffusion process of Charged Dust Particles in Capacitively Coupled RF Discharge System

W.X. Chew, S.V. Muniandy and C.S. Wong

*Plasma Research Laboratory, Department of Physics, University of Malaya,
50603 Kuala Lumpur, Malaysia*

Abstract. Dusty plasma is loosely defined as electron-ion plasma with additional charged components of micron-sized dust particles. In this study, we developed a particle diagnostic technique based on particle tracking velocimetry to investigate the dynamics of micron-sized titanium oxide particles in Argon gas capacitively coupled rf-discharge. The particle trajectories are constructed from sequence of image frames and treated as sample paths of charged Brownian motion. At specific sets of plasma parameters, disordered liquid-like dust particle configuration are observed. Mean-square-displacement of the particle trajectories are determined to characterize the transport dynamics. We showed that the dust particles in disordered liquid phase exhibit anomalous diffusion with different scaling exponents for short and large time scales, indicating the presence of slow and fast modes which can be related to caging effect and dispersive transport, respectively. A Gaussian model with varying scaling exponent is proposed as candidate model for observed anomalous transport.

Keywords: Dusty plasma, transport process, Brownian motion.

Hands on Research in Complex Systems

17-29th June 2012
Shanghai Jiao Tong University, China.

Hands-On Research in Complex Systems
Advanced Study Institute --- 17-29 June 2012
Shanghai Jiao Tong University (Shanghai, People's Republic of China)
Sponsored by Abdus Salam International Centre for Theoretical Physics
and Shanghai Jiao Tong University

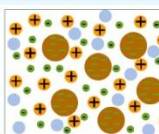
Fractal analysis of dynamics light scattering intensity fluctuation in disordered dusty plasmas

W.X. Chew, S.S. Safaai, S.V. Muniandy, S.L. Yap and C.S. Wong.

Plasma Technology Research Centre, Department of Physics, University of Malaya, 50603 Kuala Lumpur, Malaysia.

Introduction

Dusty or complex plasmas are plasmas containing charged micron-sized dust particles [1]. The charged dust particles experience complex interactions with each other and the background plasma as well. By controlling the charge or temperature of the dust particles, one can alter the physical state of dusty plasma that range from highly-ordered crystal-like, partially ordered liquid-like and highly disordered gas-like states. One way to differentiate such physical state experimentally is by calculating the radial pair correlation function, $g(r)$, from the snapshot of dust layer. However, pair correlation fails in describing disordered gas-like state.

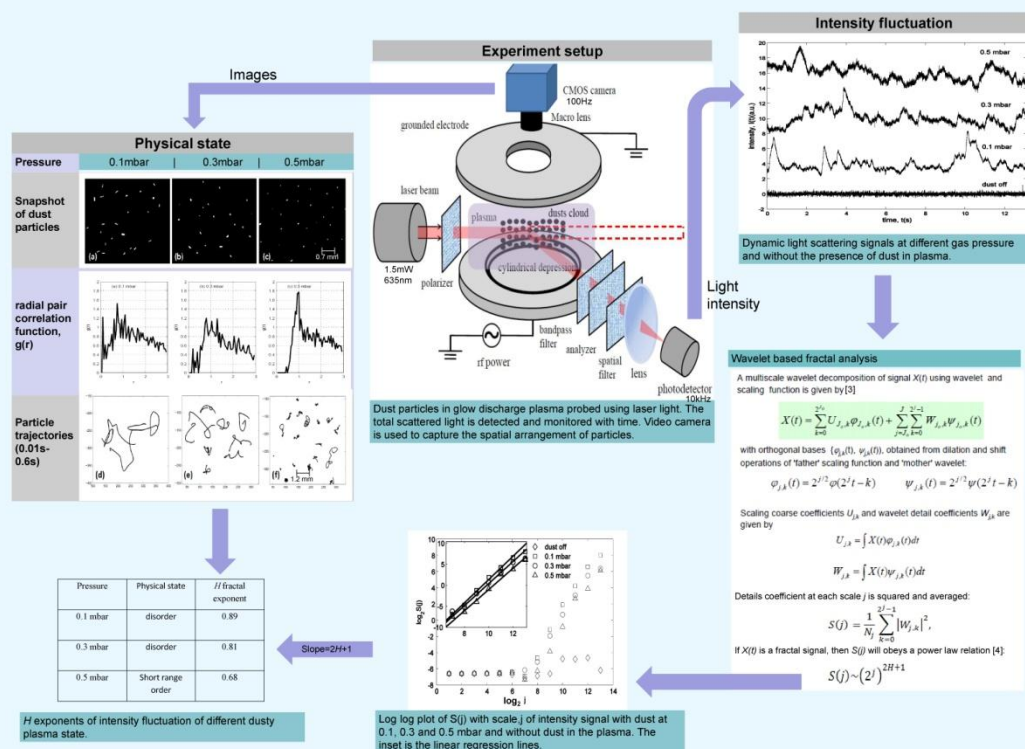


Here, we propose the use of **dynamic light scattering** technique together with fractal analysis of the signal as an alternative way to probe the state of dusty plasma. **Fractal analysis** is a powerful tool for understanding complex system and dynamics. Characteristics in time series $X(t)$ can be described through **scale invariance** property, namely $X(at) \equiv a^H X(t)$, where a is a scale factor, $0 < H < 1$ is the H -self-similar exponent [2].

Objectives

The main objectives of this study are:

- To characterize physical state of dusty plasma especially the disorder state through **fluctuation behavior** in **dynamic light scattering signal**.
- To characterize the light intensity fluctuation using **wavelet based fractal analysis**.



Appendix B: Matlab scripts

B1: Signal processing and correlation analysis in DLS experiment

```
%there are five section in this correlation analysis of DLS signal:
%(1)bandstop filtering, (2) wavelet detrend (3)empirical ACF
%calculation, (4)ACF averaging, (5)ACF model fitting
%-----
%(1) bandstop filtering
%key in the names of input raw data, and click Ctrl+enter to run within
%this cell.
%three spectrum will appear, select the [Fp1,Fst1,Fst2,Fp2] for bandstop
%filter.
clear all,clc,close all
name='09dona' %-----
A_bandstopFilter(name)
clear all,clc%,close all
name='09donb' %-----
A_bandstopFilter(name)
clear all,clc%,close all
name='09donc' %-----
A_bandstopFilter(name)
%clear all,clc,close all
%name='09donb'
%A_bandstopFilter(name)
%%
%(2)wavelet detrending
clear all,clc,close all
name='09dona' %-----
B_waveletdetrend(name)
clear all,clc
name='09donb' %-----
B_waveletdetrend(name)
clear all,clc
name='09donc' %-----
B_waveletdetrend(name)
%clear all,clc
%name='09donb'
%B_waveletdetrend(name)
%%
%(3) ACF calculation
clear all,clc,close all
name1='09dona' %-----
name2='09donb' %-----
name3='09donc' %-----
C_getACF(name2,8000) %specify the input data one by one with the lag time %-----
-----
%%
%(4) averaging the ACF data
clear all,clc,close all
name='09'; %-----
c1=load('09dona_ac.dat'); %-----
c2=load('09donb_ac.dat'); %-----
c3=load('09donc_ac.dat'); %-----
%change this to reduce or add number of data for averagin; default is 3
%sets of data
l=min([size(c1,2),size(c2,2),size(c3,2)]); %length of the shortest ACF %-----
-----
aveC=mean([ c1(2,1:l);c2(2,1:l);c3(2,1:l)]); %mean of three acf %-----
-----
```

```

lag=c2(1,1:l);
plot(lag,aveC)
acf=cat(1,lag,aveC);
save([name 'meanACF.dat'], 'acf', '-ascii')
%%
% ACF fitting, remember to specify the exclusion region in D_fitACF function
% first!!
clear all, clc, close all
[a s d f z x c v ]=D_fitACF('09meanACF') %-----

```

Main Functions

```

function A_bandstopFilter(name)
%this script uses Chebyshev II bandstop filter to remove power line interference present
%in raw signal.
%a raw spectrum will be shown for selecting the region to be filtered.
%Once finish you can see the result signal and save the signal.
% Load original 1D signal.
x = load([name '.dat']);
% sampling rate
Fs=10000; %-----
%cut to closest dyadic length:
dl=floor(log2(length(x)));
xx=x(1:2^dl);
%demean and normalize
a=xx-mean(xx);
aa=a./std(a);
%check original power spectrum
[ff,yy]=fftpsd(aa,Fs);
title('raw power spectrum')
xlim([30 80]) %shown only the first interference peak
%-----
%input parameters:Fp1,Fst1,Fst2,Fp2,Ap1,Ast,Ap2,Fs (F=freq,A=amplitude,p=pass,st=stop)
[fff,ppp]=ginput(4); %select the [Fp1,Fst1,Fst2,Fp2]
d1=fdesign.bandstop(fff(1),fff(2),fff(3),fff(4),2,10,2,Fs);
hd1=cheby2(d1,'matchexactly','stopband');
yy1=filter(hd1,aa);
y1=(yy1-mean(yy1))./std(yy1);
clear yy1
[fff,ppp]=ginput(4);%select the [Fp1,Fst1,Fst2,Fp2] for second time
d2=fdesign.bandstop(fff(1),fff(2),fff(3),fff(4),5,20,5,Fs);
hd2=cheby2(d2,'matchexactly','stopband');
yy2=filter(hd2,y1);
y2=(yy2-mean(yy2))./std(yy2);
clear yy2
xlim([10^2 10^2.3]) %shown only the second interference peak
[fff,ppp]=ginput(4);%select the [Fp1,Fst1,Fst2,Fp2]
d3=fdesign.bandstop(fff(1),fff(2),fff(3),fff(4),5,20,5,Fs);
hd3=cheby2(d3,'matchexactly','stopband');
yy3=filter(hd3,y2);
y3=(yy3-mean(yy3))./std(yy3);
clear yy3 y2
out=y3;
%plot the filtered spectrum
fftpsd(out,Fs);
title('bandstop filtered')
%plot the raw and filtered signal
figure
subplot(211)
plot(xx)
title('raw signal')

```

```

subplot(212)
plot(out)
title('bandstop filtered signal')
%saving the filtered signal
save([name '_bs.dat'],'out','-ascii')

```

function B_waveletdetrend(name)

```

%this decompose the signal using wavelet decomposition at scale j and reconstruct a
%coarse scale signal at scale j-1 and subtracted it from the original
%signal to give a detrended signal.
%default wavelet is db4
wvletdb=4;% wavelet type
%input data
x = load([name '_bs.dat']);
% Perform decomposition at level j of s using db1.
j=floor(log2(length(x)))
[c,l] = wavedec(x,j,['db' num2str(wvletdb)]);
%reconstructed at scale
k=j-1
% Reconstruct signal from the level k approximation:
xa8 = wrcoef('a',c,l,['db' num2str(wvletdb)],k);
detc=x-xa8;
%plotting the figure
figure
subplot(311);plot(x);title('Original signal') % title ('original signal');
subplot(312);plot(xa8); title('reconstructed signal')% title ('signal recon. from ca5');
ylim([-5 5])
subplot(313);plot(detc); title('detrended signal')% title ('signal recon. from cd2');%trend
figure
plot(detc)
%saveing the detrended signal
save([name '_wd.dat'],'detc','-ascii')

```

function C_getACF(name,lag)

```

%this script calculate the autocorrelation function(ACF) of input time series
%until the specified lag time
data= load([name '_wd.dat']);
%sampling interval=1/10k
nsi=1/10000;%0.0032;%-----
%autocorrelation calculation
[c,lags]=xcorr(data,lag,'coeff');
%selecting the ACF with positive lag time
plag=lags(lag+1:2*lag+1).*nsi;%in second
pc=c(lag+1:2*lag+1)';
acorr=cat(1,plag,pc); %turn the ACF and lag time into a two column matrix
save([name '_ac.dat'],'acorr','-ascii')% saving the two column matrix
%plotting the ACF
plot(data)
figure
plot(plag,pc)
kk=find((pc<=0))
min(kk) %give the lag time where ACF turn right below zero.

```

function [cB goodB cD goodD cBD goodBD cF goodF]=D_fitACF(name)

```

%fit the empirical ACF with four different correlation model: ballistic,
%diffusive, ballistic-diffusive and fractional ornstein-uhlenbeck model.
%before fitting, specify which part of ACF to be excluded in the fitting
%general exclusion rule:
%(1)first point of ACF is one, but the next point
%there's a sharp drop to below one, hence for better fitting, the first
%point is excluded.
%(2) excluded negative ACF

```

```

%(3) excluded part with sudden bump when ACF is decaying, which is caused
%by non-stationary effect.
acf= load([name '.dat']);
t=acf(1,:);
c=acf(2,:);
%exc=[]
%exc=find( c<=0 | c==1 |t>=0.6);%exclusion rules for 0.1
%exc=find( c<=0 | c==1 |t>=0.5);%exclusion rules for 0.3
%exc=find(c<=0 | c==1 );%exclusion rules for 0.5
%exc=find(c<=0 | c==1 );%exclusion rules for 0.8
exc=find(c<=0 | c==1 | t>=0.65);%exclusion rules for 0.9
inc=find(c<1 & c>0);% index of positive ACF region without first point
x1=t(inc(1));
x2=t(inc(end));
figure%displaying excluded region
plot(t,c)
hold on
plot(t(exc),c(exc),'o')
xlim([x1 x2])
ylim([0 1])
title('marked points are region excluded in fitting')
figure
[cB,goodB]=createFitB(t,c,exc);
xlim([x1 x2])
ylim([0 1])
figure
[cD,goodD]=createFitD(t,c,exc);
xlim([x1 x2])
ylim([0 1])
figure
[cBD,goodBD]=createFitBD(t,c,exc);
xlim([x1 x2])
ylim([0 1])
figure
[cF,goodF]=createFitFOU(t,c,exc);
xlim([x1 x2])
ylim([0 1])

```

B2: Image processing and particle tracking

Image processing

```

clear all
close all
clc
%This code perform spatial denoise on input grayscale image, output as binary image
%before you run, please do the following:
%(1)specify the parameter in every setion specified with long dash
%(2)create a output folder with the name of 'bi'
mode=0 %-----
%0=test mode(show one result without saving)
%1=(process all image frames and save data)
%<spatial denoise>, -----
lnoise=1; %lnoise=size of noise,
lobject=3; %lobject=size of dust grain
%loop for calling image file
D = dir('proc\0100*.bmp')%-----
%star is the number sequences in your data name,
%e.g. to import data01.bmp,data02.bmp,data03.bmp, type 'data0*.bmp' as the
%filename. Note that D only have the numerical information.

```

```

if mode==0
size=1;
else
size=numel(D);
end
%create empty cell
imcell = cell(1,size);
for i = 1:size
imcell = imread(['proc\' D(i).name']);%the name of directory your image is stored, same with D-----
-----
if mode==0
figure(1)
imshow(imcell)
else
end
%transform image to 2D binary field
bwcell=im2bw(imcell);
clear imcell
%fprintf('spatial denoising...');
outcell=bpass(bwcell,lnoise,lobject);
clear bwcell
if mode==0
figure(2)
imshow(outcell)
else
end
%saving the results in binary image format
if mode==1
imwrite(outcell,['bi\' D(i).name']);
clear outcell
else
end
end
end

```

Particle location identification

```

clear all,close all,clc
%This code finds particle position
%before you run, please do the following:
%(1)specify the parameter in every setion specified with long dash
pg=0 %-----
%0=test mode(show one result without saving)
%1=(process all image frames and save data)
%directories of binary images, cannot be grayscale!!
D = dir('bi\0100*.bmp');%-----
if pg==0
size=1;
else
%number of frames
size=numel(D);
end
imcell = cell(1,size);
%position list
poslst=0;
%start loop for position estimation
for i=1:size
fprintf(num2str(i));
fprintf('\n')
%load the image file
img=imread(['bi\' D(i).name']);
%input variable

```

```

%size to calculate centroid from lobject in bpass.m
lobject=3; %-----
szc=lobject+10; %-----
%diamter of the window over which to average to calculate the centroid.
%should be big enough to capture the whole particle but not so big that it captures others.
szpk=lobject+10; %-----
%if your data's noisy, (e.g. a single particle has multiple local
% maxima), then set this optional keyword to a value slightly larger than the diameter of your particle.
%pkfnd
%maximum intensity in grayscale image
maxth=max(max(max(img)));
th=2;%-----
%the minimum brightness of a pixel that might be local maxima. refer to the
%value of maximum intensity, maxth
%estimation of particles position
pkcoor=pkfnd(img,th,szpk);
%centroid calculation
cent=cntrd(img,pkcoor,szc,0);
%position list for tracking (x | y | frame)
if poslst==0
    %initial list
    poslst=cent(:,1:2);
    t=zeros(1,length(cent(:,1)));
    poslst=cat(2,poslst,t');
else
    %subsequent list
    clear t
    xy=cent(:,1:2);
    t(1:length(cent(:,1)))=i-1;
    t=t';
    xy=cat(2,xy,t);
    poslst=cat(1,poslst,xy);
end
if pg==0
    %plot as particle estimated position%-----
    figure(1),
    imshow(imread(['bi\' D(i).name']))
    figure(1),hold on
    pkx=pkcoor(:,1);
    pky=pkcoor(:,2);
    scatter(pkx,pky,'r')
    %plot centroid
    figure(2),
    imshow(img)
    figure(2),hold on
    scatter(cent(:,1),cent(:,2),'r+')
else
    end
clear cent
clear pkcoor
clear img
end
if pg==1
    save poslst.mat poslst %output filename
else
    save oneframeposlst.mat poslst %particle positions of the first image frame
end

```

Particle tracking

```
clear all,close all,clc
% This code perform particle tracking and shows the particles trajectory
% before you run, please do the following:
% (1) specify the parameter in every setion specified with long dash
% (2) if parameter 'newlist' return zero matrix, try minus 'mxt' with 1
load('poslst.dat'); % output from Blocateparticle.m
% one of the input image as backdrop-----
filename='proc\010000.bmp';
svcom=0 %-----
% 0=test mode(show one result without saving)
% 1=(process all image frames and save data)
savefile='01mbar.mat'; % output name-----
% tracking variables
%-----
maxdisp=12; % maximum distance in one frame
param.good=2;% minimum travel length
param.mem=0;% particle lost time
param.quiet=1; %text display
param.dim=2; %tracking dimension
mxt=10; %track particles that last for this long
% calling track.m
res=track(poslst,maxdisp,param);
save res.mat res
clear res
% plot the tracked particles trajectories and save the particles
% position,time and ID
figure(1)
set(gca,'color',[0 0 0])
ipic=imread(filename);
colormap('default')
hold on
load('res.mat')
% empty newlist
newlist=[];
% loop for filtering particle match the criteria
for i=1:res(size(res,1),4)
    fprintf(num2str(i))
        fprintf('\n')
    % filter that choose only particle last from 0th frame til mxt-th frame
    % Q:is i-th data contain mxt-th time frame and started at time 0? if YES
    % then continue
    if find(res(:,4)==i & res(:,3)==mxt) & find(res(:,4)==i & res(:,3)==0)~=0
        % find the index of particles that matches above criteria.
        index=find(res(:,4)==i & res(:,3)<=mxt);
        % x,y,t,id of particles
        x=res(index,1);
        y=res(index,2);
        t=res(index,3);
        id=zeros(length(x),1);
        id(:,1)=i;
        xyt=cat(2,x,y,t,id);
        % create a new list
        newlist=cat(1,newlist,xyt);
        % plot line with rainbow color gradient,initial blue,later red
        rainbowplot(x,y)
        % mark of particle id by plotting a point on the graph
        xmarks=size(ipic,1);
        ymarks=size(ipic,2);
        hh=plot(xmarks,ymarks,'b');
        legend(hh,num2str(i));
```



```

h=colorbar;
ylabel(h,'time (frame)','fontsize',22)
legend off
clear x y t id index xyt
else
end
end
%save as
if svcom==1
save(savefile,'newlist');
else
end
%number of particle satisfy criteria
fprintf('number of particle satisfy criteria')
length(unique(newlist(:,4)))
%plot particle with their id
index=find(newlist(:,3)==0);
x=newlist(index,1);
y=newlist(index,2);
id=newlist(index,4);
clear newlist
%marking of particle ID on figure
figure(2)
imshow(ipic);
hold on
plot(x,y,'or')
for i=1:length(x)
a=x(i)+5;
b=y(i);
c=id(i);
h=text(a,b,num2str(c))
set(h,'Color','w')
end

```

Pair correlation

```

clear all,clc,close all %-----
% Calculate Pair Correlation Function of randomly distributed points
%g(r) is like a histogram with user defined 'bin size', which is like the
%annular ring with thickness=bin size, r-distance away from one of the
%particle.
%input particle coordinates (x,y)
%CM=load('gasCM.dat');
CM=load('liqCM.dat');
%CM=load('liqCM.dat');
[numP, junk] = size(CM);
figure
scatter(CM(:,1),CM(:,2))
keynum=50;%determine the 'bin size'/annular ring size
maxgr=5*keynum;%maximum of r,choose before edge effect appear (particle near picture's edge don't
have symmetrical neighbors distribution)
imgarea=max(CM(:,1))*max(CM(:,2)); %area of image(unit in pixel), approximated by the farther
particle from origin.
partdensty=numP/imgarea %particle density~number of particle/ area of image;
IPD=1/sqrt(partdensty); %interparticle distance~1/sqrt(particle density)
PCorr = [];
for i = 1:maxgr;
PCorr(i) = 0; % Initialize PCorr to all zeros
end
for i = 1:numP
for j = i+1:numP

```

```

dist = sqrt( ( CM(i,1) - CM(j,1) )^2 + ( CM(i,2) - CM(j,2) )^2 ); %distance between each pairs of particles
d_int = round( keynum*dist/IPD );%grouping distances into categories.
if d_int < maxgr
PCorr(d_int) = PCorr(d_int) + 1; %count the frequency for different distance categories.
end;
end
end;
%plot(PCorr)
for i = 3:maxgr
    %normalized by the annular area and total number of particles
    nPCorr(i) = PCorr(i) / ( numP*pi*(( i+0.5)*IPD/keynum )^2 - ( i-0.5)*IPD/keynum)^2 );
end
npPCorr=nPCorr./partdensty;%normalize by average particle density
pPCorr=2.5.*npPCorr(1:end-1); %a correction factor for g(r) converge to one for large r
RoverIPD=[1:maxgr-1]./keynum; %construct x-axis which is r normalized by interparticle distance
figure
plot(RoverIPD,pPCorr)
xlabel('r / IPD')
ylabel('g(r),a.u.')
grid on

```

Velocity histogram

```

clear all ,close all,clc
%this code finds the particle speed distribution (2D)
%information regards experiment setting
%mm/pix ratio-----
pix=0.0233;
%s/frame ratio-----
fr=0.01;
%input:particle x,y positions (output of Ctrackparticle-----
list=load('addinlist.dat');
%number of bins in histogram-----
bin=15
%particle id's
id=unique(list(:,4));
%empty cells for x and y's increments
cumvx=[];
cumvy=[];
cumv=[];
%loop calling every particle to calculate particle first increment and
%velocity
for i=1:length(id)
    index=find(list(:,4)==id(i));
    x=list(index,1);%arbitrary axis x
    y=list(index,2);
    l=length(x);
    vx(i,1:l-1)=(x(2:end)-x(1:end-1)).*pix./fr; %velocity in x
    vy(i,1:l-1)=(y(2:end)-y(1:end-1)).*pix./fr;
    %cumvx=cat(2,cumvx,vx(i,:)); %ensemble averaged velocity
    %cumvy=cat(2,cumvy,vy(i,:));
    v=sqrt(vx(i,:).^2+vy(i,:).^2); %average of speed of both x y component
    cumv=cat(2,cumv,v);
    clear v
end
%unit is mm per s
meanv=mean(cumv)
varv=var(cumv)
hist(cumv,bin)
%title(['histrogram of v_y, var=' num2str(varvy) ])
xlabel('velocity, mm/s')

```

```
save v01.dat cumv -ascii %-----  
saveas(gcf,'result\hist.fig')  
saveas(gcf,'result\hist.jpg')
```